

LOCKHEED MARTIN ENERGY RESEARCH LIBRARIES



3 4456 0515284 8

ORNL-5182

*Cy 1*



# Metals and Ceramics Division Materials Science Annual Progress Report for Period Ending June 30, 1976

OAK RIDGE NATIONAL LABORATORY  
CENTRAL RESEARCH LIBRARY  
DOCUMENT COLLECTION  
**LIBRARY LOAN COPY**

DO NOT TRANSFER TO ANOTHER PERSON

If you wish someone else to see this document, send in name with document and the library will arrange a loan.

ORNL-7864  
1976-1-071

## OAK RIDGE NATIONAL LABORATORY

OPERATED BY UNION CARBIDE CORPORATION FOR THE ENERGY RESEARCH AND DEVELOPMENT ADMINISTRATION

Printed in the United States of America. Available from  
National Technical Information Service  
U.S. Department of Commerce  
5285 Port Royal Road, Springfield, Virginia 22161  
Price: Printed Copy \$6.00 ; Microfiche \$2.25

This report was prepared as an account of work sponsored by the United States Government. Neither the United States nor the Energy Research and Development Administration/United States Nuclear Regulatory Commission, nor any of their employees, nor any of their contractors, subcontractors, or their employees, makes any warranty, express or implied, or assumes any legal liability or responsibility for the accuracy, completeness or usefulness of any information, apparatus, product or process disclosed, or represents that its use would not infringe privately owned rights.

ORNL-5182  
Distribution  
Category UC-25

Contract No. W-7405-eng-26

METALS AND CERAMICS DIVISION MATERIALS SCIENCE ANNUAL PROGRESS REPORT  
FOR PERIOD ENDING JUNE 30, 1976

Compiled by C. J. McHargue, Manager, Materials Science

Edited by Sigfred Peterson

SEPTEMBER 1976

OAK RIDGE NATIONAL LABORATORY  
Oak Ridge, Tennessee 37830  
operated by  
UNION CARBIDE CORPORATION  
for the  
ENERGY RESEARCH AND DEVELOPMENT ADMINISTRATION

LOCKHEED MARTIN ENERGY RESEARCH LIBRARIES



3 4456 0515284 8



## FOREWORD

Since most programs of the Metals and Ceramics Division report progress on a quarterly or semiannual schedule, the need for an annual report has diminished. However, work supported by the Office of Materials Science, Division of Physical Research is usually published in the open literature. In order to give a view of this program in the Metals and Ceramics Division an annual report has been prepared. It consists of abstracts of papers published or presented during the year ending June 30, 1976, and summaries of work in progress.

During this reporting period a number of new programs have been started and others phased out in order to reflect the broadened responsibilities of the Division of Physical Research to the Energy Research and Development Administration compared with the Atomic Energy Commission. By the start of FY 1977, it is estimated that the thrust of these studies will be 32% nuclear energy, 36% nonnuclear energy, and 32% multidirectional-base research.

Following the reports of our technical progress is an appendix listing (1) assignments of our staff in other organizations, (2) guest assignments in our section, (3) staff changes, (4) joint appointments of our staff with the University of Tennessee for the academic year 1975-1976, (5) papers presented at technical meetings, and (6) publications.

C. J. McHargue



## CONTENTS

SUMMARY . . . . .	xiii
1. STRUCTURE OF MATERIALS . . . . .	1
1.1 THEORETICAL RESEARCH . . . . .	1
1.1.1 Electronic States of Substoichiometric Compounds and Application to Palladium Hydride. . . . .	1
1.1.2 A Band Theory Calculation of the Fermi Surface of Technetium . . . . .	1
1.1.3 Defect Annealing and Clustering in the Elastic Interaction Force Field . . . . .	2
1.1.4 Numerical Solutions of the General Rate Equations for Point Defects and Defect Clusters . . . . .	2
1.1.5 Bonding Properties of Stepped Transition Metal Surfaces . . . . .	2
1.1.6 Electronic Structure of Stepped Transition Metal Surfaces . . . . .	3
1.1.7 Cluster Calculations of the Electronic Structure of Transition Metal Surfaces . . . . .	3
1.1.8 Oxygen Chemisorption on a Small Aluminum Cluster . . . . .	3
1.1.9 A Surface Molecule Study of Oxygen Chemisorption on Aluminum . . . . .	4
1.1.10 Electron Phonon Interaction in Cubic Systems: Application to Niobium . . . . .	4
1.1.11 Gap Anisotropy and $T_C$ Enhancement: General Theory and Calculation for Nb, Using Fermi Surface Harmonics . . . . .	5
1.1.12 Superconductivity in the Transition Metals . . . . .	5
1.1.13 A One-Dimensional Model for Transition Metals and Their Alloys . . . . .	5
1.1.14 Exact Spectral Density Function for a One- Dimensional Model of an Amorphous Solid . . . . .	6
1.1.15 Spectral Density Functions for Amorphous Solids . . . . .	6
1.1.16 The Quasicrystalline Approximation: Comparison of the Spectral Density with Exact Results . . . . .	6
1.1.17 The Effects of Short-Range Order on the Spectral Density Function for a One-Dimensional Amorphous Solid . . . . .	7

1.1.18	Cluster Shape and Critical Exponents Near Percolation Threshold . . . . .	7
1.1.19	Cluster Size and Boundary Distribution Near Percolation Threshold . . . . .	7
1.2	X-RAY DIFFRACTION RESEARCH . . . . .	8
1.2.1	Raman Resonance Scattering of X Rays . . . . .	8
1.2.2	Quantitative X-Ray Fluorescent Analysis Using Fundamental Parameters . . . . .	9
1.2.3	X-Ray Monochromator Design for Synchrotron Radiation . . . . .	9
1.2.4	The Detection of Structurally Forbidden Bragg Maxima in $V_3Si$ . . . . .	10
1.2.5	The Crystal Structure of Monoclinic Europa . . . . .	10
1.2.6	Crystal Structure of $LiTe_3$ . . . . .	11
1.2.7	Recent Experimental Results from the ORNL 10-m Small-Angle X-Ray Scattering Spectrometer . . . . .	11
1.2.8	Report of the IUCr Commission on Crystallographic Apparatus International Project for the Calibration of Absolute Intensities in Small-Angle X-Ray Scattering . . . . .	12
1.2.9	Application of SAXS for Characterization of Pyrocarbon Coatings . . . . .	12
1.2.10	Studies of Catalysts: Cobalt Molybdate . . . . .	13
1.2.11	A Study of the Structure of Collagen Fibrils by Small-Angle X-Ray Scattering . . . . .	13
1.2.12	X-Ray Excitation of Surface Plasmons on Spherical Voids in Metals . . . . .	14
1.2.13	A New Small-Angle X-Ray Scattering Facility Utilizing a Rotating Anode, Pin-Hole Collimation and a Position-Sensitive Proportional Counter . . . . .	14
1.3	FUNDAMENTAL CERAMICS STUDIES . . . . .	15
1.3.1	Physical Structure of Coal . . . . .	15
1.3.2	Transmission Electron Microscope Observations of Porosity in Coal . . . . .	17
1.3.3	Optical and Electron Microscopy of Vapor-Deposited Silicon Carbide . . . . .	17
1.3.4	Small-Angle X-Ray Scattering Studies of Porosity in Pyrocarbons . . . . .	17

1.3.5	Structural Characterization of HTGR Pyrocarbon Fuel Particle Coatings . . . . .	18
1.3.6	Deformation of Ceramics . . . . .	18
1.3.6.1	Deformation of Ceramic-Metal Composites . . . . .	18
1.3.6.2	Erosion Processes in Ceramics . . . . .	18
1.3.7	Fission Product Compounds . . . . .	19
1.3.7.1	Compatibility of Fuel, Fission Products, and Construction Materials .	19
1.3.7.2	Fission Product Transport in Advanced Nuclear Fuels . . . . .	19
1.4	CRYSTAL PHYSICS . . . . .	20
1.4.1	Oxygen Partial Pressure Versus Phase Equilibria and Directional Solidification in the Cr-O-Mo System . . . . .	20
1.4.2	Directional Solidification by Internal Zone Melting of Cr <sub>2</sub> O <sub>3</sub> -Mo Eutectic Composites . . . . .	20
1.4.3	Mathematical Modeling of Internal Zone Growth . . . . .	21
1.4.4	The Growth of Large-Diameter UO <sub>2</sub> -W Composites. .	21
1.4.5	The Unidirectional Solidification of CeO <sub>2</sub> -Transition Metal Systems . . . . .	22
1.4.6	Directional Solidification of an LiF-20 mole % CaF <sub>2</sub> Eutectic Melt by the Edge-Defined, Film-Fed (EFG) Method . . . . .	23
1.4.7	Boundary Layer Model of Thin Film in the EFG Process . . . . .	23
1.4.8	Fabrication of a Large Autoclave for Growing Quartz Crystals for Acoustic Loss ( <i>Q</i> ) Measurements . . . . .	23
1.4.9	Single-Crystal Synthesis of Pure and Rare-Earth-Doped CaO by Mass Transport in Molten CaF <sub>2</sub> ·LiF Solvent . . . . .	24
1.4.10	Single-Crystal Growth of Monoclinic Eu <sub>2</sub> O <sub>3</sub> from Molten NaF Solvent . . . . .	24
1.4.11	Bridgman Growth of Several Pure and Actinide-Doped Halide Single Crystals . . . . .	25
1.4.12	Vibrational Spectra of Synthetic Single-Crystal Tephroite, Mn <sub>2</sub> SiO <sub>4</sub> . . . . .	25
1.4.13	Self-Luminescence of Several Curium-Doped Alkaline-Earth and Lanthanum Halides . . . . .	25

1.4.14	Electron Paramagnetic Resonance Investigations of Divalent $^{253}\text{Es}$ in $\text{SrCl}_2$ and $\text{BaF}_2$ . . . . .	26
2.	DEFORMATION AND MECHANICAL PROPERTIES . . . . .	27
2.1	THE PHASE TRANSFORMATION CHARACTERISTICS OF A URANIUM + 14 at. % NIOBIUM ALLOY . . . . .	27
2.2	AGING INDUCED SHAPE INSTABILITY IN AN ELASTICALLY BENT U-7.5 wt % Nb-2.5 wt % Zr ALLOY . . . . .	27
2.3	PRECIPITATION-HARDENED ALUMINUM FOR POSSIBLE APPLICATION AS STABILIZING COMPONENT IN SUPERCONDUCTING MAGNETS AND TRANSMISSION LINES . . . . .	28
2.4	ROLLING AND RECRYSTALLIZATION OF (110)[ $\bar{1}\bar{1}0$ ] TANTALUM SINGLE CRYSTALS . . . . .	29
2.5	THE EFFECTS OF ORIENTATION ON THE ROLLING AND RECRYSTALLIZATION BEHAVIOR OF TANTALUM SINGLE CRYSTALS .	29
2.6	METAL SURFACE DEFORMATION . . . . .	30
2.7	HYDROGEN ABSORPTION INDUCED DEFORMATION IN SINGLE- CRYSTAL NICKEL FOILS . . . . .	33
3.	PHYSICAL PROPERTIES AND TRANSPORT PHENOMENA	
3.1	MECHANISMS OF SURFACE AND SOLID STATE REACTIONS . . . . .	35
3.1.1	Reactions of Fe-Cr Alloys in Mixed-Gas Environments . . . . .	35
3.1.2	Ceramic-Metal Composites . . . . .	36
3.1.3	Diffusion in Vanadium-Titanium Alloys . . . . .	36
3.1.3.1	Interdiffusion and Intrinsic Diffusion in Binary Vanadium- Titanium Solid Solutions at 1350°C . .	36
3.1.3.2	Intrinsic Diffusion and Vacancy Flow Effects in Vanadium- Titanium Alloys from 900 to 1600°C . .	37
3.1.4	Anomalous Fast Diffusion Processes . . . . .	37
3.1.4.1	Solute and Solvent Diffusion for an Alloy in Dissociative Equilibrium . . .	38
3.1.5	Tritium Diffusion in Oxides. . . . .	38
3.1.6	Oxygen Diffusion in Niobium and Niobium- Zirconium Alloys . . . . .	38
3.1.7	Older Programs . . . . .	39
3.1.7.1	Interface Stability During the Oxidation of Binary Alloys . . . . .	39

3.1.7.2	Microstructures of the Scales Formed on Zircaloy-4 in Steam at Elevated Temperatures . . . . .	39
3.1.7.3	Sputter Sectioning of Diffusion Specimens . . . . .	41
3.1.7.4	Oxidation of Refractory Metal Alloys . . . . .	41
3.1.7.5	Gas-Solid Reactions for BCC Alloys. . . . .	41
3.2	PHYSICAL PROPERTIES RESEARCH . . . . .	42
3.2.1	Transport in Nonmetals . . . . .	42
3.2.1.1	Lattice Thermal Conductivities in Electrically Insulating Crystals . . . . .	42
3.2.1.2	Electrical Conductivities of Some Ferrite Crystals . . . . .	43
3.2.2	Physical Properties of Metals . . . . .	43
3.2.2.1	Analysis of Experimental Data . . . . .	43
3.2.2.2	Iron and Dilute Iron Alloys . . . . .	44
3.2.2.3	Niobium . . . . .	45
3.2.2.4	Specific Heat of Actinides . . . . .	46
3.2.3	Apparatus Development . . . . .	46
3.2.3.1	Thermal Expansion Apparatus . . . . .	46
3.2.3.2	CODAS Development . . . . .	47
3.3	SUPERCONDUCTING MATERIALS . . . . .	47
3.3.1	The Influence of Yttrium on the Superconducting Properties of Nb-Ti Alloys . . . . .	48
3.3.2	The Peak Effect in Superconducting Nb-Hf Alloys . . . . .	48
3.3.3	Direct Observation of the Flux Distribution in the Mixed State of V-Ga Alloys Using a Scanning Electron Microscope . . . . .	49
3.3.4	Bending of Flux Lines by Transport Currents in Type-II Superconductors Measured by Neutron Diffraction . . . . .	49
3.3.5	Magnetic History Effects and Wave-Form Asymmetry in ac Magnetization Measurements on Type-II Superconductors . . . . .	49
3.3.6	Tensile Properties of Superconducting Composite Conductors and Nb-Ti Alloys at 4.2 K . . . . .	50
3.3.7	Performance of Multifilamentary Nb <sub>3</sub> Sn Under Mechanical Load . . . . .	50

3.3.8	Thermomechanical Heat Generation in Copper and an Nb-Ti Superconducting Composite . . . . .	51
3.3.9	Inhomogeneities in Superconducting Niobium Surfaces . . . . .	51
3.3.10	Work in Progress - Advanced Superconducting Materials . . . . .	52
3.3.10.1	Superconductivity in $\text{LiTi}_2\text{O}_4$ . . . . .	52
3.3.10.2	Superconductivity in $\text{PbMo}_6\text{S}_8$ . . . . .	52
3.3.10.3	Superconductivity Properties of Sputter-Deposited $\text{Nb}_3\text{Al}$ and $\text{Nb}_3(\text{Al}_3\text{Ge})$ . . . . .	52
3.3.10.4	Microstructural Studies of Hard Superconductors . . . . .	52
4.	RADIATION EFFECTS . . . . .	55
4.1	EXPERIMENTAL STUDIES AND EVALUATIONS . . . . .	55
4.1.1	Neutron Experiments on Aluminum Alloys . . . . .	55
4.1.2	Direct Observation of Coated Voids . . . . .	56
4.1.3	Correlation of Neutron- and Nickel-Ion Damage in Pure Nickel . . . . .	57
4.1.4	Swelling Resistance in a Type 316 Stainless Steel . . . . .	59
4.1.5	Void Nucleation in Alloys . . . . .	60
4.1.6	Effect of Structural Inhomogeneity on the Swelling of Nickel Binary Alloys . . . . .	61
4.1.7	Tracing the Evolution of Bubbles in Helium-Injected Aluminum by Means of Positron Annihilation . . . . .	62
4.1.8	Low-Activation Materials for Fusion Reactors: Radiation Damage Considerations in Aluminum Alloys . . . . .	63
4.1.9	Simulation of Helium Effects: Introduction of Helium from Charged Particle Accelerators and Alpha Particle Sources . . . . .	64
4.2	THEORETICAL STUDIES . . . . .	65
4.2.1	Effect of a Surface Layer on Void Nucleation . . . . .	65
4.2.2	The Effect of Stress-Induced Diffusion on Void Nucleation . . . . .	67
4.2.3	Some Aspects of Void and Loop Nucleation and Growth in the Vicinity of a Finite Dislocation Loop . . . . .	68

4.2.4	Evolution of Dislocation Density and Dose Exponents of Void Growth . . . . .	69
4.2.5	Growth Kinetics of Frank Loops in Nickel during Electron Irradiation . . . . .	72
4.2.6	Transient and Steady-State Diffusion Solution for Point Defects in a Stress Field . . . . .	73
4.2.7	Diffusion of Point Defects to a Toroidal Sink in a Finite Medium . . . . .	73
4.2.8	Morphologies of Precipitates on Voids and Loops Resulting from Irradiation-Induced Segregation . . . . .	74
4.2.9	Distributions of Point Defects in Bounded Media Under Irradiation . . . . .	74
4.2.10	The Use of Pressurized Eccentric Tubes to Study the Effect of Hydrostatic Stress on Swelling . . . . .	75
4.3	FACILITY, EQUIPMENT, AND EXPERIMENT DEVELOPMENT . . . . .	78
4.3.1	The Simulation of Radiation-Enhanced Creep . . . . .	78
4.3.2	The Oak Ridge CN Van de Graaff Facility for Heavy Ion Radiation Damage Studies . . . . .	79
4.3.3	Experiments with the ORNL Heavy-Ion Bombardment Facility . . . . .	80
4.3.4	EBR-II Row 7 Irradiation Experiment . . . . .	81
4.3.4.1	Precipitation of Solute Elements During Irradiation . . . . .	82
4.3.4.2	Irradiation Creep Simulation . . . . .	82
4.3.4.3	Segregation of Solute Elements to Grain Boundaries . . . . .	83
4.3.4.4	Correlation of Neutron Damage with Ion Damage . . . . .	83
4.3.4.5	Swelling in Neutron Irradiated Pure Binary and Ternary Alloys . . . . .	83
4.3.4.6	Effect of Stress on Swelling . . . . .	84
4.3.4.7	Neutron-Induced Defect Characterization of Several BCC Metals and Alloys . . . . .	84
4.3.4.8	Atom-Probe, Field-Ion Microscope Investigation of Radiation Damage in Refractory Metal Alloys . . . . .	84
4.3.4.9	Status of Experiment . . . . .	85
4.3.5	Analytical Electron Microscopy . . . . .	85
4.3.6	High-Voltage Electron Microscopy . . . . .	86

APPENDIX . . . . .	87
1. STAFF ASSIGNMENTS . . . . .	87
2. GUEST ASSIGNMENTS . . . . .	87
3. STAFF CHANGES . . . . .	88
4. ORNL-UT JOINT APPOINTMENTS FOR ACADEMIC YEAR 1975-1976 . . . . .	88
5. PRESENTATIONS AT TECHNICAL MEETINGS . . . . .	89
6. PUBLICATIONS . . . . .	95
Publications Pending . . . . .	100
Patent . . . . .	102
Theses . . . . .	102
ORGANIZATION CHART . . . . .	103

## SUMMARY

### 1. STRUCTURE OF MATERIALS

#### 1.1 Theoretical Research

The constant-energy KKR band theory techniques originated by the Theory Group have been further developed and used to calculate the electron-phonon coupling constant for many metals. These results have been used to gain a deeper understanding of the conditions under which high superconducting transition temperatures,  $T_c$ , might be attained. Coupling these results with the newly developed Fermi surface harmonics made it possible to calculate gap anisotropy for niobium, and has led to a realistic theory for the upper critical field  $H_{c2}$  in hard superconductors. These band theory techniques have been extended to treat hcp metals, and the Fermi surface of technetium has been calculated for the first time.

The multiple-scattering cluster technique has been used to study the electronic states and orbitals on flat and stepped surfaces. From these studies general information about bonding on metal surfaces can be obtained, and in addition the bonding of oxygen on an aluminum surface has been analyzed in detail.

Our studies of electronic states in disordered systems have led to a model calculation for a one-dimensional "transition metal alloy" that can be used for a critique of the techniques presently being used in studies of real alloy systems. Our model calculations of the spectral density function of disordered solids  $A(\vec{k}, E)$  have been used for the same purpose, but they have also yielded new physical insights into this little-understood quantity and have allowed us to explain an experiment on an amorphous magnet carried out at this laboratory. Our CPA calculation on the palladium hydride system is the first realistic theory for electronic states in substoichiometric compounds.

We have developed a numerical technique to study the transient and stationary states of defect annealing and clustering for quenching, annealing, and irradiation situations.

#### 1.2 X-Ray Diffraction Research

Final phases of the instrumentation for the 10-m small-angle x-ray scattering spectrometer have been completed; experiments with such diverse specimens as neutron-irradiated metals, catalysts, collagen fibrils, and nu-bodies from chicken chromosomes have been carried out to test the capabilities of this machine. Performance to date meets or exceeds that expected by extrapolations from our experience with a smaller system. A technically useful characterization of pyrocarbon coatings for use on reactor fuel pellets has been achieved with results from small-angle x-ray scattering measurements.

Our predictions that weak space-group-forbidden x-ray reflections may arise in certain crystals because of anharmonic thermal vibrations or nonspherical electron distributions have been borne out by experiments with a  $V_3Si$  crystal. Since the important superconducting properties of such compounds must be related to the details of the thermal motion, we expect our measurements to contribute to our understanding of this phenomenon.

Applications of monochromatic x-ray sources to excite fluorescent x-rays in a sample of interest have (1) increased the sensitivity of fluorescence analysis for trace elements by several orders of magnitude, (2) enabled more precise quantitative interpretations of x-ray fluorescence data to be made, and (3) permitted us to find and study a Raman resonance scattering effect previously obscured by background noise.

The crystal structure of  $LiFe_3$  was described with the help of modulated three-dimensional structure ( $MS_3$ ) groups. This work would seem to be among the first applications of modulated symmetry theory to be approximate solutions of superstructures in which atom parameters are related in special ways not apparent from their space groups. Progress in selection and initial characterization of monoclinic europia crystals for structure analysis is reported.

### 1.3 Fundamental Ceramics Studies

Studies of vapor deposited coatings of pyrocarbon and silicon carbide have been completed. The size, shape, and distribution of porosity and minerals in coal has been investigated, and the initial results have been reported. Work has continued on the evaluation of fission product and reactor structural material compatibility, as well as on the preparation of large europium oxide single crystals for detailed study of the properties of this potential neutron absorber material. Studies have been initiated on fission product transport in advanced LMFBR fuels, on erosion of ceramics, and on the deformation of ceramic-metal fiber composites.

### 1.4 Crystal Physics

Indications are that  $P_{O_2}$  plays an extremely important role in control of metal oxide-metal eutectic solidification. Thermochemical data and oxidation-reduction experiments have permitted reasonable control of the Cr-O-Mo system. On the basis of predictions of the mathematical modeling of the internal zone growth technique, the sample diameter has been increased from 2 to 5 cm to avoid the severe instability of the induction-coupled power in samples of  $Cr_2O_3$ -Mo at certain combinations of controllable system parameters. As we scaled up the  $UO_2$ -W diameter from 2 to 3 cm it appears that for the first time, in this system, we are being troubled with a less severe instability effect. Nevertheless we achieved melts in 450-g ingots, obtained improved tungsten fiber continuity, and increased

size and length of cells. The search for coupled eutectic metal oxide-metal systems of intermediate temperatures (less than about 2000°C) was reinitiated. A few experiments indicate that  $\text{CaO}_2\text{-Ni}$  may be such a system.

The edge-defined, film-fed (EFG) method was used to directionally solidify the eutectic  $\text{LiF-20 mole \% CaF}_2$ . The purpose of these experiments is to find a well-behaved system as a model for gaining better understanding of the potential and limitations of the EFG process. As an example we have numerically solved the time-dependent mass-transfer problem for a binary liquid crystallizing to a eutectic structure under conditions imposed by the EFG process.

Fabrication of a new, larger hydrothermal autoclave is complete. It will have an internal diameter of 32 mm, compared with our present 22-mm bombs. This will permit the growth of quartz crystals (RbOH solution based) of sufficient size for direct measurement of acoustic loss ( $Q$ ) of fabricated oscillator plates.

Pure and rare-earth-doped  $\text{CaO}$  crystals have been grown by mass transport in molten  $\text{CaF}_2\cdot\text{LiF}$  solvent. This suggests that this technique will be applicable to preparation of actinide-doped  $\text{CaO}$  single crystals for electron paramagnetic resonance studies. Monoclinic  $\text{Eu}_2\text{O}_3$  crystals have been grown from molten  $\text{NaF}$  solvent. Needlelike crystals  $0.2 \times 0.2 \times 5$  mm with low Na and F solvent impurity content have been grown. Bridgman growth of  $\text{RbCaF}_3$ ,  $\text{LaBr}_3$ , and  $\text{CaBr}_2$  doped with  $^{244}\text{Cm}$  and  $\text{SrCl}_2$  doped with  $^{249}\text{Bk}$  has been successful. These crystals are being used for optical and luminescence studies. Raman, infrared, and visible absorption spectra of our crystals of  $\text{Mn}_2\text{SiO}_4$  have been measured. Self-luminescence of several curium-doped alkaline-earth and lanthanum halides has been studied and is being prepared for publication. An EPR investigation of  $^{253}\text{Es}^{2+}$  in  $\text{SrCl}_2$  and  $\text{BaF}_2$  has been published.

## 2. DEFORMATION AND MECHANICAL PROPERTIES

Shape instability in U-7.5 wt % Nb-2.5 wt % Zr alloy was explained on the basis of an interaction of aging mechanisms and preferred orientations caused by mechanical twinning. The martensitic transformation to monoclinic  $\alpha''$  in a monotectoid uranium-niobium alloy was observed to take place both athermally and isothermally. The precipitation process in aluminum-gold alloys and its effect on the residual resistivity ratio and microhardness were investigated. The effects of initial orientation on the deformation and recrystallization behavior of rolled tantalum single crystals were studied by optical and electron metallography, x-ray line broadening and pole figure analyses, and microhardness testing. Studies were initiated on the surface deformation that accompanies wear and erosion. Hydrogen embrittlement of nickel single crystals was studied by transmission electron microscopy.

### 3. PHYSICAL PROPERTIES AND TRANSPORT PHENOMENA

#### 3.1 Mechanisms of Surface and Solid-State Reactions

Ceramic-metal composites ( $\text{Cr}_2\text{O}_3\text{-Mo}$ ) resisted attack at  $1000^\circ\text{C}$  in a variety of  $\text{CO-CO}_2$  mixtures but reacted readily in sulfur-bearing atmospheres. We began a program to characterize the reactions of iron-chromium alloys in mixed-gas environments in terms of the properties of individual reaction products. Studies of interdiffusion processes in vanadium-titanium alloys between  $900$  and  $1600^\circ\text{C}$  were essentially completed, the results showing that the vacancy wind phenomenon influences intrinsic diffusion fluxes to a greater degree than theoretically predicted. Interstitial diffusion of oxygen in niobium was slowed significantly by the addition of 1 at. % Zr, presumably because of clustering of oxygen about the zirconium atoms. We initiated projects to investigate tritium diffusion in oxides and the mechanism of anomalous fast diffusion in metals; a theoretical treatment of certain aspects of the latter phenomenon was completed. Several older programs involving the oxidation of uranium-base and refractory metal alloys and the microstructure of oxide scales formed on Zircaloy were completed or are being phased out.

#### 3.2 Physical Properties Research

The thermal conductivity of polycrystalline CsCl, CsBr, and CsI was measured and compared with previous results on rubidium halides. The electrical conductivities of some single-crystal spinel ferrites were studied. Improved procedures to separate the Lorenz number and lattice conductivity values of metals were developed. Transport property measurements on iron and dilute iron alloys were completed and analyzed to show the behavior of the Lorenz number and the lattice thermal resistance of pure iron. The electrical resistivity and Seebeck coefficient of niobium were measured to  $1600$  K. The specific heats of  $^{241}\text{Am}$ ,  $\text{PuC}_{0.82}$ ,  $\text{PuC}_{0.90}$ ,  $\text{PuC}_{1.51}$ , and  $\text{Eu}_2\text{O}_3$  were measured. Computer-operated data acquisition systems were used for thermal expansion measurements, for a technique to obtain the thermal diffusivity and thermal conductivity of salt cores, and for temperature measurements on oxidizing zirconium samples.

#### 3.3 Superconducting Materials

The influence of metallurgical variables (precipitate and dislocation structure) on superconducting critical current density was studied in Nb-Ti alloys containing yttrium particles, and in Nb-Hf alloys (the Nb-Hf alloys exhibit dramatic peak effects). The fluxoid lattice was imaged in  $\text{V}_3\text{Ga}$  by a decoration technique and the use of scanning electron microscopy. Neutron diffraction was used to study the bending of flux lines

by transport currents in Nb-13% Ta alloys. Alternating current measurements on Nb-Ta samples revealed magnetic history effects, which are believed to be related to the defect structure of the fluxoid lattice.

The mechanical properties of superconducting composite conductors were determined at 4.2 K. The stress-induced degradation of critical current density was studied in multifilamentary Nb<sub>3</sub>Sn conductors. Plastic deformation and stress-strain hysteresis loops were found to be significant sources of heat generation in superconducting composites.

Inhomogeneities in niobium surfaces were found responsible for high values of upper critical field and strong flux pinning near the specimen surface.

Work in progress on the advanced superconductors LiTi<sub>2</sub>O<sub>4</sub>, PbMo<sub>6</sub>S<sub>8</sub>, Nb<sub>3</sub>Al, and Nb<sub>3</sub>(Al<sub>3</sub>Ge) is described.

#### 4. RADIATION EFFECTS

The Radiation Effects Program is concerned with understanding the effects of variations in composition and microstructure on swelling behavior and mechanical properties changes arising from elevated-temperature neutron irradiation. It complements and supports applied work sponsored by the LMFBR and fusion reactor programs by examining relatively simple systems and by conducting studies aimed at identifying mechanisms controlling damage.

During the past year swelling and postirradiation mechanical property measurements were completed on high-purity aluminum and a series of commercial aluminum alloys irradiated to exposures of up to 260 dpa in the High Flux Isotope Reactor. The 6061 alloy, which swelled a negligible amount and retained at least 10% elongation in tensile tests, showed the best performance of the group. Studies of small impurity additions to aluminum indicated that elements that caused large changes in lattice parameter reduced swelling. In highly irradiated commercially pure aluminum, spherical shells or coatings rich in silicon were found on the voids.

A correlation experiment designed to compare the temperature dependence of damage produced by neutron and nickel ion bombardment in nickel showed that the 3000-fold increase in damage rate in the ion bombardment experiment increased the temperature for peak swelling by about 200°C.

Ion bombardment was used to study the early stages of interstitial dislocation loop formation in high- and low-swelling stainless steels. Loops in the low-swelling steel appeared to be more stable and grew to larger sizes before unfauling. Silicon, the element responsible for the swelling resistance of the steel, was found to be segregated to the dislocation loops.

A series of two-phase aluminum, copper, and nickel alloys heat-treated to produce a variety of coherent and incoherent precipitate structures was irradiated to examine the effects of microstructure on

swelling behavior. In the case of copper alloys spherically symmetrical coherency strains retarded swelling, while strains of tetragonal symmetry suppressed it for 1-MeV electron exposures of up to 40 dpa.

Positron annihilation was shown to be a useful technique for monitoring the migration and precipitation of helium into bubbles in aluminum.

An evaluation of commercial aluminum alloys for fusion reactor first-wall applications indicated that swelling and ductility loss will preclude their use at temperatures above 473 K (200°C).

Techniques for implanting helium in metals for studying high-temperature embrittlement were reviewed and shown not to provide a complete simulation of the processes occurring during elevated-temperature neutron irradiation. The techniques were recommended for identifying mechanisms of embrittlement.

A theoretical investigation of formation of a thin layer of differing elastic properties surrounding a void as a result of solute segregation showed a significant change in the image interaction of self-interstitials with voids. It was concluded that the formation of a surface layer that provides an activation barrier for the interstitials is probably necessary for void nucleation, although a large dislocation bias or change in surface energy as a result of impurity contamination could provide the driving force. Other studies examined nucleation in the region of an existing interstitial dislocation loop. Void nucleation was shown to be more likely in the region above (or below) the plane of the loop. Dose exponents for swelling were evaluated for limiting cases for models that have been proposed and shown to depend on microstructure. Since several regimes may be traversed in a long-time irradiation, extrapolation of short-term results is questionable unless evolution of the microstructure is known. An evaluation of the growth of interstitial dislocation loops in nickel during electron irradiation indicated that the ratio of sink strength for interstitials to that for vacancies increased with increasing loop size. A numerical technique for describing diffusion of point defects in a stress field was developed and applied to small dislocation loops in quenched aluminum. An analytical solution was developed for diffusion of point defects to a toroidal sink in a finite medium. Calculations based on surface energy considerations were initiated to describe the morphologies of precipitate particles resulting from segregation of impurities to radiation-induced defects. Vacancy and interstitial profiles produced by ion bombardment were calculated for the temperature range where vacancies are mobile. Peak concentrations were broadened and displaced from the point of maximum generation rate. Calculation of the deflection of pressurized eccentric tubes during irradiation showed that the deflection can be used to evaluate the effect of a hydrostatic stress on swelling.

Progress on the development of the ORNL irradiation creep experiment and the CN Van de Graaff facility are reported along with a summary of heavy ion bombardments made during the year. A major experiment to be irradiated in a Row 7 position of EBR-II was designed and constructed. Experiments being conducted with DPR support are described. Developments in analytical and high-voltage electron microscopy facilities are reported.

## 1. STRUCTURE OF MATERIALS

### 1.1 THEORETICAL RESEARCH J. S. Faulkner

We have contributed to the development of models for point defect annealing and clustering in finite media, the Korringa-Kohn-Rostoker and discrete variational method approaches for calculating electronic states in ordered solids, the coherent-potential approximation for obtaining the electronic states in disordered solids, and cluster methods for treating a range of problems in the theory of surfaces and condensed matter. We are using these techniques to gain an understanding of the properties of technologically interesting materials in their normal states and after radiation damage.

#### 1.1.1 Electronic States of Substoichiometric Compounds and Application to Palladium Hydride<sup>1</sup> -- J. S. Faulkner

A theory for the electronic states of substoichiometric compounds based on the coherent-potential approximation is described. Extensive numerical calculations have been carried out on palladium hydride. These results and the applicability of the theory to this system and other systems will be discussed.

#### 1.1.2 A Band Theory Calculation of the Fermi Surface of Technetium<sup>2</sup> -- J. S. Faulkner

Although technetium has no stable isotopes, it has some interesting properties. For example, its transition temperature for superconductivity is the highest of any hcp metal. We have recently adapted a revised version of our KKR band theory programs to calculate the constant-energy surfaces of hcp materials without interpolation. This allows us to calculate the integrated density of states, the Fermi energy ( $E_F$ ), the density of states at  $E_F$ , and the Fermi surface topology in great detail. We will report such calculations for technetium.

---

<sup>1</sup>Abstract of *Phys. Rev.* B13: 2391-93 (1976).

<sup>2</sup>Abstract of a paper presented at the solid-state meeting of the American Physical Society, Atlanta, Georgia, March 29-April 1, 1976.

1.1.3 Defect Annealing and Clustering in the Elastic Interaction Force Field<sup>3</sup> - M. H. Yoo, W. H. Butler, and L. K. Mansur

The effective capture radius for recombination and the bias factors of Frank loops for point defects have been calculated by a numerical solution of the steady-state diffusion equation. Employing these results we have obtained from the general rate equations the steady-state diffusion profiles of vacancies and interstitials in bounded media, namely the half-space and the foil. Effects of spatial variation of defect production, thermal emission of vacancies, bias factors of sinks, and the image interaction of point defects with free surfaces on the defect diffusion profiles are described.

1.1.4 Numerical Solutions of the General Rate Equations for Point Defects and Defect Clusters - M. H. Yoo

Based on the rate theory model of the homogeneous nucleation and subsequent growth of defect clusters, a system of partial differential rate equations is formulated to account for point defect conservation and growth of defect clusters. Each of the total  $m + n$  equations for  $m$  types of mobile defects and  $n$  types of fixed internal sinks is divided into a number ( $l$ ) of equations for spatial positions (one dimension) by a procedure known as the method of lines. The total of  $(m + n) \times l$  rate equations, typically 100, are solved simultaneously by use of the stiff integrator package called GEAR-B. This numerical technique is used to study the transient and stationary states of defect annealing and clustering for quenching, annealing, and irradiation situations.

1.1.5 Bonding Properties of Stepped Transition Metal Surfaces<sup>4</sup> - G. S. Painter, R. O. Jones,<sup>5</sup> and P. J. Jennings<sup>6</sup>

Electronic structure calculations for small metallic clusters are analyzed to determine (1) how electrons are distributed spatially and

---

<sup>3</sup>Abstract of pp. 804-11 *Fundamental Aspects of Radiation Damage in Metals* (Proc. Int. Conf., Gatlinburg, Tenn., October 6-10, 1975) CONF-751006, Vol. 2.

<sup>4</sup>Abstract of a paper to be published in the Proceedings of the NBS Conference on the Electron Factor in Catalysis on Metals, Gaithersburg, Maryland, December 8-9, 1975.

<sup>5</sup>Institut für Festkörperforschung der Kernforschungsanlage, Jülich, West Germany.

<sup>6</sup>School of Physical Sciences, Murdoch University, Murdoch, Australia.

energetically in small crystallites and at surfaces, (2) how electrons respond to surface disorder (kinks, steps, reduced coordination number), and (3) how electronic characteristics are related to chemically active surface sites.

1.1.6 Electronic Structure of Stepped Transition Metal Surfaces<sup>7</sup> --  
G. S. Painter, P. J. Jennings<sup>6</sup> and R. O. Jones<sup>5</sup>

The multiple-scattering approach has been used to determine the electronic structure and orbital charge distributions for clusters of iron, nickel, and copper atoms in a simple stepped surface. The density of states at the Fermi energy is by far the largest in the case of iron, and the relatively inert copper is distinguished by the absence of pronounced charge lobes present at the step in the other elements. For all three elements, the stepped surface shows a variety of bonding orbitals not present on the flat surface.

1.1.7 Cluster Calculations of the Electronic Structure of Transition Metal Surfaces<sup>8</sup> -- R. O. Jones,<sup>5</sup> P. J. Jennings,<sup>6</sup> and G. S. Painter

The electronic structure and charge distributions for 13-atom clusters of  $3d$  transition metals (Fe, Ni, Cu) have been calculated by use of a scattered wave technique. The cluster geometry is chosen to display features of stepped and flat surfaces. Many states in the band show pronounced charge lobes in the neighborhood of edge and corner atoms, suggesting that these are active sites in these metals. These lobes are more extensive for lighter elements in the series and, for a given element, more diffuse at lower energies in the  $d$ -band. Charge expansion from the center of the cluster to the edge atoms is a general feature, and the stepped surfaces show a variety of bonding orbitals not present on the flat surface.

1.1.8 Oxygen Chemisorption on a Small Aluminum Cluster<sup>9</sup> -- J. Harris<sup>5</sup>  
and G. S. Painter

The chemisorption of oxygen on the (100) surface of aluminum is studied within the Hartree-Fock-Slater self-consistent field model with a multiple-scattering method. Good agreement is obtained with the

---

<sup>7</sup>Abstract of *J. Phys. C* 8: L199-L202 (1975).

<sup>8</sup>Abstract of *Surf. Sci.* 53: 409-28 (1975).

<sup>9</sup>Abstract of *Phys. Rev. Lett.* 36: 151-53 (1976).

spectral results of the jellium calculation of Lang and Williams when the oxygen-metal distance approaches their equilibrium separation. For adsorption at a hole site, we argue that the  $O(2p)$  resonance should be deeper in the band and broader than suggested by the jellium model.

1.1.9 A Surface Molecule Study of Oxygen Chemisorption on Aluminum<sup>2</sup> ---  
G. S. Painter and J. Harris<sup>5</sup>

The bonding of oxygen and a small cluster of aluminum atoms is studied within the Hartree-Fock-Slater self-consistent field model by a multiple-scattering technique. The electronic structure and local density of states calculated for several adsorbate-surface separations are compared with available experimental spectral data. The possibility of correlating theoretical and experimental results to ascertain stable bonding sites is discussed.

1.1.10 Electron Phonon Interaction in Cubic Systems: Application to Niobium<sup>10</sup> --- W. H. Butler, J. J. Olson,<sup>11</sup> J. S. Faulkner, and B. L. Gyorffy<sup>12</sup>

To a good approximation the electron-phonon coupling parameter,  $\lambda$ , which determines the superconducting transition temperature  $T_c$  and the electron-phonon mass enhancement, may be written as the product of two factors: one that depends upon the phonon frequencies  $(M\langle\omega^2\rangle)^{-1}$ , and a purely electronic factor,  $\eta$ . This latter quantity is determined by the band structure and the electron-phonon matrix elements. In this paper we develop a method of calculating  $\eta$  from first principles, making only the rigid muffin-tin approximation to describe the electron-phonon coupling. As an illustration we evaluate  $\eta$  for niobium and discuss the significance of the calculation with regard to the validity of describing the electron-phonon interaction in transition metals by the rigid muffin-tin approximation. We also attempt to isolate those features of the band structure that appear to have the strongest effect on  $T_c$ .

---

<sup>10</sup>Abstract of a paper submitted to the *Physical Review*.

<sup>11</sup>Present address, Physics Department, University of California at San Diego.

<sup>12</sup>H. H. Wills Physics Laboratory, Royal Fort, Bristol, U.K.

1.1.11 Gap Anisotropy and  $T_c$  Enhancement: General Theory and Calculation for Nb, Using Fermi Surface Harmonics<sup>13</sup> — W. H. Butler and P. B. Allen<sup>14</sup>

A general theory is given of the anisotropy of the energy gap and the resulting transition temperature ( $T_c$ ) enhancement of pure superconductors. The frequency dependence of the gap  $\Delta(k, \omega)$  is approximated by the two-square-well form of McMillan, but otherwise an exact algebraic solution of the strong-coupling Eliashberg equations is given, valid for arbitrarily large anisotropy. In the limit of weak anisotropy a simple perturbative formula is also derived. The method of solution relies on the use of expansion functions called Fermi surface harmonics (FSHs), which are velocity polynomials orthonormalized on the Fermi surface. Methods for explicit construction of these functions are described. As an application of these techniques the mass enhancement and gap anisotropy are calculated for niobium in an approximation that includes all electronic anisotropy but neglects the contribution to the anisotropy that arises from phonons. The rms gap anisotropy in this model is 6%, which is not inconsistent with most of the current experimental data. The resulting  $T_c$  enhancement is predicted to be 0.7% or 0.06 K.

1.1.12 Superconductivity in the Transition Metals<sup>2</sup> — W. H. Butler

We have calculated the electron-phonon mass enhancement and superconducting transition temperature,  $T_c$ , for eight cubic transition metals using the rigid muffin-tin approximation of Gaspari and Gyorffy, but including rigorously the effects of nonspherical energy bands. These calculations were made possible by the numerical efficiency of the KKR technique when operated in the constant-energy search mode. We find that the rigid muffin-tin approximation is quite adequate for obtaining a qualitative first-principles understanding of the variation of  $T_c$  in the transition metals, but the matrix elements should probably be reduced by screening effects. We find that processes in which the electron scatters from a  $d$  state to an  $f$  state are the primary contributors to the electron-phonon interaction in the transition metals.

1.1.13 A One-Dimensional Model for Transition Metals and Their Alloys<sup>10</sup> — W. H. Butler

We develop the one dimensional analogs of multiple scattering theory and KKR band theory. The muffin-tin CPA turns out to be quite simple in

---

<sup>13</sup>Abstract of a paper to appear in proceedings of the Second Rochester Conference on  $d$ - and  $f$ -band Superconductors (Rochester, New York, April 30, 1976).

<sup>14</sup>Department of Physics, State University of New York, Stony Brook.

one dimension when written in terms of the logarithmic derivatives of the radial Schrödinger equation. For transition metals we develop a one-dimensional model that includes the effects of hybridization and resonant scattering. Using this model we calculate the change in the density of states due to the addition of a single impurity. A number of surprising effects, which are outside the realm of tight-binding models and which seem to have three-dimensional analogs, are observed.

1.1.14 Exact Spectral Density Function for a One-Dimensional Model of an Amorphous Solid<sup>2</sup> - D. G. Hall<sup>15</sup>

The results of an exact machine calculation of the spectral density function  $A(q,\omega)$  for a one-dimensional model of an amorphous solid are presented. The model contains an adjustable short-range-order parameter, and  $A(q,\omega)$  is obtained for several values of that parameter. The calculated  $A(q,\omega)$  are discussed in a general way, and features such as broadening and the redistribution of states are shown as departures from the behavior of  $A(q,\omega)$  for the ordered system.

1.1.15 Spectral Density Functions for Amorphous Solids<sup>16</sup> - D. G. Hall<sup>15</sup> and J. S. Faulkner

The spectral density function  $A(\vec{Q},\omega)$ , proportional to the imaginary part of the single-particle Green's function  $G(\vec{Q},\omega)$ , is calculated exactly for a one-dimensional model of an amorphous solid. In addition to a Hamiltonian that describes electrons in the tight-binding approximation or spin waves, we also treat one that describes phonons. The insight gained from the model calculation is applied to recent neutron scattering results of Mook et al.

1.1.16 The Quasicrystalline Approximation: Comparison of the Spectral Density with Exact Results<sup>17</sup> - D. G. Hall<sup>15</sup>

The quasicrystalline approximation (QCA) for electronic excitations in a one-dimensional liquid metal is examined by comparing the spectral density  $A(k,E)$  to exact numerical results. The numerical method is briefly described, and the limitations of the QCA are indicated.

---

<sup>15</sup>Under appointment to the Graduate Laboratory Participation Program Administered by ORAU for ERDA.

<sup>16</sup>Abstract of a paper to be published in the Proceedings of the Conference on Neutron Scattering, Gatlinburg, Tenn., June 6-10, 1976.

<sup>17</sup>Abstract of a paper submitted to *Solid State Communications*.

1.1.17 The Effects of Short-Range Order on the Spectral Density Function for a One-Dimensional Amorphous Solid<sup>10</sup> — D. G. Hall<sup>15</sup> and J. S. Faulkner

The spectral density  $A(Q, E)$  is calculated exactly for a one-dimensional model of an amorphous solid. The model contains an adjustable short-range-order parameter  $\alpha$ , and  $A(Q, E)$  is calculated for several values of  $\alpha$ . The harmonic oscillator Hamiltonian appropriate to lattice vibrations and a tight-binding Hamiltonian describing in a simplified way either electrons or spin waves are studied for nearest neighbor interactions. The calculated spectral densities are compared with the recent neutron scattering measurements of Mook, Wakabayashi, and Pan.

1.1.18 Cluster Shape and Critical Exponents Near Percolation Threshold<sup>18</sup> — P. L. Leath<sup>19</sup>

The shape of the large, random clusters, occurring near percolation threshold  $c_0$ , is shown to be such that the mean cluster boundary-to-bulk ratio  $\langle b \rangle / \langle n \rangle$  gives  $c_0$ . A Monte Carlo calculation yields that the cluster size distribution is proportional to a Gaussian in  $b/n$ , which is independent of concentration and narrows to a delta function as  $n \rightarrow \infty$ ; the asymptotic behavior gives  $c_0$  and the critical exponents.

1.1.19 Cluster Size and Boundary Distribution Near Percolation Threshold<sup>10</sup> — P. L. Leath<sup>19</sup>

It is shown that the shape of the large, random clusters, near the critical percolation concentration  $c_0$ , is such that their mean boundary  $\langle b \rangle$  is proportional to their mean bulk  $\langle n \rangle$ , and this is illustrated by an argument that shows that the dimension of the boundary is the same as that of the bulk. The resulting ratio  $\langle b \rangle / \langle n \rangle$  is simply related to the critical concentration  $c_0$ . The detailed results of a Monte Carlo calculation, previously reported, are given for  $c < c_0$  on a simple, square lattice; they yield an empirical formula for the probability distribution  $P(n, b)$  for finding a cluster of size  $n$  and boundary  $b$  that is proportional to a Gaussian in  $b/n$ , which is independent of concentration and which narrows to a delta function at  $b/n = \alpha_0$ ,  $n \rightarrow \infty$ . The asymptotic behavior of the Gaussian form gives the critical exponents  $\beta = 0.19 \pm 0.16$  and  $\gamma = 2.34 \pm 0.3$ . It gives  $\alpha_0$  corresponding to the critical concentration  $c_0 = 0.587 \pm 0.14$ , in agreement with previous determinations.

---

<sup>18</sup>Abstract of a paper submitted to *Physical Review Letters*.

<sup>19</sup>Work carried out at ORNL while a summer guest. Permanent address, Department of Physics, Rutgers University, New Brunswick, N. J.

## 1.2 X-RAY DIFFRACTION RESEARCH — H. L. Yakel and Bernard Borie

The work accomplished by the X-Ray Diffraction Group in the past year was highlighted by the successful synthesis of components of the 10-m small-angle x-ray scattering spectrometer. Preliminary results from the instrument demonstrate the unique advantages of the combination of high-intensity x-ray source, two-dimensional position-sensitive detector, and dedicated on-line computer system. Advances in other areas of our program are also indicated among the following abstracts and brief descriptions of work in progress.

### 1.2.1 Raman Resonance Scattering of X Rays<sup>20</sup> — C. J. Sparks, Jr.

Though Raman resonance scattering of photons has been theoretically predicted and observed in the visible energy region, we recently reported the first observation of a Raman resonance-like scattering of x rays in the keV energy region.<sup>21</sup> These resonance-scattered x rays occur with increasing intensity as the energy of the incident x rays approaches an absorption edge of the target atom. The energy of the resonance-scattered x rays is less than the incident energy by an amount equal to the binding energy of the next electron shell above the shell nearest resonance. The intensity of the resonance-scattered x rays was independent of scattering angle. Comparison of the intensity of this inelastic resonance scattering with the real part of the anomalous dispersion corrections to the coherent atomic scattering factors for x rays showed the processes to be the same. The cross section is predicted by the  $\vec{p} \cdot \vec{A}$  term in second-order perturbation theory, a term previously neglected in inelastic x-ray scattering calculations.

Since this resonance scattering occurs when the electron is in a virtual state of excitation, this process provides for a new kind of x-ray spectroscopy in contrast to the usual observations made after the electron is photojected from the atom. Fine structure in our recent observation of the energy spectrum from this inelastic resonance scattering process gives information on the energy levels of the outer electron shells. This information is carried by higher energy x rays, permitting information to be obtained from the bulk rather than the near surface, as has been the usual case.

---

<sup>20</sup>Abstract of an invited paper presented at the Midwinter Solid State Research Conference on Deep Level Spectroscopy, University of California, Irvine, Jan. 12-16, 1976.

<sup>21</sup>C. J. Sparks, Jr., *Phys. Rev. Lett.* 33: 262-65 (1974).

1.2.2 Quantitative X-Ray Fluorescent Analysis Using Fundamental Parameters<sup>22</sup> -- C. J. Sparks, Jr.

A monochromatic source of x rays for sample excitation permits the use of pure elemental standards and relatively simple calculations to convert the measured fluorescent intensities to an absolute basis of weight per unit weight of sample. Only the mass absorption coefficients of the sample for the exciting and the fluorescent radiation need be determined. Besides the direct measurement of these absorption coefficients in the sample, we consider other techniques, which require fewer sample manipulations and measurements. These fundamental parameter methods permit quantitative analysis without recourse to the time-consuming process of preparing nearly identical standards.

1.2.3 X-Ray Monochromator Design for Synchrotron Radiation<sup>23</sup> --  
C. J. Sparks, Jr. and J. B. Hastings

The advantages of singly curved monochromators for use in the x-ray energy spectrum of synchrotron radiation has been generally overlooked. Several centimeters of horizontal beam divergence can be focused at the sample or the detector to increase the intensity on the samples and to improve both the spatial and energy resolution in some x-ray spectroscopy and scattering experiments. Design considerations for the optics of these monochromators and the advantage of their applications for certain experiments are given.

1.2.4 The Detection of Structurally Forbidden Bragg Maxima in V<sub>3</sub>Si --  
Bernard Borie

The detection of weak reflections forbidden by the space group in diamond, silicon, and germanium is common. They are caused by non-spherical electron distributions about the atomic nucleus and by the anharmonic character of the thermal motion. We have developed a general theory<sup>24</sup> to predict which of the forbidden reflections in other structures

---

<sup>22</sup>Invited review paper given at the 24th Annual Denver X-Ray Conference, Aug. 6-9, 1975. Published in *Advances in X-Ray Analysis*, Vol. 19, pp. 19-52, ed. by R. W. Gould et al., Kendall/Hunt, Dubuque, Iowa, 1976.

<sup>23</sup>Abstract of paper presented at the Second Annual Stanford Synchrotron Radiation Project Users Group Meeting, Stanford Linear Accelerator Center, Stanford, Calif., SSRP Report 75/11, Oct. 23-24, 1975.

<sup>24</sup>B. Borie, "Thermally Excited Forbidden Reflections," *Acta Cryst.* A30(Part 3): 337-41 (May 1974).

should be excited in this manner, and we have applied it to the A15 structure. Within the limiting sphere of Cu  $K\alpha$  radiation for  $V_3Si$  we predict the excitation of three such maxima:  $hkl \approx 410, 430, \text{ and } 531$ . We have undertaken a search for them.

We report the observation of very weak 410 and 430 reflections and confirmation that 322 (which shares a common Bragg angle with 410) remains absent. In our measurements we have taken care to avoid contributions due to surface contaminants and the Renninger effect. We expect shortly to search for 531.

The measurements have been made by use of an energy-sensitive solid-state detector, so that in addition to the coherently diffracted Cu  $K\alpha$  radiation we have simultaneously measured the V  $K\alpha$  fluorescent intensity. The ratio of these count rates will allow us to convert our data to absolute units by a novel and powerful new method (due to C. J. Sparks). Our experiment will constitute its first application.

Since the important superconducting properties of compounds with the A15 structure must be related to the details of the thermal motion, we expect our measurements to contribute to our understanding of this phenomenon.

#### 1.2.5 The Crystal Structure of Monoclinic Europia -- Harry L. Yakel

The structure of monoclinic samarium sesquioxide ( $B-Sm_2O_3$ ) was reported in 1957 by D. T. Cromer,<sup>25</sup> who studied a crystal grown by a flame-fusion technique.<sup>26</sup> A limited number of diffraction data were collected, they were not corrected for absorption, and the structure was solved by Patterson projections followed by Fourier and least squares refinements. An agreement factor of only 11% was achieved.

It is doubtlessly correct to assume that the structure of  $B-Eu_2O_3$  is isomorphous with that of  $B-Sm_2O_3$ . However, uncertainties regarding the relative stabilities of  $B-Eu_2O_3$  and cubic  $C-Eu_2O_3$ , and especially regarding the possible effects of impurities (e.g., hydroxyl ions) on the stability of either phase, suggest that a reexamination of the crystal structure(s) of europia grown under carefully controlled conditions would be useful. To this end, we have begun studies of monoclinic europia growth from  $NaF-Eu_2O_3$  melts on which a small thermal gradient has been imposed (Sect. 1.4.10 of this report). The resulting europia crystals contain no contaminants from the flux, and have been exposed only to atmospheres from which oxygen and water have been rigorously excluded.

Preliminary selection and x-ray diffraction characterization of the crystals have been completed. Usefully dimensioned perfect  $B-Eu_2O_3$

---

<sup>25</sup>D. T. Cromer, "The Crystal Structure of Monoclinic  $Sm_2O_3$ ," *J. Phys. Chem.* 61: 753--55 (1957).

<sup>26</sup>R. M. Douglass and E. Staritzky, "Samarium Sesquioxide,  $Sm_2O_3$ , Form B," *Anal. Chem.* 28: 552 (1956).

crystals occurred rather seldom; objects with the superficial qualities of acceptable crystals frequently comprised aggregates of crystals of similar orientation, each noticeably tipped about an average  $\vec{b}$  axis direction. Despite this difficulty, a small, perfect monoclinic europia crystal has been mounted inside a 0.1-mm-diam capillary in a helium-filled dry box. Since the capillary was sealed inside the box, this specimen has never been exposed to an oxygen- or water-containing environment. A second small, perfect B-Eu<sub>2</sub>O<sub>3</sub> crystal was removed from the dry box, mounted and examined in the normal laboratory atmosphere. Single-crystal x-ray diffraction data sets will be collected from both crystals; careful comparisons of the data themselves and of the crystal structures derived from them should serve to (1) refine and amend the earlier results of Cromer,<sup>25</sup> and (2) indicate the scope of any structural consequences of the differing histories of the two crystals.

1.2.6 Crystal Structure of LiTe<sub>3</sub><sup>27</sup> -- Diane Y. Valentine,<sup>28</sup> O. B. Cavin, and Harry L. Yakel

The crystal structure of LiTe<sub>3</sub> has been analyzed from x-ray and neutron powder diffraction data, and from photographically recorded x-ray single-crystal diffraction data. The proposed structure is based on harmonically related positional displacements of tellurium atoms from a reference structure whose rhombohedrally centered hexagonal unit cell has  $|\vec{A}| = 8.7144 \pm 0.0003 \text{ \AA}$  and  $|\vec{C}| = 5.3363 \pm 0.0002 \text{ \AA}$ . Displacements are in basal plane directions; the wave vector of the harmonic function describing them is parallel to  $\vec{C}$  and has a wavelength of  $4|\vec{C}|$  from  $-103^\circ\text{C}$  to  $150^\circ\text{C}$ . The unique axial ratio ( $\cong\sqrt{3}/8$ ) of the hexagonal cell of the reference structure is also maintained over this temperature range. While the actual structure must be classified as a superstructure, the symmetry relationships developed for modulated three-dimensional structure (MS<sub>3</sub>) groups are applicable to its derivation. The proposed displacements produce sections normal to  $\vec{C}$  in which segments of tellurium-like chains can be distinguished. These sections are separated by metal-like layers that occur as the displacements become small. Lithium atoms are regularly distributed in channels parallel to  $\vec{C}$ .

1.2.7 Recent Experimental Results from the ORNL 10-m Small-Angle X-Ray Scattering Spectrometer<sup>29</sup> -- R. W. Hendricks

The development of the ORNL 10-m small-angle x-ray scattering spectrometer, which uses a two-dimensional position-sensitive proportional

---

<sup>27</sup>Abstract of paper to be submitted to *Acta Crystallographica*.

<sup>28</sup>Chemistry Division.

<sup>29</sup>Abstract of paper to be presented at Small-Angle Scattering Symposium Summer Meeting, American Crystallographic Association, Evanston, Ill., Aug. 8-12, 1976.

counter, was described at the Clemson (winter 1976) ACA meeting. Since then the machine has been tested with a wide variety of scattering specimens. Among these are (1) neutron-irradiated aluminum, molybdenum, and nickel containing voids, (2) collagen fibrils, (3) nu-bodies extracted from chicken nucleii, and (4) a commercial hydrotreating catalyst. In this paper, we describe the operating characteristics of the spectrometer as determined by incident beam flux, slit-edge parasitic scattering, electronic noise, system deadtime, and data handling procedures. The results will be compared with similar performance characteristics of the Kratky camera and our 2-m spectrometer with a one-dimensional position-sensitive detector.

1.2.8 Report of the IUCr Commission on Crystallographic Apparatus International Project for the Calibration of Absolute Intensities in Small-Angle X-Ray Scattering<sup>29</sup> -- L. B. Shaffer<sup>30</sup> and R. W. Hendricks

As a result of informal discussions held at the Second International Conference on Small-Angle Scattering of X-Rays in Graz, Austria (1970), a project to test the reproducibility and comparative accuracy of the various absolute intensity calibration techniques in current use was organized. The proposal was accepted as an official project of the Commission on Crystallographic Apparatus of the International Union of Crystallography. In the project, the absolute differential x-ray scattering cross sections of standard samples of glassy carbon and polystyrene were calibrated in eight different laboratories using five different calibration techniques and two different x-ray wavelengths. The results have been intercompared by use of a variety of statistical techniques. It is concluded that angularly dependent errors associated with determining the zero of angle, dead-time corrections, and collimation corrections are more important in accounting for discrepancies between laboratories than are differences in the absolute intensity calibration methods themselves.

1.2.9 Application of SAXS for Characterization of Pyrocarbon Coatings<sup>29</sup> -- P. Krautwasser<sup>31</sup> and R. W. Hendricks

Small-angle x-ray scattering measurements proved to provide a very sensitive method for the characterization of pyrocarbon coatings deposited on nuclear fuel kernels. The size distribution of voids up to 1000 Å

---

<sup>30</sup>Anderson College, Anderson, Indiana 46011.

<sup>31</sup>Institut für Reaktorwerkstoffe, Kernforschungsanlage Jülich, 517 Jülich, BRD, on assignment to ORNL.

in diameter depends strongly on the deposition conditions of the coatings. As determined by transmission electron microscopy, a variation of these conditions leads to different microstructures, which can be distinguished by their typical pore size distributions. The evaluation of the pore spectra rather than the total porosity is therefore needed. This also allows the investigation of the influence of the different pore sizes on other material properties. The total porosity of the pyrocarbons is almost entirely due to pores smaller than 25 Å, whereas the resistance to oxidation is influenced by the concentration of pores of about 50 Å in diameter. The strength of pyrocarbon coatings depends strongly on the number of pores in the size range of 200 to 1000 Å. The influence of the variation of the deposition parameters on material properties can therefore be predicted by SAXS measurements, or conversely, these measurements can be used to control the deposition condition of pyrocarbon coatings. In this contribution we will demonstrate correlations between the pore size distribution determined by SAXS and deposition conditions, immersion density, oxidation rate, and fracture strength in various pyrocarbons.

1.2.10 Studies of Catalysts: Cobalt Molybdate<sup>29</sup> -- J. S. Lin, E. L. Fuller, Jr.,<sup>28</sup> and R. W. Hendricks

A commercial hydrotreating catalyst consisting of 3% cobalt oxide and 9% molybdenum oxide supported on approximately 80-Å-diam silica-promoted alumina crystallites (Harshaw CoMo 401 T) has proven to be useful in a wide variety of processes, including the synthetic production of fuels. As a part of an ongoing program of catalyst research, we are investigating the structure and surface properties of this material under a variety of conditions with gas adsorption, transmission electron microscopy (TEM), and small-angle x-ray scattering in an attempt to correlate these properties with catalytic activity. We have varied the chemical composition, crystallite sizes, and pore structure by chemical treatment (hydration and oxidation reduction) and heat treatment (isochronal annealing to 1000°C). The pore size distributions and surface areas have been determined as a function of specimen treatment in the ORNL 10-m small-angle x-ray scattering spectrometer, which uses a two-dimensional position-sensitive proportional counter. The correlation of these studies with the gas adsorption and TEM results will be reported. Additionally, the inhomogeneity of the as-received material has been examined by determining the small-angle scattering patterns from different sections of the pellets.

1.2.11 A Study of the Structure of Collagen Fibrils by Small-Angle X-Ray Scattering<sup>29</sup> -- R. H. Stinson,<sup>32</sup> T. Kurg,<sup>32</sup> and R. W. Hendricks

Phasing problems have prevented a satisfactory determination of the one-dimensional electron density distribution along the 680-Å unit cell

---

<sup>32</sup>Department of Physics, University of Guelph, Guelph, Ontario N1G 2W1.

of native tendon collagen. A method of solution is presented in which improved intensities of reflections were measured on the ORNL 10-m small-angle x-ray scattering spectrometer, which uses a two-dimensional position-sensitive proportional counter. Heavy metal compounds, including phosphotungstic acid and uranyl acetate, were used for phase determination. The heavy metal stains were located from electron micrographs. The locations are in agreement with those determined from difference Patterson maps. The resulting electron density distribution will be compared with that predicted by various models of the fibril assembly.

1.2.12 X-Ray Excitation of Surface Plasmons on Spherical Voids in Metals<sup>33</sup> - T. L. Ferrell,<sup>34,35</sup> J. C. Ashley,<sup>34</sup> and R. W. Hendricks

The cross section for x-ray excitation of surface plasmons on a spherical void in an electron gas is derived by use of the hydrodynamical approximation. The result is compared with the cross sections for elastic scattering from the void and other inelastic processes, such as scattering from bulk plasmons, in order to provide information on the feasibility of detecting such surface plasmon excitations experimentally. Possible applications to the study of the mechanisms of void nucleation and growth are discussed.

1.2.13 A New Small-Angle X-Ray Scattering Facility Utilizing a Rotating Anode, Pin-Hole Collimation and a Position-Sensitive Proportional Counter<sup>36</sup> - J. Schelten<sup>37</sup> and R. W. Hendricks

A new small-angle x-ray scattering facility that uses a 6-kW rotating anode, pin-hole collimation, and a position-sensitive proportional counter was developed. As presently constructed, the minimum scattering vector  $\kappa (= 4\pi \sin \theta/\lambda)$  that can be reached with Cu K $\alpha$  radiation is  $5 \times 10^{-3}/\text{\AA}$ . Under these conditions the flux incident on the specimen has been found to be  $6 \times 10^5$  photons/sec. The system has several advantages compared with traditional long-slit geometries; namely, (1) it can quantitatively measure anisotropic scattering distributions, (2) it avoids large mathematical corrections of the data for slit-smearing effects, and

---

<sup>33</sup>Abstract of paper to be published in *Philosophical Magazine*.

<sup>34</sup>Health Physics Division.

<sup>35</sup>Permanent address: Physics Department, Appalachian State University, Boone, N.C. 28608.

<sup>36</sup>Abstracted from *J. Appl. Cryst.* 8: 421-29 (1975).

<sup>37</sup>On research assignment from Institut für Festkörperforschung der Kernforschungsanlage, D517 Jülich, West Germany.

(3) it minimizes double Bragg scattering in crystalline materials and multiple diffuse scattering in amorphous or liquid materials. To illustrate the performance of this instrument, the scattering curves obtained from four widely different samples are shown. These are: polyethylene, a neutron-irradiated aluminum single crystal containing voids, a dilute suspension of Ludox spheres, and duck tendon collagen. Quantitative comparisons of the performance with a Kratky camera and with the neutron small-angle scattering facility in Jülich are given.

### 1.3 FUNDAMENTAL CERAMICS STUDIES -- C. S. Yust

The objectives of this program are the investigation and elucidation of the fundamentals of high-temperature phenomena in ceramic solids. The topics of immediate interest are the deformation of ceramic systems, erosion processes in refractory oxides, and the stability of ceramic phases at high temperature. In addition, the types, sizes, and distribution of the microconstituents in coal are being studied by transmission electron and optical microscopy and small-angle x-ray scattering. Fission product distribution and compound stability in advanced nuclear fuels are studied.

#### 1.3.1 Physical Structure of Coal -- C. S. Yust and L. A. Harris

Studies of the physical structure of coal have been started in order to increase the understanding of its physical and chemical nature and the relationship of its nature to coal processing parameters. Several metallurgical techniques have been adapted to determine the microstructure of the exinite and inertinite regions of an Eastern Kentucky bituminous coal. The size and distribution of porosity give information about the internal surface area and permeability related to the kinetics of conversion processes. The size, shape, hardness, and composition of mineral inclusions may influence the erosion processes, catalyst fouling, and removal of entrained solids in the gas or liquid produced.

Pores in the exinite (a region relatively high in hydrogen content) have the unusual shapes shown in Fig. 1.1. The colloidal-size particles (250 Å diam) contain no element heavier than sodium (lower limit of detection) except calcium. An electron diffraction pattern obtained with a 15-Å beam is being analyzed to identify the calcium compound. These pores and particles strongly suggest a naturally occurring catalyzed reaction. We are trying to define the composition of any gas in the pore.

The inertinite (a constituent relatively high in carbon) is very granular, upper right of Fig. 1.1, and contains much larger pores than would be deduced from gas absorption techniques.

An example of a mineral inclusion is shown in Fig. 1.2. This particle is about 2 μm on a side, contains many sharp angular corners, and is much harder than the matrix. It consists of titanium, iron, and silicon. Other minerals have been identified as quartz particles intimately mixed with the exinite and inertinite and particles rich in aluminum and silicon.



Fig. 1.1. Transmission Electron Micrograph of Exinite Region of a High-Volatile Bituminous Coal. Colloidal particles are associated with each large ( $\sim 0.5 \mu\text{m}$ ) pore. 60,000 $\times$ .



Fig. 1.2. Scanning Transmission Electron Micrograph of Mineral Inclusion in Inertinite. This particle contains titanium and lesser amounts of iron and silicon. 20,000 $\times$ .

1.3.2 Transmission Electron Microscope Observations of Porosity in Coal<sup>38</sup> - L. A. Harris and C. S. Yust

Samples of a high-volatile bituminous coal (HVab) were examined by transmission in a high-voltage electron microscope (1 MeV). The porosity observed within the exinite and inertinite constituents of this coal falls primarily into the mesopore size range (20 to 500 Å). Small particles (~250 Å diam) were seen in most of the exinite pores and are believed to have catalyzed the pore formation.

1.3.3 Optical and Electron Microscopy of Vapor-Deposited Silicon Carbide<sup>39</sup> - C. S. Yust and V. J. Tennery

The coatings on HTGR fuel particles include a layer of silicon carbide formed by the thermal decomposition of methyltrichlorosilane in a fluidized bed. The silicon carbide layer serves as a diffusion barrier for solid fission products. The microstructure of the coating is therefore of particular interest and was studied by optical and electron microscopy. The coatings consist of columnar grains, radially aligned. Optical transmission studies revealed regions of optical anisotropy, although the coating is almost entirely composed of cubic  $\beta$ -silicon carbide. Transmission electron microscopy reveals a large degree of faulting on {111} planes and extensive partial dislocation formation on the fault planes. Annealing lowered the dislocation content of the coatings but did not vary the fault plane density significantly. The microstructure of the silicon carbide coatings formed on the spherical fuel particles was more heavily faulted than those that had been deposited on flat disks by other investigators.

1.3.4 Small-Angle X-Ray Scattering Studies of Porosity in Pyrocarbons - H. P. Krautwasser<sup>40</sup>

The size distribution of voids in pyrocarbons was determined from SAXS and correlated with the deposition conditions and with behavior during deformation and irradiation. The pore size spectrum influences specific properties, in contrast to the belief that total porosity is the most significant factor. The total porosity is determined by pores smaller than 25 Å; resistance to oxidation is influenced by pores about 50 Å diam; strength depends on the number of pores having diameters of 200 to 1000 Å.

---

<sup>38</sup>Abstracted from *Fuel* 55(3): 233-36 (July 1976).

<sup>39</sup>Abstract of a paper to be submitted to the *Journal of the American Ceramic Society*.

<sup>40</sup>On assignment from KFA, Jülich, to ORNL.

### 1.3.5 Structural Characterization of HTGR Pyrocarbon Fuel Particle Coatings<sup>39</sup> – V. J. Tennery, C. S. Yust, H. P. Krautwasser,<sup>40</sup> and R. L. Beatty

The combined use of three characterization techniques to assess the irradiation stability of propylene-derived pyrocarbon has provided an improved understanding of its structural properties, which are important to the mechanical integrity of the pyrocarbon during exposure to fast neutrons. The characterization techniques include oxygen plasma etching, small-angle x-ray scattering, and transmission electron microscopy. The results obtained by applying these methods to a set of pyrocarbon coatings that were subsequently irradiation tested in the High Flux Isotope Reactor are compared. The characterization clearly shows that in these pyrocarbons the microstructure associated with mechanical stability at high fast neutron fluences has spheroidal growth features ranging in size from less than 0.1  $\mu\text{m}$  to about 1  $\mu\text{m}$  and a relatively homogeneous distribution of a fine fibrous carbon around the larger growth features. The characterization techniques each provide portions of the microstructural data needed for assessing a given pyrocarbon material.

### 1.3.6 Deformation of Ceramics

#### 1.3.6.1 Deformation of Ceramic-Metal Composites – C. S. Yust

A study of the deformation characteristics of metal-fiber-reinforced ceramic-matrix composites is in progress. The initial stages of this study involve the development of specimen preparation techniques for both mechanical testing and transmission electron microscope study of the deformed samples. Samples of a composite consisting of molybdenum fibers in a chromia matrix have been thinned successfully by ion etching. Preliminary examination of the microstructure of this composite system shows very little evidence of grown-in dislocation content. Chemical microanalysis by x-ray fluorescence in the electron beam suggests that some chromium may be dissolved in the molybdenum fibers.

#### 1.3.6.2 Erosion Processes in Ceramics – C. S. Yust

A study of erosion in ceramics has begun. The objective is a more complete understanding of subsurface damage mechanisms in well-defined ceramic systems that approximate commercial refractory compositions. Erosion damage will be simulated by single point indentation tests, by surface scratch and abrasion tests, and by bombardment of test surfaces with a variety of particles. The influence of such parameters as temperature, atmosphere, composition, and microstructure will be explored. Presently, preparation of samples is in progress in the system  $\text{Al}_2\text{O}_3\text{-SiO}_2$ . Quantitative electron microscopy techniques (TEM and STEM) will be used to characterize the response to erosion and wear.

### 1.3.7 Fission Product Compounds

#### 1.3.7.1 Compatibility of Fuel, Fission Products, and Construction Materials -- J. Brynestad and S. L. Bennett

Tellurium is a fission product and causes intergranular embrittlement in some transition-metal base construction materials in nuclear reactors. The stabilities of selected transition metal tellurides are being determined by measuring vapor pressure by the Knudsen effusion weight-loss technique with a recording vacuum thermobalance. The experimental study of the Ni-Ni<sub>3</sub>Te<sub>2-x</sub> system has just been completed. Independent mass-spectrometric experiments showed that the gaseous species in this system are monomeric and dimeric tellurium. Since the nickel telluride dissociation and the dissociation equilibrium  $\text{Te}_2(g) \rightleftharpoons 2\text{Te}(g)$  must be simultaneously satisfied, the partial pressure of Te<sub>2</sub> (or Te) can be related to the experimentally measured rate of mass loss as well as to the temperature, the effective orifice area, and the equilibrium constant for the above reaction. Several experiments were performed over the temperature region 800-1000°C with effective orifice areas varying by a factor of 20. There were no changes, within experimental error, in the derived Te<sub>2</sub> (or Te) partial pressures, demonstrating that equilibrium had been achieved within the Knudsen cells. The composition of the Ni<sub>3</sub>Te<sub>2-x</sub>/Ni<sub>3</sub>Te<sub>2-x</sub> + Ni phase boundary over this temperature range was found to be Ni<sub>3</sub>Te<sub>1.77</sub> ± 0.02. Values of  $S_{298}^\circ$ ,  $H_T^\circ - H_{298}^\circ$  and  $S_T^\circ - S_{298}^\circ$  have been estimated for Ni<sub>3</sub>Te<sub>1.77</sub>. The third-law  $\Delta H_{298}^\circ$  for the decomposition of this phase into Ni and Te<sub>2</sub>, based on these estimates and the experimental Te<sub>2</sub> pressures, is in good agreement with  $\Delta H_{298}^\circ$  derived from the second law treatment.

#### 1.3.7.2 Fission Product Transport in Advanced Nuclear Fuels -- R. L. Beatty

Studies at ORNL have been concerned with the structure and properties of unirradiated advanced nuclear fuels as well as the stability and migration of impurities (e.g., fission products). One question that arises when such studies are used to predict in-service behavior is the extent to which equilibrium thermodynamics can be used in the dynamic system. The Swiss Federal Institute for Reactor Research has irradiated several carbide fuels under well documented conditions. We have accepted their offer for a staff exchange to compare predicted behavior with experiment. Problems under investigation based on the final fission product distribution are the thermal, microstructural, and compositional effects on diffusional and vapor transport rates, and the chemically stable forms of the various fission products.

#### 1.4 CRYSTAL PHYSICS -- G. W. Clark

The growth of crystals of refractory materials is our central theme. Frequently very specific crystals (composition, phase, purity, perfection, size, etc.) are required to characterize physical properties uniquely or are required in technical devices for their optimum operation. Such suitable crystals are often difficult to obtain; hence, we conduct a continuing program to devise and improve methods of crystal growth, to develop increased understanding of crystal growth processes and kinetics, and to provide crystals needed in research. Crystals are grown by several methods: by internal zone growth, by temperature-gradient zone melting, from molten-salt solvents, from supercritical aqueous systems, by edge-defined film-fed growth, and by the Verneuil method. During this report period, our crystals were shared for investigating electron spin resonance, optical and elastic properties, deformation, diffusion, field emission, and electronic oscillator quality. We are investigating selected physical properties, both those related to the crystal growth process and those important for characterizing new compounds and eutectic structures. Of specific consideration is the use of metal oxide-metal eutectic composites as MHD electrode material and turbine components.

##### 1.4.1 Oxygen Partial Pressure Versus Phase Equilibria and Directional Solidification in the Cr-O-Mo System -- J. D. Holder and G. W. Clark

Oxygen partial pressure,  $P_{O_2}$ , for solid-liquid phase equilibria of  $Cr_2O_3$ ,  $Cr_2O_3$ -Cr eutectic, and  $Cr_2O_3$ -Mo eutectic has been estimated from (1) available thermomechanical data on the  $Cr_2O_3$ -Cr- $O_2$  equilibria, (2)  $Cr_2O_3$  oxidation and reduction experiments, and (3) Mo oxidation and reduction experiments. The solubility of refractory metals in oxides as a function of dissolved oxygen and  $P_{O_2}$  is also suggested from recent experiments conducted elsewhere. All indications are that  $P_{O_2}$  plays an extremely important role in the oxide-metal eutectic solidification by controlling phase volume ratios, growth rate limitations, and liquid superheat requirements.

Gas mixing and  $P_{O_2}$  monitoring equipment is presently being built and tested. Initial experiments will involve a study of phase equilibria as a function of temperature and  $P_{O_2}$  at near-eutectic compositions. Later experiments will be constructed to test directional solidification versus  $P_{O_2}$  in this system.

##### 1.4.2 Directional Solidification by Internal Zone Melting of $Cr_2O_3$ -Mo Eutectic Composites -- J. D. Holder and G. W. Clark

The study of the internal zone melting and directional solidification of  $Cr_2O_3$ -Mo is continuing. Scale-up of sample diameter from 2 to 5 cm has

been successful as predicted by the mathematical modeling of IZG by Hartzell and Sekerka.<sup>41</sup> The concept of internal susceptors has been developed and was instrumental in scale-up. A zone approximately 2 cm long has been moved through a 5-cm length of a hot-pressed mixture of Cr<sub>2</sub>O<sub>3</sub> and Mo powders (Cr<sub>2</sub>O<sub>3</sub>-20 mole % Mo). Our present effort is to perfect crystal quality for mechanical and physical property determinations. Control of electrical conductivity by metal or cation doping has been demonstrated and should prove valuable for further scale-up attempts.

#### 1.4.3 Mathematical Modeling of Internal Zone Growth -- R. A. Hartzell,<sup>41</sup> R. F. Sekerka,<sup>41</sup> J. D. Holder, and G. W. Clark

A collaboration between persons of the Department of Metallurgy and Materials Science, Carnegie-Mellon University and this group at ORNL, which was made more formal by ERDA subcontract support in late 1973, has been most fruitful. The intent was to develop a mathematical model of the internal zone growth technique and then utilize the predictive capacities of this model to improve our present internal zone growth system and to extend the use of this technique to a more general method of solidification. The complexity of this model describing induction coupling and heat transport in metal oxide-metal systems evolves through the facts that the electrical conductivity of the system is a strong function of temperature and that electrical conductivity appears as a parameter in both equations. Thus, the induction coupling and heat transport equations are coupled.

The first exciting prediction of the model was the probable existence of a coupled power or sample temperature instability associated with other controllable system parameters. At the same time we were being stopped by erratic experimental system behavior that we did not recognize as an instability.

As the model has been refined and our laboratory experience matured, it appears that we will be able to predictably skirt along the edge of the instability to reach our goal of directionally solidifying many complex eutectic systems.

The modeling continues to support the conviction that there are many, many opportunities yet untouched for using this general technique of internal zone growth.

#### 1.4.4 The Growth of Large-Diameter UO<sub>2</sub>-W Composites -- A. T. Chapman<sup>42</sup> and G. W. Clark

Last year we reported the successful growth of large UO<sub>2</sub> single crystals using the internal centrifugal zone growth technique with ingots

---

<sup>41</sup>Department of Metallurgy and Materials Science, Carnegie-Mellon University. Work supported by ERDA subcontract.

<sup>42</sup>Consultant from the School of Ceramic Engineering, Georgia Institute of Technology.

up to 25 mm in diameter. Efforts to make similar size increases for the  $\text{UO}_2\text{-W}$  composite structures met with difficulty because of the inability to achieve well-sintered and densified ingots before internal melting. We found it necessary to presinter the  $\text{UO}_2\text{-W}$  samples in controlled  $P_{\text{O}_2}$  to produce the needed sample characteristics. Using  $\text{UO}_2\text{-W}$  ingots weighing approximately 450 g and up to 30 mm in diameter, we have successfully internally melted these samples using a 10-kW induction generator operating at 3.5 MHz. The resultant eutectic structures showed major increases in the length and size of the cells and, consequently, improved tungsten fiber continuity compared with the smaller (approximately 20-mm-diam) ingots. In the large ingots the longitudinal heat losses, especially at the upper end, appear to be sufficient to distort the desirable flat liquid-solid interface across the internal molten zone. The possibility of decreasing the induction frequency used during solidification and/or providing insulation to better control end heat losses are under consideration.

#### 1.4.5 The Unidirectional Solidification of $\text{CeO}_2$ -Transition Metal Systems — A. T. Chapman<sup>42</sup> and G. W. Clark

During the last seven years, the growth of refractory metal oxide-metal eutectic structures has been achieved in a variety of systems. Almost all systems exhibiting aligned structures consist of oxide and metal combinations that have eutectic temperatures well above 2000°C. Efforts to extend this technology to include transition metals (i.e., Ni, Cr, Fe, Co) have been unsuccessful. Analysis of the high-temperature metal oxide-metal systems displaying eutectic structures suggests that oxide stoichiometry is perhaps the most important parameter affecting the solubility of the metal in the molten oxide. Consequently, a solidification study was initiated in the  $\text{CeO}_2$ -transition metal system. Ceria was selected as the host oxide because of its comparatively low melting point and its large variations in O/Ce ratios that may be controlled by use of  $\text{CO}_2\text{-CO}$  and  $\text{H}_2\text{O-H}_2$  gas mixtures. The direct internal zone melting of  $\text{CeO}_2\text{-x-Ni}$  samples produced some interesting microstructures. Starting with  $\text{CeO}_2\text{-15 wt % NiO}$  samples melted in a reducing atmosphere spherical  $\text{CeO}_2$  grains surrounded by a continuous layer of nickel metal could be produced when the molten zone was rapidly translated through the sample. Using much slower (approximately 3 cm/hr) solidification rates produced primarily isolated droplets of nickel metal in the  $\text{CeO}_2$  matrix, but in some areas partially aligned short nickel platelets were present. These results suggest that the growth of aligned eutectic structures in the  $\text{CeO}_2$ -transition metal systems is feasible, and experimental work is continuing.

1.4.6 Directional Solidification of an LiF-20 mole % CaF<sub>2</sub> Eutectic Melt by the Edge-Defined, Film-Fed (EFG) Method - J. D. Holder, C. B. Finch, and G. W. Clark

The EFG method was used to solidify cylindrical samples (5 mm diam by 3 cm) of a lamellar LiF-20 mole % CaF<sub>2</sub> eutectic. The experiments were conducted in argon at 800 to 850°C, using a platinum crucible and nickel die. Wettability of the die was improved by introduction of small amounts of oxygen into the system, an effect possibly related to the formation of a NiO film on the die surface. Melts of eutectic and LiF-rich (18 mole % CaF<sub>2</sub>) compositions were successfully solidified at rates between 3 and 40 mm/hr, and the resulting microstructures were analyzed with an eye to gaining a better understanding of the potential and limitations of the EFG process.

1.4.7 Boundary Layer Model of Thin Film in the EFG Process - J. D. Holder, C. B. Finch, and G. W. Clark

A numerical solution to the time-dependent mass transfer problem for a binary liquid crystallizing to a eutectic structure under the conditions imposed by the edge-defined film-fed growth process was developed. The results predict shorter transient periods to steady state in EFG than in typical Bridgman or zone melting directional solidification techniques. An increased sensitivity to growth rate perturbations is also predicted as the film thickness decreases. We are presently seeking an experimental model system to verify our predictions.

1.4.8 Fabrication of a Large Autoclave for Growing Quartz Crystals for Acoustic Loss ( $Q$ ) Measurements - O. C. Kopp<sup>43</sup> and G. W. Clark

Fabrication of a new, larger hydrothermal autoclave based on a previous design<sup>44</sup> is complete. The internal diameter of 32 mm (1.25 in.) compared with 22 mm (0.875 in.) for the present autoclaves will permit us to grow a number of quartz crystals large enough for fabricating oscillator plates for the measurement of acoustic loss ( $Q$ ). Previously, the size limitation imposed by the vessels permitted us to obtain only

---

<sup>43</sup>Research Participant from the Department of Geological Sciences, University of Tennessee, Knoxville.

<sup>44</sup>O. C. Kopp, G. W. Clark, and T. G. Reynolds, "Replaceable Liner-Type Autoclave with Modified Bridgman Closures," *Rev. Sci. Instr.* 34: 1262-63 (1963).

one direct measurement of  $Q$  for RbOH-grown quartz.<sup>45</sup> The availability of acoustic loss data for several crystals grown with RbOH should enable us to answer important questions concerning the perfection of our quartz in some detail.

1.4.9 Single-Crystal Synthesis of Pure and Rare-Earth-Doped CaO by Mass Transport in Molten  $\text{CaF}_2 \cdot \text{LiF}$  Solvent - C. B. Finch and G. W. Clark

Crystals of CaO up to 2 mm on edge were grown from a high-temperature solution in  $\text{CaF}_2 \cdot \text{LiF}$  between 1150 and 1200°C. Experiments were conducted in dry air, using platinum vessels and a solution temperature differential between nutrient and crystallizing nuclei 10 cm above of approximately 20°C. Growth runs of approximately three weeks produced crystals of cubic habit approximately 3 mm on edge. Crystals were grown doped with  $\text{Gd}^{3+}$ , and spectroscopic analysis indicated that at least one-fourth of the gadolinium introduced to the system is incorporated in the crystal. This suggests that this growth technique will be applicable to preparation of actinide-doped CaO single crystals, where it is of interest to determine the EPR of actinide ions in an octahedrally coordinated site symmetry.

1.4.10 Single-Crystal Growth of Monoclinic  $\text{Eu}_2\text{O}_3$  from Molten NaF Solvent - S. L. Bennett, J. Brynstad, G. W. Clark, C. B. Finch, and H. L. Yakel

The optimum conditions for growth of high-purity single crystals of monoclinic  $\text{Eu}_2\text{O}_3$  from molten NaF solvent were sought in the temperature range 1100 to 1200°C. The limited change in the solubility of  $\text{Eu}_2\text{O}_3$  in NaF with temperature (solubility was about 0.3 wt % at both 1150 and 1200°C) dictated that continued emphasis be placed on experiments involving mass transport from nutrient to seed over solution temperature differentials ranging between 10 to 30°C. The experiments were conducted with vertical sealed platinum vessels about 10 cm tall under an atmosphere of argon. Efforts were made to eliminate  $\text{H}_2\text{O}$  or  $\text{OH}^-$  from the starting reagents and growth environment. Crystal-growth runs up to three weeks long produced transparent, needle-like crystals up to  $0.2 \times 0.2 \times 5$  mm in size, which were colorless to slightly pink. Spectrochemical analysis indicated 3 ppm Na and 3 ppm F as the only solvent impurities. X-ray diffraction and optical goniometric studies indicated that the  $[b]$  crystallographic axis coincides with the longest crystal dimension (i.e., needle axis). Selected crystals are being used in x-ray structure determinations and in an x-ray diffraction study of the surface degradation of  $\text{Eu}_2\text{O}_3$  in the presence of moisture.

---

<sup>45</sup>O. C. Kopp and P. A. Staats, "Measurement of  $Q$  for RbOH-Grown Quartz," *J. Phys. Chem. Solids* 36: 356 (1975).

1.4.11 Bridgman Growth of Several Pure and Actinide-Doped Halide Single Crystals - C. B. Finch

Conventional melt growth techniques were used to prepare single crystals of  $\text{RbCaF}_3$ ,  $\text{LaBr}_3$ , and  $\text{CaBr}_2$  for optical and luminescence studies. The crystals were prepared in platinum, vitreous carbon, or quartz containers, which were lowered through a  $20^\circ\text{C}/\text{cm}$  thermal gradient at approximately 2 mm/hr. Crystals of the above compounds were also doped with  $^{244}\text{Cm}$ . Single crystals of  $\text{SrCl}_2$  doped with  $^{249}\text{Bk}$  were grown for electron spin resonance studies.

1.4.12 Vibrational Spectra of Synthetic Single-Crystal Tephroite,  $\text{Mn}_2\text{SiO}_4$  - H. D. Stidham,<sup>46</sup> J. B. Bates,<sup>47</sup> and C. B. Finch

The Raman, infrared, and visible absorption spectra of synthetic tephroite,  $\text{Mn}_2\text{SiO}_4$ , have been measured. The bands observed in the vibrational spectra are assigned to the  $\vec{k} \approx 0$  transverse optical modes of  $\text{Mn}_2\text{SiO}_4$ , and several longitudinal optical mode frequencies of  $\nu_3$  were estimated from features observed in transverse magnetic reflection spectra. The Raman-active components of the internal modes of  $\text{SiO}_4^{4-}$  do not appear to interact with the motions of  $\text{Mn}^{2+}$  ions, but the infrared components of  $\nu_2$  and  $\nu_4$  appear to be highly mixed with the external modes of the manganese sublattice.

1.4.13 Self-Luminescence of Several Curium-Doped Alkaline-Earth and Lanthanum Halides - C. B. Finch and J. P. Young<sup>48</sup>

The self-excited radioluminescence spectra of several alkaline-earth and lanthanum halides doped with approximately 0.1 at.%  $^{244}\text{Cm}$  were recorded between 273 and  $600^\circ\text{K}$  in the wavelength range 0.2 to 2  $\mu\text{m}$ . The host crystals investigated included  $\text{CaF}_2$ ,  $\text{SrF}_2$ ,  $\text{BaF}_2$ ,  $\text{RbCaF}_3$ ,  $\text{LaF}_3$ ,  $\text{SrCl}_2$ , and  $\text{LaCl}_3$ . With the exception of  $\text{LaCl}_3$ , all the samples display a strong emission peak in the vicinity of 0.6  $\mu\text{m}$ . In addition, the fluorite-structure fluorides ( $\text{CaF}_2$ ,  $\text{SrF}_2$ ,  $\text{BaF}_2$ ) exhibit a broad peak at 0.30  $\mu\text{m}$ , while the isostructural  $\text{SrCl}_2$  and nonisostructural  $\text{LaCl}_3$  both have similar broad peaks at 0.40  $\mu\text{m}$ . The 0.60- $\mu\text{m}$  peak has greatest intensity at approximately 400 K in all crystals studied, where it occurs. The 0.30- and 0.40- $\mu\text{m}$  peaks, while strong at room temperature, are quenched on heating to 400 K. No luminescence emission was detected from  $\text{ThO}_2$  or  $\text{CeO}_2$  doped with similar amounts of  $^{244}\text{Cm}$ .

---

<sup>46</sup>On leave from Department of Chemistry, University of Massachusetts, Amherst.

<sup>47</sup>Solid State Division.

<sup>48</sup>Analytical Chemistry Division.

1.4.14 Electron Paramagnetic Resonance Investigations of Divalent  $^{253}\text{Es}$  in  $\text{SrCl}_2$  and  $\text{BaF}_2$ <sup>49</sup> - L. A. Boatner,<sup>50</sup> R. W. Reynolds,<sup>51</sup> C. B. Finch, and M. M. Abraham<sup>47</sup>

The electron paramagnetic resonance (EPR) spectrum of  $^{253}\text{Es}^{2+}$  ( $5f^{11}$  electronic configuration) has been observed in the cubic single-crystal hosts  $\text{BaF}_2$  and  $\text{SrCl}_2$ . The spectrum obtained at about 24 GHz and a temperature of 4.2 K exhibited a well-resolved eight-line hyperfine pattern ( $I = 7/2$ ) for  $^{253}\text{Es}^{2+}$  in both host crystals. The magnetic field positions of the observed transitions were independent of the magnetic field orientation, but line width anisotropies were present. The EPR spectrum of  $^{253}\text{Es}^{2+}$  was described by the spin-Hamiltonian

$$H = g\mu_B \vec{H} \cdot \vec{S} + A\vec{I} \cdot \vec{S}$$

with  $S = 1/2$ ,  $I = 7/2$ , and  $g = 5.825 \pm 0.006$ ,  $A = 12.18 \pm 0.03/\text{m}$  for the  $\text{BaF}_2$  host and  $g = 6.658 \pm 0.003$ ,  $A = 13.82 \pm 0.02/\text{m}$  for  $\text{SrCl}_2$ . The significant difference between the measured  $g$ -values for the two hosts indicates that the  $\text{Es}^{2+}$  ground state is a  $\Gamma_6$  doublet in  $\text{BaF}_2$  and a  $\Gamma_7$  doublet in  $\text{SrCl}_2$ . Although a similar change in ground states between  $\text{BaF}_2$  and  $\text{SrCl}_2$  has been observed for the rare-earth analog of  $\text{Es}^{2+}$  (i.e.,  $\text{Ho}^{2+}$  with a  $4f^{11}$  electronic configuration), a corresponding effect is not necessarily expected for  $\text{Es}^{2+}$  in view of the known importance of intermediate-coupling effects in the actinide series. The observation of such a correspondence provides an additional example of the increasing "rare-earth-like" behavior of the actinides with increasing atomic number.

---

<sup>49</sup>L. A. Boatner, R. W. Reynolds, C. B. Finch, and M. M. Abraham, *Phys. Rev. B* 13: 953 (1976).

<sup>50</sup>Ecole Polytechnique Fédérale de Lausanne, Laboratoire de Physique Expérimentale, CH-1007 Lausanne, Switzerland.

<sup>51</sup>Advanced Technology Center, Dallas, Texas.

## 2. DEFORMATION AND MECHANICAL PROPERTIES

R. A. Vandermeer

The emergence of Materials Science as a discipline is anchored on the premise that important relationships obtain between the microstructure of a material and its properties. This group seeks to discover and characterize these relationships, with particular emphasis on deformation and mechanical behavior in materials of relevance to nuclear and other energy-related fields.

### 2.1 THE PHASE TRANSFORMATION CHARACTERISTICS OF A URANIUM + 14 at.% NIOBIUM ALLOY<sup>1</sup> - R. A. Vandermeer

The transformation of the elevated-temperature bcc phase during both continuous cooling and isothermal aging in a uranium-niobium alloy of the monotectoid composition has been investigated with dilatometry and x-ray diffraction. During rapid cooling to room temperature two transformation stages were detected. The end product phase was the metastable monoclinic  $\alpha''$  modification, which was assumed to form martensitically with an accompanying volume expansion of 0.48%. For the fastest quenching rate the  $M_s$  temperature was 160°C; the  $M_f$  was about 50°C. The  $M_s$  temperature increased slightly with a decrease in cooling rate. Aging at temperatures above  $M_s$  and below 375°C caused  $\alpha''$  to be produced isothermally rather than athermally. The lattice parameters of  $\alpha''$  formed isothermally differed from those found after quenching. This and other evidence to be presented suggest the possible interplay of solute segregation processes with the martensitic transformation. This alloy exhibited a wide range of mechanical properties depending on heat treatment, including the curious shape memory effect. Because of the intimate connection of the shape memory effect and martensitic phase transformation, this study was conducted to provide information regarding transformation characteristics to be used in later shape memory studies.

### 2.2 AGING INDUCED SHAPE INSTABILITY IN AN ELASTICALLY BENT U-7.5 wt % Nb-2.5 wt % Zr ALLOY<sup>2</sup> - R. A. Vandermeer

The U-7.5 wt % Nb-2.5 wt % Zr alloy when quenched from 1073 K was found to exist at room temperature as a metastable phase, which was a slight tetragonal distortion of the elevated-temperature body-centered-cubic (bcc) phase. Flat, as quenched specimens have been elastically

---

<sup>1</sup>Abstract of talk presented at the Annual Meeting of the Metallurgical Society of AIME, Feb. 22-28, 1976, Las Vegas, Nevada.

<sup>2</sup>Abstract of a paper published in *Metall. Trans.* 7A(6): 871-78 (June 1976).

deformed in four-point bending to maximum outer fiber stresses below the stress required for plastic deformation to occur but into a range of stress where pseudoelastic behavior has been observed. Aging of these elastically bent specimens in an oil bath at 423 K, while constrained by the bending jig, resulted in a permanent deflection and shape change. Further isothermal aging, after removal from the bending apparatus, caused increasing deflection and continued shape instability in spite of the absence of the applied load. X-ray examination of samples cut from a bent and aged specimen revealed important preferred orientation and lattice parameter differences between the tension and compression regions and the high- and low-stress parts of the specimen. These observations are described and compared with previous findings on quenched samples of this alloy that had been either deformed separately or aged separately. A rationalization of the shape instability is presented. Elastic twin nucleation and growth, preferred orientations, solute segregation, and the interplay of all these seem to be involved.

### 2.3 PRECIPITATION-HARDENED ALUMINUM FOR POSSIBLE APPLICATION AS STABILIZING COMPONENT IN SUPERCONDUCTION MAGNETS AND TRANSMISSION LINES<sup>3</sup> - R. A. Vandermeer, J. C. Ogle, and C. E. Zachary

In large superconducting magnets and in the proposed underground superconducting power transmission lines, ultrahigh-purity aluminum is a candidate material for the component serving to carry fault currents and to provide a path for the rated current should the superconductor temporarily go normal. If the aluminum could also mechanically support the superconductor assembly, certain design simplifications and weight savings might be realized. Unalloyed high-purity aluminum, though electrically suitable at the low temperatures, does not have sufficient strength to accomplish this. This research is exploring the possibility of manipulating the dispersant in a dilute, precipitation hardenable alloy whose solid solubility is extremely limited, in such a way as to strengthen aluminum while retaining a reasonably high conductivity.

Alloys containing 0.07, 0.12, and 0.26 wt % Au in zone-refined aluminum were prepared. Specimens were solution heat-treated at 873 K for 16 hr and quenched into an ice-brine solution. Aging treatments were carried out at 371, 460, 510, 575, and 625 K for times up to 1000 hr. The residual resistivity ratio was found to depend sensitively on the defect and precipitate state of these alloys. The strengthening of the alloys was monitored by means of Vickers microhardness tests. In this paper some correlations established between mechanical and electrical properties of these alloys will be presented.

---

<sup>3</sup>Abstract (revised) of paper to be presented at the Second International Conference on Mechanical Behavior of Materials, Aug. 16-20, 1976, Boston, Mass.

#### 2.4 ROLLING AND RECRYSTALLIZATION OF (110)[ $\bar{1}\bar{1}0$ ] TANTALUM SINGLE CRYSTALS<sup>1</sup> — W. B. Snyder, Jr.<sup>4</sup> and R. A. Vandermeer

Although much knowledge has been gained in past years concerning the rolling and recrystallization behavior of iron and iron-silicon single crystals, a paucity of information exists on single crystals of the bcc refractory metals. The present investigation is a study of the effects of rolling conditions on the orientation stability and recrystallization behavior of (110)[ $\bar{1}\bar{1}0$ ] single crystals of tantalum. Optical metallography, microhardness, transmission electron microscopy, and x-ray diffraction were used to characterize the effects of rolling and recrystallization. Rolling under conditions of high friction produces transverse strains that are not symmetric with respect to the specimen midplane. Rolling with lower friction forces or under more nearly ideal strain conditions produces symmetric transverse strains with respect to the specimen midplane. A "double barreling" effect at specimen edges occurs under all straining conditions. As a result of these strain inhomogeneities, the character of deformation banding varies through the crystal thickness. Crystal instability is explained by the Taylor theory of plasticity using Dillamore's treatment of pencil glide in bcc metals. Optical microscopy and microhardness indicate that the rate of recrystallization depends strongly on the character of the macroscopic deformation banding.

#### 2.5 THE EFFECTS OF ORIENTATION ON THE ROLLING AND RECRYSTALLIZATION BEHAVIOR OF TANTALUM SINGLE CRYSTALS<sup>5</sup> — W. B. Snyder, Jr.<sup>4</sup>

This investigation was concerned with establishing the effects of orientation on the deformation and recrystallization behavior of rolled tantalum single crystals. Crystals with initial orientations of (001)[ $\bar{1}\bar{1}0$ ], (112)[ $\bar{1}\bar{1}0$ ], (111)[ $\bar{1}\bar{1}0$ ], and (110)[ $\bar{1}\bar{1}0$ ] were rolled to 80% thickness reduction and examined with optical and electron metallography, x-ray line broadening and pole figure analyses, and microhardness testing. A summation of the important conclusions follows:

The (001)[ $\bar{1}\bar{1}0$ ] and (112)[ $\bar{1}\bar{1}0$ ] crystals maintained their initial orientation during rolling and produced microstructures of more or less uniform distributions of dislocations. Slight increases in x-ray line broadening and microhardness indicated that little lattice curvature and stored energy remained in these crystals after rolling. In addition, pole figure analyses indicate that very little spread in orientation existed in the deformed crystals. During rolling, the (111)[ $\bar{1}\bar{1}0$ ] crystal reoriented by a  $10^\circ$  rotation toward the more stable (112)[ $\bar{1}\bar{1}0$ ]. The

---

<sup>4</sup>Staff Member, Development Division, Y-12 Plant.

<sup>5</sup>This contribution summarizes a Dissertation presented to the University of Tennessee as partial fulfillment of Ph.D. requirements of W. B. Snyder, Jr. R. A. Vandermeer was faculty advisor.

moderate reorientation of the (111)[ $\bar{1}\bar{1}0$ ] crystal during rolling created a fairly uniform dislocation cell structure with more or less random misorientations throughout the crystal. Lattice curvature as determined from both transmission electron microscopy and pole figure analysis was greater than for the stable crystals. Microhardness and x-ray line broadening measurements suggested that the amount of stored energy in the moderately reoriented crystal was greater than that in the stable crystals.

Significant reorientation occurred in the (110)[ $\bar{1}\bar{1}0$ ] crystal with concomitant formation of deformation bands. Deformation bands consisted of alternate {001}  $\langle 100 \rangle$  and {111}  $\langle 110 \rangle$ -to- $\langle 112 \rangle$  oriented regions separated by a transition band of mixed orientations. Orientations of alternate bands were affected by rolling conditions. Microstructures within the bands were quite inhomogeneous, varying from dense uniform dislocation arrays to a definite cell structure. Crystals that formed deformation bands during rolling exhibited the greatest increase in orientation spread and stored energy of any crystals.

Crystal stability and reorientation could be partly explained by assuming plane strain deformation and using the Taylor theory of plasticity as applied to pencil glide in bcc metals. Reorientations produced from deformation banding could be better interpreted by applying Taylor's theory to the strain state of axisymmetric compression rather than plane strain.

Annealing of crystals with small amounts of lattice curvature or orientation spread produced large subgrains, which were only slightly misoriented from one another. On the other hand, recrystallized grains were formed in those crystals that had sufficient lattice curvature to produce dislocation cell structures. Crystals containing deformation bands of alternate orientation recrystallized at a lower temperature than those crystals that reoriented wholly to single orientations. The lowered recrystallization temperature was believed due to the increased lattice curvature generated by deformation bands.

Recrystallized grains were nucleated by the polygonization and growth of dislocation cells in the deformed crystal. Growth and impingement of these nuclei resulted in recrystallized grains that had orientations that were originally in the deformed crystals.

Results of this experiment suggested that a critical amount of lattice curvature was necessary to cause natural recrystallization in rolled single crystals.

Deformation banding occurred in the (110)[ $\bar{1}\bar{1}0$ ] crystal but not in the (111)[ $\bar{1}\bar{1}0$ ] crystal. Thus it appeared that there could be a critical orientation within this  $35^\circ 16'$  range where banding would start.

## 2.6 METAL SURFACE DEFORMATION - R. W. Carpenter

The wear characteristic of metals subject to rubbing surface deformation is expected to depend on the deformation substructure immediately beneath the deformed surface. Since erosion is a combination of wear and corrosive attack, all aspects of surface deformation need to be investigated. An experimental method to examine dislocation arrays immediately below such deformed surfaces has been developed by use of an analytical electron microscope. A small scratch was made along the

surface of a large-grained annealed 1100 aluminum wafer specimen with a hemispherical stylus loaded to about 35 mg. The scratched surface was preserved while the wafer was thinned to electron transparency from the unscratched back surface. The specimen was examined in an analytical electron microscope in the following imaging modes:

(1) Scanning secondary electron images were used to characterize the external deformation caused by the scratch, Fig. 2.1.

(2) Scanning transmission (STEM) images were used to examine the dislocation arrays adjacent to and directly underneath the scratch in thick regions of the foil, Fig. 2.2. Note that the dislocation array is about 4 times the width of the stylus mark.

(3) Transmission electron images (TEM) were used to examine the dislocation arrays beneath the scratch in thinner regions of the foils, and to determine the Burgers vectors of the dislocations in the arrays, Fig. 2.3. Multiple slip had occurred. Stereomicroscopy showed that the dislocations extend into the specimen only about 4 times the width of the stylus mark.

The work is continuing, and environmental effects will be studied with the modifications to the high-voltage (1 MV) electron microscope.



Fig. 2.1. Surface Stylus Mark on 1100 Aluminum Specimen. Scanning Electron Micrograph at 20 kV, 15,000 $\times$ .



Fig. 2.2. The Dislocation Array in the Subsurface Volume of the Specimen Directly Under the Stylus Mark Shown in Fig. 2.1. Scanning Transmission Electron Micrograph at 120 kV, 15,000 $\times$ .



Fig. 2.3. A Conventional Transmission Electron Micrograph (TEM) of the Subsurface Dislocation Array of Fig. 2.2. Note the small loop contrast along the edge of the array. 120 kV. 12,625 $\times$ .

## 2.7 HYDROGEN ABSORPTION INDUCED DEFORMATION IN SINGLE-CRYSTAL NICKEL FOILS<sup>6</sup> - R. W. Carpenter and G. S. Bauer<sup>7</sup>

Hydrogen was introduced into annealed single-crystal nickel foils by thinning in an active acid solution at 300 K. At this temperature the hydrogen mobility is high enough for the hydrogen to diffuse easily through the electron-transparent regions of the foil. Examination of the foils by transmission electron microscopy showed the foils to be severely deformed as a result of the hydrogen absorption. Thinning identical specimens in the same acid solution at a lower temperature, 220 K, where the hydrogen mobility is too small to penetrate the electron-transparent regions, resulted in undeformed specimens. The deformation characteristic of hydrogen absorption consisted of cracks at the foil edges that terminated in microtwins in thicker regions of the foil. The microtwins terminated in turn in planar arrays of unit slip dislocations. Evidence for local reduction of the stacking fault energy was found in the form of dissociated unit slip dislocations on slip planes immediately ahead of the twin tips. The observations are being analyzed in terms of contemporary models for twinning and crack nucleation.

---

<sup>6</sup>Summary of a paper to be presented at the Sixth European Congress on Electron Microscopy, Jerusalem, 1976.

<sup>7</sup>Permanent address: Institut für Festkörperforschung, Kernforschungsanlage Jülich, Federal Republic of Germany, on assignment to ORNL.



### 3. PHYSICAL PROPERTIES AND TRANSPORT PHENOMENA

#### 3.1 MECHANISMS OF SURFACE AND SOLID STATE REACTIONS -- J. V. Cathcart

We investigate fundamental mechanisms of gas-solid reactions and of solid-state diffusion processes. The long-term goals of this work are to develop a more comprehensive understanding of the role of alloying elements in the kinetics of gas-metal reactions and to characterize the influence on diffusion processes of the interactions between the diffusing species and defects in the host lattice. Because diffusion is an integral part of many gas-metal reactions, these dual goals are obviously interrelated.

During the past year this research has encompassed programs designed to study (1) the reaction of iron-chromium alloys in high-temperature, mixed-gas environments; (2) the reactions of ceramic-metal composites in similar environments; (3) interstitial diffusion of tritium in oxides and of oxygen in alloys; (4) the phenomenon of anomalous fast diffusion in metals; and (5) interdiffusion processes in metals. These projects provide basic information relevant to the behavior of structural materials used in coal conversion processes, the development of high-temperature materials, the tritium containment problem in fusion reactors, and hydrogen embrittlement of metals.

##### 3.1.1 Reactions of Fe-Cr Alloys in Mixed-Gas Environments -- R. A. McKee, G. F. Petersen, and J. J. Campbell

We initiated a study of the oxidation, sulfidation, and reactions in mixed oxygen-sulfur potentials of a series of iron-chromium alloys between 600 and 900°C. Such alloys are likely candidates for use in various components in coal conversion plants, and while the oxidation and, to a lesser extent, the sulfidation of these alloys have been the subject of earlier investigations, the reactions are so complex (multiphase scale formation, wide ranges of defect concentrations, sensitivity to ambient oxygen or sulfur pressures, etc.) that additional information is needed regarding the properties of the various reaction products formed. We plan to characterize the total reaction in terms of the properties of the individual reaction products and their interactions with each other.

We are beginning with an investigation of the sulfidation of the alloys and their pure components, and most of our efforts this year have been directed toward apparatus design and construction. A device for measuring sulfur pressure, based on the same principle as that used to measure oxygen pressures with a calcia-stabilized ZrO<sub>2</sub> cell, was built and is being tested. Microbalances suitable for measuring the kinetics of either sulfidation or oxidation reactions have been set up. We have also obtained and installed a large magnet, which will be used to measure magnetic susceptibility and to determine the nature of the charge carriers in the reactions products by means of Hall effect measurements. Conductivity measurements are also planned where appropriate, and an effort is under way to prepare the single crystals of FeS and CrS to be used.

### 3.1.2 Ceramic-Metal Composites -- J. V. Cathcart and G. F. Petersen

In cooperation with the Crystal Physics and Fundamental Ceramics Groups, we have continued our efforts to characterize ceramic-metal composites in various high-temperature environments. We tested  $\text{Cr}_2\text{O}_3$ -Mo composites in a variety of CO-CO<sub>2</sub> mixtures at 1000°C. Some of the  $\text{Cr}_2\text{O}_3$  evaporated at high CO/CO<sub>2</sub> ratios (reducing conditions), and a limited attack of the ends of the molybdenum rods occurred at high oxygen potentials. In all cases, however, the degradation of the composite was superficial. In H<sub>2</sub>S and sulfur vapor, on the other hand, the composites were severely attacked, disintegrating completely in a few hours in sulfur at a pressure of about 30 kPa (0.3 atm). We are currently testing other oxides, e.g. MgO, in an effort to find an oxide that is more resistant to sulfur attack.

### 3.1.3 Diffusion in Vanadium-Titanium Alloys -- P. T. Carlson and L C Manley, Jr.

#### 3.1.3.1 Interdiffusion and Intrinsic Diffusion in Binary Vanadium-Titanium Solid Solutions at 1350°C<sup>1</sup> -- P. T. Carlson

Interdiffusion coefficients, intrinsic diffusion coefficients, and vacancy wind parameters have been determined in the vanadium-titanium system at 1350°C with the use of infinite, solid-solid diffusion couples. The experimentally determined diffusion coefficients were compared with the values predicted from the models of Darken, Manning, and Dayananda with the use of available tracer diffusion and thermodynamic information and were found to be larger than those calculated from the three models. Vacancy wind parameters, determined experimentally, reflected a greater influence of the vacancy wind phenomenon on the intrinsic diffusion flux of each species than that calculated on the basis of Manning's theory. In particular, the faster diffusing component is enhanced and the slower diffusing component is retarded to a greater degree than is theoretically predicted. Furthermore, experimental and predicted values of intrinsic diffusivity ratios,  $D_V/D_{Ti}$ , were compared, and the results suggest an increased effect of vacancy flow on the intrinsic fluxes with respect to the magnitude of this phenomenon calculated from Manning's treatment. The vacancy wind effect is shown to be an important factor in the consideration of intrinsic diffusion fluxes and their relation to tracer diffusion and thermodynamic information in the vanadium-titanium system.

---

<sup>1</sup>Abstract of paper published in *Metall. Trans. A* 7A(2): 199-208 (1976).

### 3.1.3.2 Intrinsic Diffusion and Vacancy Flow Effects in Vanadium-Titanium Alloys from 900 to 1600°C<sup>2</sup> - P. T. Carlson and L C Manley, Jr.

Intrinsic diffusion coefficients and vacancy wind parameters have been determined on the vanadium-titanium system from 900 to 1600°C with the use of infinite, solid-solid diffusion couples. The experimentally determined quantities reflect a greater influence of the vacancy wind phenomenon on the intrinsic diffusion flux of each species than that calculated on the basis of Manning's theory. In particular, the diffusion rate of the faster diffusing component is enhanced and that of the slower diffusing component is retarded to a greater degree than is theoretically predicted. A comparison of the experimental and predicted intrinsic diffusivity ratios,  $D_V/D_{Ti}$ , further suggests the increased effect of vacancy flow on the intrinsic fluxes. The discrepancies between the experimental and theoretical values are examined in terms of the assumptions of the random alloy model used in the theoretical treatment. Specifically, the random alloy model assumes a monovacancy mechanism of diffusion, while tracer diffusion results in pure vanadium suggest an additional contribution due to di-vacancies.

### 3.1.4 Anomalous Fast Diffusion Processes - R. A. McKee, P. T. Carlson, and L C Manley, Jr.

The diffusion rates of noble metals and Group II-B elements in lead are higher, in some instances by six orders of magnitude, than the corresponding self-diffusion rates for lead. Recently attempts have been made to explain this phenomenon in terms of the dissociative mechanism of diffusion in which a substitutionally dissolved solute atom is thermally activated into an interstitial position. The degree of coupling between the resulting vacancy and the interstitial and the energy of formation of the substitutional vacancy are assumed to influence the subsequent diffusion rate. This same general process or some modification of it may also explain the anomalous diffusion behavior of iron in carbon steels and may well influence diffusion through oxide (or sulfide) scales formed on high-temperature alloys.

The mechanism of dissociative diffusion is neither fully confirmed nor completely understood, and we have initiated a study of the process in lead-cadmium alloys. A salt bath suitable for the diffusion anneals is now in operation, and single crystals of lead and dilute lead-cadmium alloys have been grown. Diffusion measurements will begin shortly. In addition a paper covering certain theoretical aspects of the dissociative diffusion mechanism has been written, the abstract of which is given below.

---

<sup>2</sup>Abstract of paper submitted for publication in *Metallurgical Transactions*.

#### 3.1.4.1 Solute and Solvent Diffusion for an Alloy in Dissociative Equilibrium<sup>3</sup> — R. A. McKee

Solute and solvent diffusion have been analyzed with the pair association theory for a dilute fcc alloy in which the solute is partitioned between the three states of unassociated substitutional solute atoms, interstitial-vacancy close pairs, and isolated interstitial solute atoms. Correlation factors are identified for solute and solvent motion, and the enhancement factor for solvent diffusion attributable to solvent-vacancy exchanges in the presence of the interstitial solute-vacancy defect is calculated. The results of the calculation present a different maximum enhancement relationship for solvent diffusion from that of previous treatments of dissociative diffusion.

#### 3.1.5 Tritium Diffusion in Oxides — R. A. Perkins and R. A. Padgett, Jr.

We are studying the interaction of tritium with defects in oxide lattices as the tritium diffuses through the oxide. This process is important in the containment of tritium generated in fusion reactors, and it is also relevant to the general problem of hydrogen embrittlement of metals. Diffusion in rutile ( $\text{TiO}_2$ ) is being investigated first because with  $\text{TiO}_2$  we can study interactions of tritium with either cation interstitial defects or anion vacancies simply by controlling the ambient oxygen pressure. During the past year we developed techniques for fixing the defect structure of  $\text{TiO}_2$ , for introducing the tritium into the oxide, and for sectioning the specimens and counting their tritium content. Preliminary diffusivity measurements were made.

#### 3.1.6 Oxygen Diffusion in Niobium and Niobium-Zirconium Alloys — R. A. Perkins and R. A. Padgett, Jr.

This project is designed to study the interactions of an interstitial diffusant (oxygen) with a substitutional impurity (zirconium) in an alloy. The experimental phase of the work is complete. The addition of 1 at. % Zr to niobium reduced the diffusion coefficient for oxygen by a factor of 4 relative to its value in pure niobium. However, the prior addition of about 1 at. % O to pure niobium has no influence on the tracer diffusivity of oxygen. The results are being interpreted in terms of the clustering of oxygen about the zirconium atoms, and a paper describing the work is in preparation.

---

<sup>3</sup>Abstract of paper submitted for publication in *Physical Review*.

### 3.1.7 Older Programs — J. V. Cathcart

Several older projects involving the oxidation of uranium-base and refractory metal alloys and a study of the morphology of the oxide scale formed on a zirconium-base alloy (Zircaloy-4) have been completed or are being phased out. The following are summaries or abstracts of papers describing this research.

#### 3.1.7.1 Interface Stability During the Oxidation of Binary Alloys<sup>4</sup> — G. J. Yurek<sup>5</sup>

The stability of a planar alloy-scale interface during the diffusion-controlled oxidation of a homogeneous, single-phase binary alloy depends on both the thermodynamic and transport properties of the system under consideration. A criterion is presented that can be employed to predict the stability of a planar alloy-scale interface for the specified reaction temperature, alloy composition, and chemical potential of the oxidant when only one component of the alloy is oxidized, anion diffusion predominates in the scale, and the solubility of oxygen in the alloy is essentially zero. A planar alloy-scale interface (a single-phase scale) is the preferred growth morphology if diffusion in the oxide phase is the rate-limiting step of the oxidation reaction. An uneven alloy-scale interface (a two-phase scale) is expected if diffusion in the alloy phase is the rate-determining step. This stability criterion is equivalent to the criterion derived by Wagner for the case of predominant cation diffusion in the scale.

#### 3.1.7.2 Microstructures of the Scales Formed on Zircaloy-4 in Steam at Elevated Temperatures<sup>6</sup> — G. J. Yurek,<sup>5</sup> J. V. Cathcart, and R. E. Pawel

The  $ZrO_2$  scales formed on Zircaloy-4 PWR tubes during corrosion in steam in the temperature range 1000 to 1300°C were found to contain a metallic phase that is relatively rich in tin (Fig. 3.1). The precise composition of the metallic phase has not been determined. Most of the metallic phase is located in a line of metallic particles, which is oriented parallel to the alloy-scale interface and located near the center of the scale. The exact morphology of the scale on either side of the particle line has not been identified. The oxide between the metallic particles and the scale-steam interface contains very little tin, except

---

<sup>4</sup>Abstract of ORNL-5116 (April 1976).

<sup>5</sup>Present address, Massachusetts Institute of Technology, Cambridge.

<sup>6</sup>Abstract of paper accepted for publication in *Oxidation of Metals*.

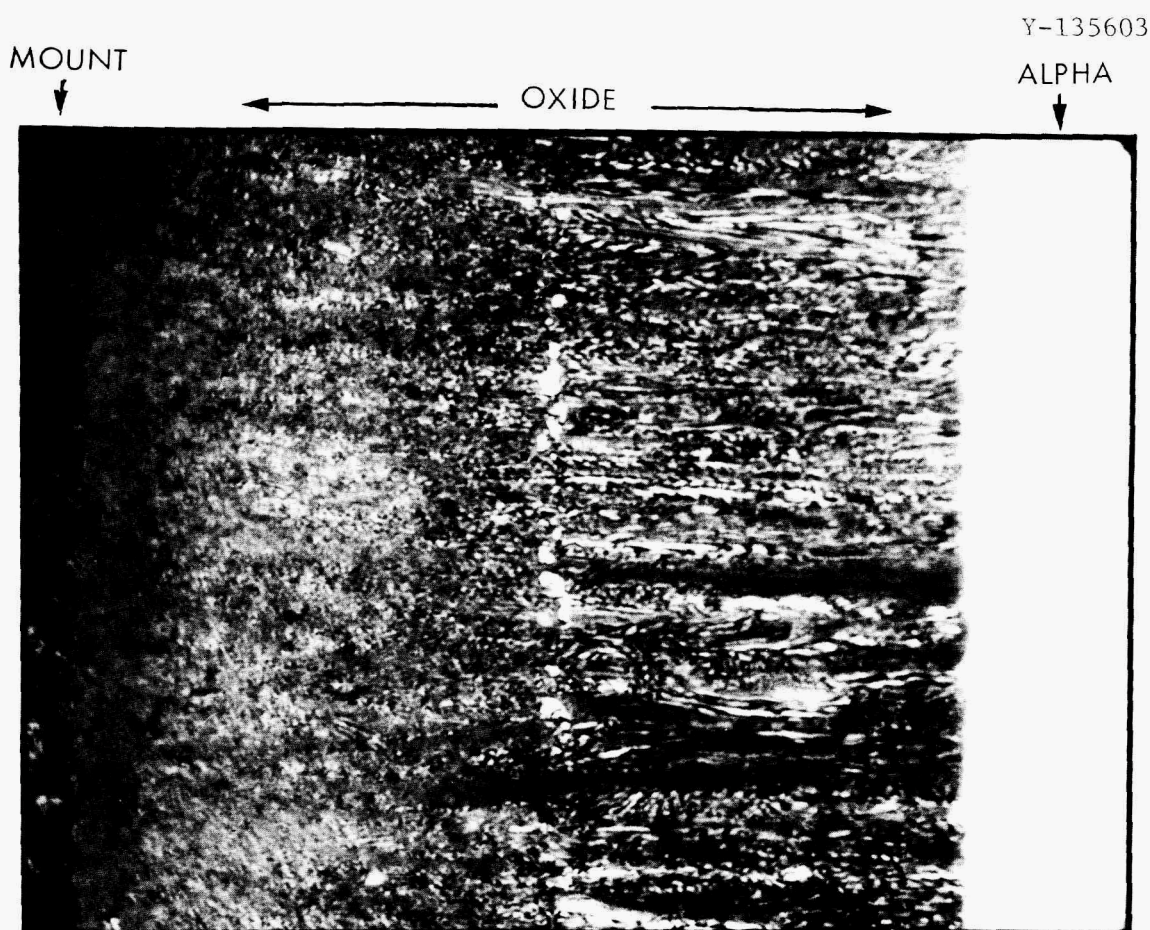


Fig. 3.1. Photomicrograph of a Cross Section through a Zircaloy-4 PWR Tube Oxidized for 201 sec at 1303°C. The bright spots near the middle of the gray-colored oxide phase are the tin-rich metallic particles. Original magnification: 2000×.

for a narrow zone adjacent to the scale-steam interface, which was formed in the beginning of the reaction. The scale between the metallic particles and the alloy-scale interface appears to consist of thin columnar grains of  $ZrO_2$  with a very fine metallic phase probably located at the  $ZrO_2$  grain boundaries. The experimental evidence presently available indicates that the metallic phase exists in the scales at the reaction temperature. If the metallic particles were rich enough in tin, then a liquid metallic phase would exist in the oxide during the reaction. Kinetic studies demonstrate that these particles move with respect to the scale-steam interface toward the center of the alloy during the course of the oxidation reaction. It appears that the presence of the line of metallic particles could, under certain conditions, markedly influence the mechanical properties of the oxide scales formed on Zircaloy-4.

### 3.1.7.3 Sputter Sectioning of Diffusion Specimens<sup>7</sup> — R. A. Perkins and R. A. Padgett, Jr.

The sectioning of diffusion specimens with shallow tracer isotope profiles (1 to 8  $\mu\text{m}$ ) by rf sputtering was investigated to determine the reliability of the method for diffusion measurements in alloy systems. A comparison of the results for  $^{51}\text{Cr}$  diffusion in Fe-17 wt % Cr-12 wt % Ni obtained from specimens sectioned by sputtering and hand grinding indicated no statistically significant difference between the two methods. The roughening of the specimen surface during sputtering did not affect the volume diffusion measurements. The composition of the material collected during sectioning differed significantly from the composition of the specimen but was constant during the sectioning series. Several sputtering parameters (power, collector temperature, gas composition, etc.) must be stabilized during the sectioning to obtain reliable results for diffusion measurements such as those made for the Fe-17 wt % Cr-12 wt % Ni alloy.

### 3.1.7.4 Oxidation of Refractory Metal Alloys — R. E. Pawel and J. J. Campbell

During oxidation at 650°C a Nb-10 wt % Hf-1 wt % Ti alloy became highly embrittled and spontaneously fractured into its individual grains as a consequence of stresses generated during oxidation. The resulting sudden exposure of fresh metal surface caused extensive specimen self-heating with an accompanying drastic increase in oxidation rate. This "ignition" phenomenon was previously observed for several tantalum-base alloys, and its occurrence with this niobium alloy suggests that such behavior may be common in this class of refractory metal alloys. The reaction was characterized in terms of its kinetics, stress generation mechanisms, and grain boundary embrittlement effects.

### 3.1.7.5 Gas-Solid Reactions for BCC Alloys — R. W. Carpenter and C. T. Liu

The kinetics of oxygen absorption at low pressure and elevated temperature was investigated<sup>8</sup> for a tantalum-base refractory alloy containing 8% W and 2% Hf. We found the oxygen absorption rate to be controlled by the transport rate across the gas-solid interface. The average oxygen concentration in the specimen is given by:

---

<sup>7</sup>Abstract of paper accepted for publication in *Journal of Vacuum Science and Technology*.

<sup>8</sup>R. W. Carpenter and C. T. Liu, *Metall. Trans. A* 6A: 2235 (December 1975).

$$\bar{C}(t) = F_0 t / l ,$$

where  $F_0$  is the time-invariant oxygen surface flux,  $t$  is time, and  $l$  is the plate-type specimen half-thickness. The average oxygen concentration is independent of the oxygen diffusion coefficient in the alloy. However, the oxygen concentration gradient is controlled by the oxygen diffusion coefficient in the temperature-pressure region we investigated. The investigation is being extended to niobium-zirconium and vanadium-titanium alloys. The results can be used to estimate the rate of oxygen contamination in these alloys during high-temperature irradiation in the high-voltage electron microscope.

### 3.2 PHYSICAL PROPERTIES RESEARCH — D. L. McElroy<sup>9</sup>

This effort aims to obtain and analyze accurate values of thermal conductivity, electrical resistivity, specific heat, coefficient of thermal expansion, and Seebeck coefficient for a variety of selected solids from 4.2 to 2600 K. Understanding the relations between these properties can provide useful insight about solids and can often provide information for systems where experimental data do not exist.

#### 3.2.1 Transport in Nonmetals

##### 3.2.1.1 Lattice Thermal Conductivities in Electrically Insulating Crystals — J. P. Moore, R. K. Williams, and F. J. Weaver

We have measured the thermal conductivity,  $\lambda$ , of polycrystalline CsCl, CsBr, and CsI from 80 to 400 K and  $\lambda$  of single-crystal CsBr from 80 to 300 K. A comparison of the low-temperature results on the two bromides indicates that phonon conduction is not influenced significantly by grain boundary scattering above 80 K. Therefore, our high-temperature results on the polycrystalline sample are a true measure of phonon conduction where other phonons are the dominant scatterers. The lattice thermal resistances ( $\lambda^{-1}$ ) of CsBr, CsI, and CsCl are roughly linear with  $T$ , with a positive deviation above about 300 K for the bromide and iodide and a negative deviation for the chloride. Previous  $\lambda^{-1}$  data<sup>10</sup> are in good agreement with the present CsI results below 250 K but are too low above 250 K. This is probably caused by photon transport through single-crystal specimens in the previous work.<sup>10</sup>

---

<sup>9</sup>Completed assignment to AERE, Harwell, September 1975.

<sup>10</sup>K. A. McCarthy and S. S. Ballard, *J. Appl. Phys.* 31(8): 1410 (1960).

The experimental  $\lambda^{-1}$  values for the three cesium compounds were compared to a theoretical equation for three-phonon umklapp scattering processes.<sup>11</sup> Best agreement, which was within a factor of 2, was obtained for the CsI, which has a mass ratio of 1.05. The positive deviation of the experimental results above the equation as the mass ratio increases is similar to the behavior of rubidium halides.<sup>11</sup> A specimen of RbF, which has a mass ratio of 4.5, has been prepared in a dry box. Measurements of  $\lambda$  and transmittance in the infrared are in progress.

### 3.2.1.2 Electrical Conductivities of Some Ferrite Crystals -- U. Roy,<sup>12</sup> W. E. Brundage,<sup>12</sup> R. K. Williams, and F. J. Weaver

The electrical conductivities,  $\sigma$ , of four high-quality<sup>13</sup> ferrite crystals were determined between about 60 and 500 K. The compositions studied were nominally  $\text{Li}_{0.12}\text{Ni}_{0.01}\text{Fe}_{2.87}\text{O}_4$ ,  $\text{Ni}_{0.26}\text{Fe}_{2.74}\text{O}_4$ ,  $\text{Li}_{0.08}\text{Ni}_{0.38}\text{Fe}_{2.54}\text{O}_4$ , and  $\text{Mn}_{0.66}\text{Ga}_{0.28}\text{Fe}_{2.06}\text{O}_4$ , and the  $\sigma$  values varied in the order given, with  $\text{Mn}_{0.66}\text{Ga}_{0.28}\text{Fe}_{2.06}\text{O}_4$  exhibiting the lowest conductivity. None of the measurements showed indications of the Verway transition, which occurs at 119 K in  $\text{Fe}_3\text{O}_4$ . The results for all of the crystals showed semiconducting behavior over this temperature range, and the activation energies for conduction were all about 0.06 eV.

### 3.2.2 Physical Properties of Metals

#### 3.2.2.1 Analysis of Experimental Data -- D. W. Yarbrough<sup>14</sup> and R. K. Williams

The methods that have been used<sup>15</sup> to extract the electronic ( $\lambda_e$ ) and lattice ( $\lambda_p$ ) thermal conductivities from experimental data are based on unnecessarily restrictive assumptions. Improved models, based on more easily defended assumptions, have been developed during the past year, and comparisons with available experimental data are now in progress.

---

<sup>11</sup>J. P. Moore, R. K. Williams, and R. S. Graves, *Phys. Rev. B* 11(8): 3107 (1975).

<sup>12</sup>Solid State Division.

<sup>13</sup>F. J. Bruni and W. E. Brundage, *J. Cryst. Growth* 19: 5-10 (1973).

<sup>14</sup>Consultant, Tennessee Technological University, Cookeville,

<sup>15</sup>R. K. Williams and W. Fulkerson, "Separation of the Electronic and Lattice Contributions to the Thermal Conductivities of Metals and Alloys," pp. 389-456 in *Thermal Conductivity, Proc. 8th Conf.*, ed. by C. Y. Ho and R. E. Taylor, Plenum Press, New York, 1969.

One of the methods uses a search routine to determine parameters for a curve fit of experimental thermal conductivity data. The model studied includes a nonlinear term,  $(A + BT)^{-1}$ , for  $\lambda_p$ . The analysis capability has been further modified to include a theoretical expression for the Lorenz function,<sup>16</sup> thus providing a model with Debye temperature, free electron concentration, and the constants in the expression for  $\lambda_p$  as adjustable parameters. Experimental thermal conductivity data for Fe, Ta, W, and Mo have been described by use of the models.

3.2.2.2 Iron and Dilute Iron Alloys -- J. W. Massey,<sup>17</sup> T. K. Holder,<sup>17</sup>  
D. W. Yarbrough,<sup>14</sup> R. K. Williams, and J. P. Moore

In the transition metals and their alloys, the total thermal conductivity,  $\lambda$ , is not solely due to the contribution from the conduction electrons,  $\lambda_e$ . The lattice or phonon conductivity,  $\lambda_p$ , acting in parallel with the electronic contribution, is frequently significant. The magnitudes of these two components in iron were studied experimentally. The method used involves determining the  $\lambda$  and electrical resistivity,  $\rho$ , of several judiciously chosen alloys and computing the magnitudes of  $\lambda_p$  and  $\lambda_e$  from the properties of pure iron and the alloys.<sup>15</sup> The two most important assumptions involved in these calculations are (1) that the solute elements do not alter  $\lambda_p$  and (2) that the solute elements do not significantly change the electronic properties of the solvent. The validity of these assumptions was tested by making measurements on a series of alloys containing 1, 3, and 5% Cr, 3% Ni, and 1% Ni + 1% Cr. Theory<sup>18</sup> indicates that nickel should have a larger effect than chromium on  $\lambda_p$ , and all the experimental results can be successfully interpreted by using the theory to account for this effect. As shown in Fig. 3.2, the results indicate that  $\lambda_p$  of iron passes through a broad maximum between 150 and 250 K, falling off at high temperatures because of increased phonon-phonon scattering. The decrease of  $\lambda_p$  below 150 K is attributed to electron-phonon scattering. The magnitude and temperature dependence of the derived  $\lambda_p$  values seem to be reasonably consistent with theory.<sup>19,20</sup> Over the temperature range of these measurements (90-400 K), the electronic Lorenz function ( $\lambda_e \rho / T$ ) was always less than the Sommerfeld value,  $L_0 [(\pi^2/3)(k/e)^2]$ , but the experimental values reached about  $0.9L_0$  at 400 K.

<sup>16</sup>A. H. Wilson, *The Theory of Metals*, 2nd ed., The Cambridge University Press, 1958.

<sup>17</sup>Graduate Student, Tennessee Technological University, Cookeville.

<sup>18</sup>B. Abeles, *Phys. Rev.* 131(5): 1906-11 (1963).

<sup>19</sup>J. M. Ziman, *Electrons and Phonons*, The Clarendon Press, Oxford, 1960, p. 321.

<sup>20</sup>J. P. Moore, R. K. Williams, and R. S. Graves, *Phys. Rev. B* 11(8): 3170-15 (1975).

ORNL-DWG 76-11020

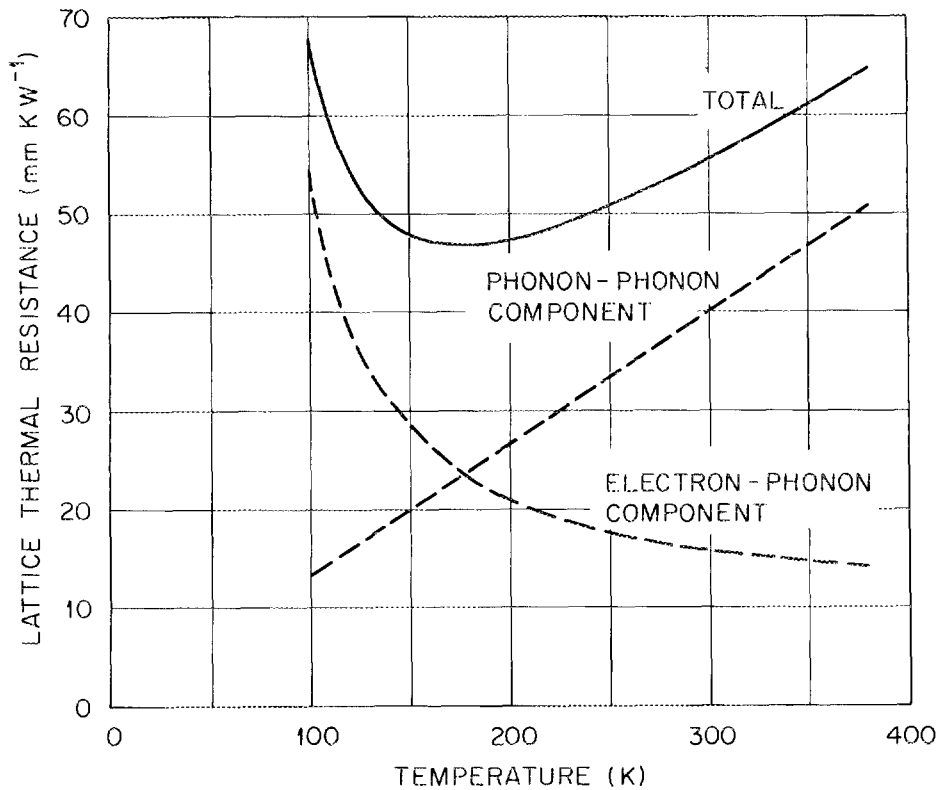


Fig. 3.2. Derived Values of the Lattice Thermal Resistance of Iron. Dashed curves show a tentative separation of the total into two components.

### 3.2.2.3 Niobium -- J. P. Moore, F. J. Weaver, and R. S. Graves

We have made thermal transport property measurements on niobium and Nb-5.05 at.% W as part of a general study of the VB and VIB transition metals and their alloys. A specimen of commercially pure niobium (<0.2 at.% impurities including gases) was fabricated for high-temperature thermal conductivity measurements, and a specimen from this stock was used to obtain Seebeck coefficient,  $S$ , and electrical resistivity,  $\rho$ , data to 1670 K. The  $\rho$  and  $S$  of niobium and Nb-5.05 at.% W nearly coincide, the  $\rho$  of the alloyed material actually being lower above 1100 K. The  $\rho$  of niobium also nearly coincides with that of tantalum up to about 900 K, but deviates negatively at higher temperatures. An approximation for the Bloch-Grüneisen function fails to describe the  $\rho$  of niobium by as much as 15% in the range 100 to 1700 K. A multiple-pass electron-beam-melted specimen of niobium has been obtained for measurement of  $\lambda$ ,  $\rho$ , and  $S$  below 400 K.

### 3.2.2.4 Specific Heat of Actinides<sup>21</sup> — D. L. McElroy

A low-temperature adiabatic calorimeter was developed to measure specific heat,  $C_p$ , values from 10 to 300 K and applied to americium-241, three plutonium carbides ( $\text{PuC}_{0.82}$ ,  $\text{PuC}_{0.90}$ ,  $\text{PuC}_{1.51}$ ) and  $\text{Eu}_2\text{O}_3$  (monoclinic and cubic). The  $^{241}\text{Am}$   $C_p$  results show a transition near 60 K with an estimated energy of 41 J/mole. Above 60 K the temperature dependence of  $C_p$  is described with a reasonable electronic term and a strongly temperature-dependent Debye temperature. Self-damage energy storage in americium near 10 K varies exponentially with time and is removed in three annealing stages centered at 80, 110, and 150 K. The  $C_p$ - $T$  values for  $\text{PuC}_{0.82}$  and  $\text{PuC}_{0.90}$  show anomalies below 150 K, where neutron diffraction has shown magnetic ordering to occur. These Schottky transitions change from being noncooperative for  $\text{PuC}_{0.82}$  to becoming cooperative for  $\text{PuC}_{0.90}$ . A  $C_p$  maximum was noted near 160 K for  $\text{PuC}_{1.51}$ , even though neutron diffraction results do not show a magnetic transition between 20 and 300 K. For  $\text{Eu}_2\text{O}_3$ ,  $C_p$  of the monoclinic structure is greater than  $C_p$  of the cubic form and exhibits a 2% anomaly near 260 K.

### 3.2.3 Apparatus Development

#### 3.2.3.1 Thermal Expansion Apparatus — T. G. Godfrey and D. L. McElroy

Improvements were effected in the computer-operated coefficient of thermal expansion (CTE) apparatus. By modifying the micrometer control circuitry, stabilizing the quartz push-rod tip, and reducing frictional forces on the push rod, the standard deviation in length data under constant conditions was reduced to  $1.5 \times 10^{-8}$  m. Measurements on irradiated HTGR fuel sticks indicate that irradiation reduces their CTE, and this reduction is proportional to the volume fraction loading of particles and the neutron fluence.

---

<sup>21</sup>Work jointly sponsored by ERDA, ORNL, and AERE, Harwell. Abstracted from two papers: D. L. McElroy, H. R. Haines, R.O.A. Hall, and J. A. Lee, "The Specific Heat of  $\text{PuC}_{1-x}$  and  $\text{Pu}_2\text{C}_3$  from 10 to 300 K," pp. 267-76 in *Plutonium 1975 and Other Actinides* (5th International Conference, Proc. Baden-Baden, Sept. 10-13, 1975), ed. by H. Blank and R. Lindmer, North Holland, Amsterdam and Oxford, 1976. R.O.A. Hall, M. J. Mortimer, D. L. McElroy, W. Müller, and J. C. Spirlet, "The Specific Heat of Americium-241 Metal from 15 to 300 K," pp. 139-46 in *Transplutonium 1975* (4th International Symposium, Baden-Baden, Sept. 13-17, 1975), ed. by W. Müller and R. Lindmer, North-Holland, Amsterdam and Oxford, 1976.

### 3.2.3.2 CODAS Development -- T. G. Godfrey and S. H. Jury<sup>22</sup>

The Computer Operated Data Acquisition System, phase III, is involved in two experiments. The first of these is the plane probe apparatus,<sup>23</sup> which was developed for studies on transport properties of relatively poor conductors. The capability of CODAS III to obtain data rapidly has been useful to oxidation experiments on zirconium in the Surface Phenomena Laboratory, where heating and cooling rates of up to several hundred degrees per second are employed. The timing accuracy of CODAS in making these temperature measurements has allowed rate constants to be calculated precisely for experiments of such short duration that the times to heat and cool contributed more than 50% to the observed reactions.

### 3.3 SUPERCONDUCTING MATERIALS -- C. C. Koch

We study the effects of metallurgical variables on the properties of superconducting materials. The superconducting property most sensitive appears to be current-carrying capacity in an applied magnetic field. It is affected by microstructural variables such as grain size, dislocation density and distribution, and morphology, composition, and volume fraction of second-phase particles. Meaningful correlation of structure and properties requires detailed knowledge of both. Consequently, some of our effort is devoted to obtaining basic metallurgical information on phase diagrams, transformation kinetics and products, and the microstructures that result from them in superconducting alloys systems. We correlate current-carrying capacity with the "model" microstructures.

This year our former emphasis on flux pinning studies is being shifted to work on advanced superconducting materials. These are the materials with the highest values of superconducting-normal transition temperature,  $T_c$ , and upper critical field,  $H_{C_2}$ .

Our laboratory has facilities to measure most of the superconducting properties of interest, such as critical current density ( $J_c$ ), ac losses,  $T_c$ , and  $H_{C_2}$ . We also measure low-temperature specific heat capacity and can study the effects of mechanical stress on superconducting properties.

We have carried on basic research in support of an applied program on stress effects in superconductors, which is funded by the Superconducting Magnet Development Program, Thermonuclear Division, ORNL.

---

<sup>22</sup>Consultant, University of Tennessee, Knoxville, TN.

<sup>23</sup>S. H. Jury and T. G. Godfrey, *A Transient Method to Measure the Thermal Conductivity and Thermal Diffusivity of Core Samples -- The Plane Probe*, ORNL/TM-4956 (in preparation).

### 3.3.1 The Influence of Yttrium on the Superconducting Properties of Nb-Ti Alloys<sup>24</sup> - C. C. Koch and J. O. Scarbrough

Composite conductors based on superconducting alloys of niobium with titanium are the present choice for the large toroidal magnets to be used for plasma containment in fusion experiments. While substantial research has been carried out on the relationship between metallurgical structure and superconducting properties in niobium-titanium alloys, a complete understanding of the mechanisms for optimizing fluxoid pinning (i.e., critical current density) is still lacking. In particular, the influence of alloying or impurity elements remains unclear. This paper presents the results of a study of the influence of yttrium additions on the metallurgy and superconducting properties of two niobium-titanium alloys. The alloy Ti-38.2 at. % Nb (55 wt % Nb) was chosen as a commercial composition that relies mainly on dislocation cell boundaries for flux pinning. We selected Ti-25 at.% Nb (39.3 wt % Nb) as an alloy in which second phase ( $\omega$  or  $\alpha$ ) precipitation is a major contributor to fluxoid pinning. We added 1 at. % Y to both alloys and determined its influence on the kinetics of precipitation, dislocation structure, and superconducting properties. Yttrium enhanced critical current density ( $J_c$ ) in cold-worked Ti-38.2 at. % Nb. Its presence modified the kinetics and morphology of  $\omega$  and  $\alpha$  precipitation in Ti-25 at. % Nb, resulting in a degraded  $J_c$  for the longer aging times at 400°C.

### 3.3.2 The Peak Effect in Superconducting Nb-Hf Alloys<sup>25</sup> - C. C. Koch, A. Das Gupta, and D. M. Kroeger

Dramatic "Peak effects" in critical current density ( $J_c$ ) versus applied magnetic field ( $H$ ) have been previously observed in Nb-38 at.% Hf alloys after solution annealing and precipitation. The nature of these peaks, previously attributed to a "matching" between the fluxoid lattice and the precipitate spacing, has been re-examined. Flux gradients have been determined by ac susceptibility methods. A marked inhomogeneity in  $J_c$  was found across the specimen diameter, and this inhomogeneity varies with field and can be correlated with the position of the "valleys" and "peaks" in  $J_c$  versus  $H$ . The temperature dependence has also been measured to separate "matching" effects from more usual pinning behavior.

Resistive measurements of  $J_c$  have revealed a marked magnetic history dependence for  $J_c$  on the low-field side of the peak. The results are being used to test the applicability of present models for flux pinning.

---

<sup>24</sup>Abstracted from paper presented at the Metallurgical Society of AIME Fall Meeting, Cincinnati, Ohio, Nov. 10-13, 1975.

<sup>25</sup>Abstracted from paper presented at the Metallurgical Society of AIME Spring Meeting, Las Vegas, Nevada, Feb. 22-26, 1976.

3.3.3 Direct Observation of the Flux Distribution in the Mixed State of V-Ga Alloys Using a Scanning Electron Microscope<sup>26</sup> -- O. Singh,<sup>27</sup> A. E. Curzon,<sup>27</sup> and C. C. Koch

The mixed state in vanadium-gallium alloys was directly observed by use of the Bitter pattern technique and a scanning electron microscope. Some parts of the specimen showed a single fluxoid state with an average fluxoid spacing of about 760 Å at 6 kG. The flux patterns were cellular in the high-defect-density regions of the surface. Surface voids and grain boundaries were the major flux pinning centres in these samples.

3.3.4 Bending of Flux Lines by Transport Currents in Type-II Superconductors Measured by Neutron Diffraction<sup>28</sup> -- D. M. Kroeger and J. Schelten<sup>29</sup>

Neutron diffraction experiments have been performed on three Nb-13% Ta specimens to obtain information about the distribution of transport currents in type-II superconductors. For sample 1, which had the lowest pinning strength, we concluded that most of the transport current was carried in a region near the surface. However, in sample 2, in which the flux pinning was homogeneous as indicated by ac flux penetration measurements, and in sample 3, in which the pinning strength was highest, a transport current was clearly carried in the bulk, and the experimental results could be explained by specific predictions of the critical state model.

3.3.5 Magnetic History Effects and Wave-Form Asymmetry in ac Magnetization Measurements on Type-II Superconductors<sup>30</sup> -- D. M. Kroeger

The voltage induced in a pickup coil wound on a superconducting niobium-tantalum specimen by a magnetic field  $H = H_{dc} + h(t)$  in some specimens depended strongly upon whether the dc field was increased or decreased to the value during measurement. In such specimens the induced wave form was asymmetric about  $V = 0$  for  $H_{dc} \lesssim 1/2 H_{C2}$ . This asymmetry did not result from large ac amplitudes with consequent variation of  $J_c$  or  $(dB/dH)_{rev}$  over the ac field cycle. The magnetic history dependence,

<sup>26</sup>Abstracted from *J. Phys. D: Appl. Phys.* 9: 611-13 (1976).

<sup>27</sup>Department of Physics, Simon Fraser University, Burnaby, British Columbia, Canada.

<sup>28</sup>Abstracted from a paper submitted for publication.

<sup>29</sup>Institut für Festkörperforschung der Kernforschungsanlage, Jülich, W. Germany.

<sup>30</sup>Abstracted from paper presented at American Physical Society 1976 March Meeting in Atlanta, Georgia. Also in *Bull. Am. Phys. Soc.* 21(3): 289 (March 1976).

in light of recent neutron diffraction experiments, which indicate that the degree of disorder or density of defects in the flux line lattice (FLL) also depends on magnetic history, suggests that  $J_c$  increases with FLL defect density. The nature of the wave form asymmetry is qualitatively consistent with this conclusion. Surface oxidation significantly alters sample behavior, indicating that the processes of flux entry and exit are involved in producing the magnetic history dependence.

### 3.3.6 Tensile Properties of Superconducting Composite Conductors and Nb-Ti Alloys at 4.2 K<sup>31</sup> — D. S. Easton and C. C. Koch

Large superconducting magnets will be used for plasma confinement in nuclear fusion energy experiments. The presence of thermal, mechanical, and magnetic forces in these coils makes the understanding of mechanical properties of the superconducting windings important. Tensile tests were made at 300, 77, and 4.2 K on commercial niobium-titanium composites with both copper and copper-nickel matrices. Tests were also conducted on niobium-titanium filaments produced by chemically removing the matrix of some composites as well as with subsized tensile samples of niobium-titanium alloys.

A pseudoelastic strain region was found in the Nb-Ti/Cu(Cu-Ni) composites and in the niobium-titanium alloys themselves. The anelastic behavior observed in the composites is typical for composites consisting of strong filaments in a weak ductile matrix. However, the pseudoelasticity found in the niobium-titanium itself was the first observation of this behavior in these alloys. Possible explanations are the formation of a reversible stress-induced martensitic transformation and/or twinning and de-twinning. The pseudoelastic strain is accompanied by audible "clicks" upon both stress loading and unloading.

The composite conductors and the niobium-titanium alloys exhibited serrated stress-strain curves. The yield-elongation serrations are apparently the major method of plastic strain in the niobium-titanium alloys at 4.2 K. Both the pseudoelastic phenomenon and the stress-strain serrations can produce an important energy loss. The well-known "training" effect in large superconducting magnets may be related to these mechanical effects.

### 3.3.7 Performance of Multifilamentary Nb<sub>3</sub>Sn Under Mechanical Load<sup>32</sup> — D. S. Easton and R. E. Schwall<sup>33</sup>

The critical current of commercial multifilamentary Nb<sub>3</sub>Sn conductor was measured under the application of uniaxial tension at 4.2 K and

---

<sup>31</sup>Abstracted from pp. 431-44 in *Shape Memory Effects in Alloys*, ed. by J. Perkins, Plenum Publishing Corp., New York, 1975.

<sup>32</sup>Abstracted from a paper accepted for publication in *Applied Physics Letters*.

<sup>33</sup>Thermonuclear Division.

following bending at room temperature. Significant reductions in  $J_c$  are observed under uniaxial loading. Results are presented for a monolithic conductor manufactured by the bronze diffusion technique and for cable conductors formed by the tin-dip technique.

3.3.8 Thermomechanical Heat Generation in Copper and an Nb-Ti Superconducting Composite<sup>32</sup> — D. S. Easton, D. M. Kroeger, and A. Moazed<sup>34</sup>

Heat generation via tensile stress in both pure copper and a superconducting niobium-titanium composite was studied at 300 and 4.2 K. Linear thermoelastic behavior was found at room temperature but not at 4.2 K. At 4.2 K, stress levels of about 88 MPa and 0.1% strain produced energy losses of 0.1 to 0.2 MJ/m<sup>3</sup>. When stress cycled under adiabatic conditions, the composite showed a temperature increase with each cycle as a result of nonlinear (hysteretic) stress-strain behavior.

3.3.9 Inhomogeneities in Superconducting Niobium Surfaces<sup>35</sup> — A. Das Gupta, W. Gey,<sup>36</sup> J. Halbritter,<sup>37</sup> H. Küpfer,<sup>37</sup> and J. A. Yasaitis<sup>38</sup>

Inhomogeneities in superconducting niobium have considerable influence on ac losses in cables; they also give bad rf results. To study inhomogeneities near niobium surfaces, the magnetic induction profile  $B(x)$  and hence the critical current density  $J_c(x)$  were determined as functions of distance  $x$  from the surface in samples that had been machined, annealed, and chemically polished or electropolished and anodized. With identical samples the magnetization and 18-kHz penetration depths were also measured as functions of dc magnetic field applied parallel to the surface. These measurements on niobium samples, which were all exposed to air, indicate that two superconducting phases exist near the surface. One of them has an  $H_{C_2}$  much higher (50%) and the other somewhat higher (10%) than  $H_{C_2}$  in the bulk. In addition, strong pinning exists near the surface, as evidenced by  $J_c$  higher than  $10^6$  A/cm<sup>2</sup>. These effects were found, although to a somewhat lesser extent, even after ultra high-vacuum annealing. The high  $H_{C_2}$  values and strong pinning near the surface, even above the bulk  $H_{C_2}$ , can be explained by the presence of inhomogeneities there.

---

<sup>34</sup>University of Tennessee.

<sup>35</sup>Abstracted from a paper to be published in *Journal of Applied Physics*.

<sup>36</sup>Now at Technische Physik, Universität, 33, Braunschweig, Germany.

<sup>37</sup>Institut für Experimentelle Kernphysik, Gesellschaft für Kernforschung mbH, Karlsruhe, Germany.

<sup>38</sup>Now at Lincoln Laboratory, Lexington, Mass.

### 3.3.10 Work in Progress - Advanced Superconducting Materials

#### 3.3.10.1 Superconductivity in $\text{LiTi}_2\text{O}_4$ - A. Das Gupta, U. Roy,<sup>39</sup> and C. C. Koch

The compound  $\text{LiTi}_2\text{O}_4$  was synthesized from an equimolar mixture of  $\text{Li}_2\text{Ti}_2\text{O}_5$  and  $\text{Ti}_2\text{O}_3$  powders. Specimens were prepared by four different techniques: (1) cold-pressing and sintering, (2) hot-pressing, (3) zone melting, and (4) reaction sintering in swaged copper tubes to produce single core and multicore conductors. Optical metallography and x-ray diffraction studies were carried out to characterize the material. The critical temperature  $T_c$  ( $\approx 11.4$  K) as well as the transverse critical current density  $J_c$  and the dc magnetization  $-M$ , as functions of the applied magnetic field  $H$ , were measured up to 7.0 T at 4.2 K. The apparent  $J_c$ , obtained by dividing the critical current by the total cross sectional area of the specimen, depended upon the densification of the material, the connectivity between the particles, and the presence in the material of the spinel phase, which is stable below about 925°C.

#### 3.3.10.2 Superconductivity in $\text{PbMo}_6\text{S}_8$ - A. Das Gupta, C. C. Koch, and D. M. Kroeger

Work has begun on the material having the highest known values for  $H_{C2}$ ,  $\text{PbMo}_6\text{S}_8$ . Powder samples have been prepared by reacting the constituents. Samples for superconducting property measurements are being made by sintering of pressed powders and by rf sputtering. The goals of this work are an understanding of the metallurgical structure of these materials and the preparation of the material into a useful form.

#### 3.3.10.3 Superconducting Properties of Sputter-Deposited $\text{Nb}_3\text{Al}$ and $\text{Nb}_3(\text{Al}_3\text{Ge})$ - D. M. Kroeger and S. D. Dahlgren<sup>40</sup>

The cooperative effort with S. D. Dahlgren of Battelle Northwest Laboratories is continuing with studies of  $\text{Nb}_3\text{Al}$  sputter deposited and heat-treated at various times and temperatures.

#### 3.3.10.4 Microstructural Studies of Hard Superconductors - C. C. Koch, D. S. Easton, A. Das Gupta, and R. Worsham<sup>41</sup>

A program has been started to use transmission electron microscopy and x-ray diffraction to study the microstructure, crystal structure, and

---

<sup>39</sup>Solid State Division.

<sup>40</sup>Battelle Northwest Laboratories.

<sup>41</sup>Physics Division.

possible phase transitions in A-15 and other high-field superconductors at liquid helium temperatures. The low-temperature electron microscope developed by R. Worsham utilizing superconducting lenses will be used in this study.



## 4. RADIATION EFFECTS

J. O. Stiegler and K. Farrell

The Radiation Effects Program has as its goal the understanding of changes in the physical and mechanical properties of metals and alloys caused by elevated-temperature neutron irradiation. Emphasis is on effects of composition and microstructure with the aim of using these metallurgical variables to minimize or control the damage. Although neutron irradiations provide the ultimate test of our ideas, simulation techniques that allow accelerated testing and evaluation of mechanisms are exploited.

Work on this program complements the radiation effects activities in the ORNL Solid State Division, which are directed at describing the primary production of point defects. Effort in the Metals and Ceramics Division is concerned with the organization of these defects into more complex configurations and with the resultant properties of heavily damaged materials. This work also parallels applied programs supported in the Metals and Ceramics Division by the Liquid Metal Fast Breeder and Fusion Reactor Programs but is aimed at uncovering mechanisms of damage by studying simple or model systems. In this report only work supported by the Division of Physical Research is described. Activities in the other programs are summarized in the progress reports for those programs.

### 4.1 EXPERIMENTAL STUDIES AND EVALUATIONS

#### 4.1.1 Neutron Experiments on Aluminum Alloys — K. Farrell and J. T. Houston

Some commercial aluminum alloys have good resistance to radiation-induced void formation and associated swelling. This resistance has now been pursued to high neutron exposures in the alloys 1100 (99% Al, balance largely insoluble Si + Fe), 8001 (99% Al, 1% insoluble Ni), 5052 (2.5% Mg in solid solution) and 6061 (1% Mg and 0.5% Si as Mg<sub>2</sub>Si precipitate). Tensile specimens of these alloys have been irradiated to fast neutron fluences up to  $1.8 \times 10^{27}$  n/m<sup>2</sup> (260 dpa) (dpa = displacements per atom) and thermal neutron fluences up to  $3.0 \times 10^{27}$  n/m<sup>2</sup> at 328 K ( $0.35T_m$ ) in the High Flux Isotope Reactor. Comparison specimens of pure aluminum were irradiated to 40 dpa. Density measurements, supported by transmission electron microscopic examination, indicate that for a damage level of about 40 dpa the pure aluminum swelled 10%, the 8001 alloy about 3%, the 1100 alloy 2%, and the magnesium-containing alloys 5052 and 6061 less than 0.3%. At 200 dpa the 8001 alloy displayed 12% swelling, the 1100 alloy 10%, the 6061 alloy 1% and the 5052 alloy less than 0.5%. At this high fluence about 5.5 wt % of insoluble silicon is formed from transmutation reactions with thermal neutrons. This silicon is less dense than the aluminum and it causes about 1% swelling, except in the 5052 alloy, where it reacts with dissolved Mg

to form  $Mg_2Si$  precipitate with an estimated net change in density of less than 1%. Thus in the 6061 and 5052 alloys the measured swelling is largely attributable to transmutation-produced silicon; very few cavities are found in these alloys.

Tensile tests on the alloys at 323, 373, and 423 K show considerable radiation hardening and loss in ductility. Most of the ductility loss results from large reductions in uniform strain brought about by the hardening. Additional embrittlement involving premature intergranular separation is evident in the 5052 alloy at exposures exceeding 20 dpa and in 1100 alloy at exposures exceeding 50 dpa. The 6061 alloy retains almost 10% elongation under all test conditions. The relatively good mechanical performance of the 6061 alloy, coupled with its high resistance to void formation and to corrosion in water, makes it a superior alloy for low-temperature light-water applications.

These observations demonstrate that chemical composition and/or precipitate structures can provide a means of minimizing void formation. Most aluminum alloys contain, in addition to their major alloying elements, many minor elements present either as tramp impurities or as deliberate additions to control grain growth or to stabilize precipitates. Of the common elements only Mg, Zn, and, to a much lesser extent, Cu have any appreciable solubility in aluminum at temperatures below about 400 K. To investigate the role of alloying elements in swelling we are studying microstructural changes in dilute (100 at. ppm level) binary alloys of Ag, Cu, Fe, Mg, Mn, Ni, Si, Sn, and Zn in a high-purity aluminum base after irradiation to 2 dpa at  $0.35T_m$ . Only Cu and Mn show a significant suppression of voids; a precipitate is developed in the Cu alloy but not in the Mn alloy. In the case of Mg there is a small suppression of swelling at the 100 at. ppm level, considerable suppression at the 1000 at. ppm level, and complete suppression at 1.66 at. %, where a precipitate of  $Mg_2Si$  is evident. Zinc has little or no effect on voids at the 100-at.-ppm level, causes only a small suppression at the 1000-at.-ppm level, and still permits some voids at the 1-at. % level despite the occurrence of extensive precipitation. We are still analyzing the microstructures in those alloys. The data suggest tentatively that suppression of void formation can be linked to lattice distortion caused by alloying elements. Of the elements so far investigated the most effective ones — Cu, Mn, and Mg — are also known to cause large changes in lattice spacing. Further alloys are now being prepared from other elements that distort the aluminum lattice.

#### 4.1.2 Direct Observation of Coated Voids<sup>1</sup> — K. Farrell, D. N. Braski, and J. Bentley

Okamoto and Wiedersich<sup>2</sup> have pointed out that whereas equilibrium segregation of foreign elements will occur at crystalline free surfaces

---

<sup>1</sup>Summary of a paper submitted to *Scripta Metallurgica*.

<sup>2</sup>P. R. Okamoto and H. Wiedersich, "Segregation of Alloying Elements to Free Surfaces During Irradiation," *J. Nucl. Mater.* 53: 336-45 (1974).

to reduce the surface free energy, an even greater degree of nonequilibrium segregation may occur in the presence of mobile point defects created during particle irradiation. The drift of vacancies and self-interstitials to the free surface will sweep dissolved impurities to the surface. In the ultimate, irradiation-induced voids should become coated with foreign elements or plated with precipitates. Evidence in support of such segregation has been obtained indirectly from study of coherency strains believed to be associated with impurities around voids or precipitates on the voids. Recently during transmission electron microscopic examination of a piece of commercially pure aluminum irradiated to very high exposures (fast and thermal fluences  $> 1 \times 10^{27}$  n/m<sup>2</sup>) we unambiguously confirmed the existence of coated voids. The voids were typically 80 to 90 nm diam, and they displayed obvious dark rims. More direct evidence of coatings on the voids was provided by the fact that many of the voids were free-standing on the surfaces of the foils, some of them retained their original shapes, and others had collapsed. These free-standing voids can exist only if they are contained in an envelope of material of different composition than the matrix and with a greater resistance to electropolishing.

Foils were tilted to project free-standing voids over large holes in the foils, and these voids were analyzed *in situ* with a finely focused electron beam ( $\sim 20$  nm diam) using energy-dispersive x-ray analysis and micro-micro diffraction. The major constituent of these voids was identified as silicon. This silicon is created in the aluminum by transmutation by thermal neutrons. An estimated 5.2 wt % Si was created. Silicon is almost insoluble in aluminum at the irradiation temperature of 328 K, and most of it appears in the microstructure as a precipitate of average particle diameter 30 to 40 nm, the balance clearly forming coatings around the voids. Such coatings are important because they might affect the growth kinetics of voids and hence may influence radiation-induced swelling (see Sect. 4.2.1).

#### 4.1.3 Correlation of Neutron- and Nickel-Ion Damage in Pure Nickel - N. H. Packan, J. O. Stiegler, and K. Farrell

Since neutron damage experiments in reactors are rather slow and expensive, use of rapid techniques that simulate displacement damage has been increasing. Bombardments with high-energy electrons and heavy ions are now used extensively to this end. A major difference between such simulations and the damage produced by neutrons lies in the much higher generation rates of point defects in the simulation cases; consequently, the resulting microstructures are different. To obtain equivalent microstructures, which is the goal of simulation, the high vacancy generation rate in the high-dose-rate simulations must be complemented by an enhanced vacancy diffusivity to allow a like proportion of defects to survive recombination and end up in clusters. Such a condition can be obtained by conducting the high-dose-rate bombardment at a higher temperature than the lower dose-rate neutron irradiation. The extent of the required temperature shift is predicted theoretically to be of the order of 150 to 200 K. We have measured a shift of this amount in pure nickel.

Recrystallized rods of zone-refined nickel were irradiated in the Oak Ridge Research Reactor (ORR) at temperatures in the range 570 to 1170 K (300 to 900°C) to develop voids. The displacement rate was  $10^{-7}$  dpa/sec, and the displacement level was approximately 1 dpa. Transmission electron microscopic examination of the irradiated rods revealed voids formed in the temperature range 570 to 780 K, and the degree of swelling was measured as a function of irradiation temperature. Void simulation experiments were made in a higher range of temperatures on disks of the same purified nickel by bombarding with a 4.0-MeV  $^{58}\text{Ni}^{2+}$  ion beam in the Oak Ridge National Laboratory 5.5-MV Van de Graaff accelerator. The displacement damage level was again 1 dpa but the displacement rate was about  $3 \times 10^{-3}$  dpa/sec, almost 3000 times faster than that in the neutron-irradiated material. The degree of swelling obtained under these conditions is compared with the neutron data in Fig. 4.1.

ORNL-DWG 76-9971

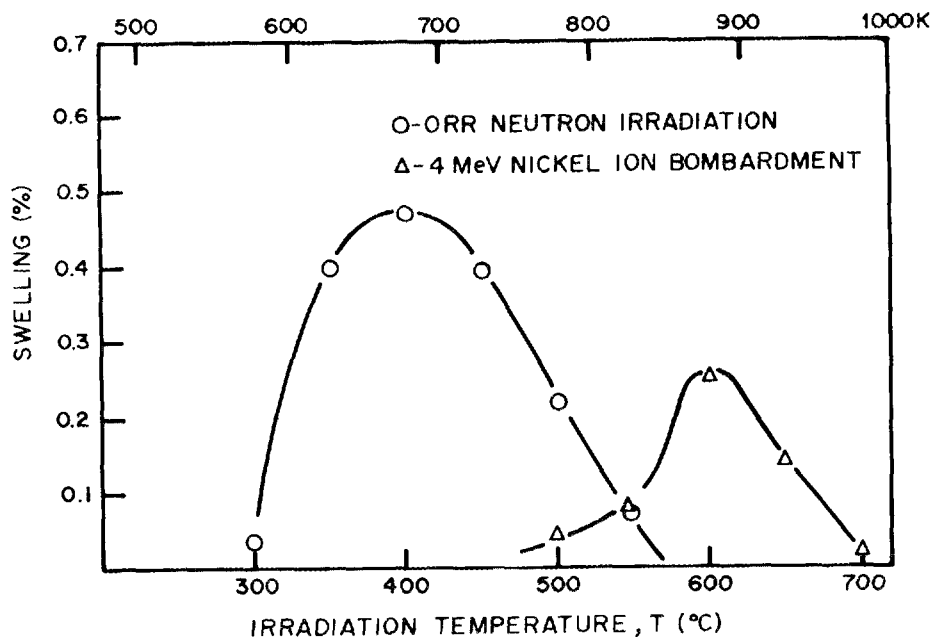


Fig. 4.1 Comparison of Swelling as a Function of Temperature for Irradiation of High-Purity Nickel by Reactor Neutrons and Nickel Ions.

The higher rate of damage during ion bombardment has clearly pushed the swelling curve about 150 to 200 K up the temperature scale. The generally higher level of swelling in the neutron-irradiated material may be largely due to its helium concentration of more than 20 at. ppm generated during irradiation. The ion-bombarded specimens contained no helium. It is well known that helium enhances void formation and swelling, especially at these low damage levels. Consistent with this view, the neutron-irradiated materials contained up to 10 times as many

voids as the ion-bombarded specimens. Future ion bombardments will be conducted with simultaneous helium implantation to simulate more closely the neutron case.

#### 4.1.4 Swelling Resistance in a Type 316 Stainless Steel<sup>1</sup> --- E. A. Kenik

It has been shown that silicon and titanium additions are critical in the high swelling resistance of the modified type 316 stainless steel designated LS1A. Extensive high-voltage electron microscopy and heavy-ion irradiations are in progress to investigate the low swelling behavior of LS1A relative to the high swelling of G7, a similar type 316 stainless steel containing less silicon and titanium. The evolution of the entire damage structure, both dislocations and voids, has been studied to determine the origin of the swelling resistance of LS1A. The step-height technique was employed for rapid swelling measurements for ion-irradiated samples. At 600 dpa, G7 exhibited a 1.02  $\mu\text{m}$  step height ( $\sim 170\%$  swelling), while LS1A exhibited a step height of about 3.5 nm ( $< 6\%$  swelling). Even at this exposure level, LS1A does not exhibit void formation. The observed step height is probably associated with the volume increase arising from the injected nickel ions.

As the dislocation substructure is a required precursor of void formation, the early stages of damage in LS1A and G7 were studied for differences in the evolution of the dislocation substructure. The faulted dislocation loops in LS1A appear more stable than those in G7, growing to larger sizes and not unfaulting as early. This behavior delays the interaction of the faulted loops and the formation of a dislocation network in LS1A.

The stability of the faulted loops in LS1A must be attributed to the action of silicon and/or titanium. The possibility that either of these elements segregates to the growing dislocation loops and thus stabilizes them was investigated with the x-ray energy analysis capability of the JEOL 100-C microscope. This technique allows the elemental analysis of 100-nm-diam areas of a thin foil by the characteristic x-rays excited by the electron beam. The major difference between the dislocation loops in LS1A and those in G7 is the large silicon segregation to the faulted dislocation loops in LS1A, which was estimated at about 4.5 at. % Si.

The segregation of silicon to the dislocation loops in LS1A could stabilize these loops in several ways. Silicon may reduce the stacking fault energy or, as an undersized atom, silicon could reduce the stress field of the interstitial loop. The silicon concentrated at the Frank dislocation might inhibit the nucleation of the Shockley partial required to unfault the dislocation loop. It appears that in LS1A the growth rate of dislocation loops decreases as the size increases. The silicon segregated at the Frank loops could reduce their ability to absorb self-interstitials preferentially. The stability of the faulted loops and the apparent decrease in preferential absorption at the larger faulted loops result in continued loop nucleation and concurrently higher dislocation density. However, as a high density of such stabilized loops is generated, the number of excess vacancies free for void formation decreases as the loops become the dominant sink for all point

defects. A similar segregation of silicon to perfect loops and dislocation segments could also reduce the preferential absorption of interstitials at these biased sinks.

#### 4.1.5 Void Nucleation in Alloys — R. W. Carpenter and J. C. Ogle

The dependence of void nucleation on alloy microstructure is being examined in several alloy systems that undergo well-known solid-state transformations. The effect has been examined in neutron-irradiated aluminum-copper alloys and electron-irradiated copper-cobalt<sup>3</sup> and copper-titanium alloys.<sup>4</sup>

The experimentally determined swelling values for neutron-irradiated aluminum-copper alloys are given in Table 4.1. The heat treatments

<sup>3</sup>R. W. Carpenter and J. C. Ogle, "The Effect of Solute Content and Precipitate Distribution on Fast Neutron Damage in Aluminum Copper Alloys," pp. 1203-12 in *Fundamental Aspects of Radiation Damage in Metals* (Proc. Int. Conf. Gatlinburg, Tenn. Oct. 6-10, 1975), Vol. 2, CONF-751006P2.

<sup>4</sup>R. W. Carpenter, "Effects of Precipitation on Electron Displacement Damage in FCC Alloys: Copper Alloys with Random and Modulated Microstructures," pp. 221-24 in *Microscopie électronique à haute tension 1975* (Proc. 4th Int. Congress, Toulouse) ed. by B. Jouffrey and P. Favord, Société Française de Microscopie Electronique, Paris, 1976.

Table 4.1. Measured Neutron Irradiation Induced Swelling

Alloy	Heat Treatment <sup>a</sup>		Preirradiation Structure	Swelling (%)
	Time (hr)	Temperature (°C)		
Al	0		Single-phase $\alpha$	12.4
Al-3.8% Cu	0		GPZ	0.07
Al-3.8% Cu	1	169	GPZ + $\theta''$	0.33
Al-3.8% Cu	10	200	$\theta'$	0.54
Al-3.8% Cu	50	200	$\theta'$	2.30
Al-1.7% Cu	0		GPZ	1.13
Al-1.7% Cu	1	169	GP + $\theta''$	0.77
Al-1.7% Cu	10	200	$\theta'$	0.68
Al-1.7% Cu	10	240	$\theta'$	

<sup>a</sup>Homogenization followed by the indicated aging treatment.

were used to form a desired microstructure before irradiation; irradiations were done in the HFIR at 328 K to about  $3 \times 10^{26}$  n/m<sup>2</sup> (>0.1 MeV). All the alloys swelled less than pure aluminum. The Al-3.8% Cu alloy shows a regular increase in swelling with progression toward the equilibrium microstructure. The Al-1.7% Cu alloy showed the reverse, a larger swelling for GP zones and somewhat less for coarser precipitates, although the magnitude of the swelling and the difference are not large.

The copper alloys were irradiated at 573 K in the 1-MV electron microscope to total displacements in the neighborhood of 40 dpa. The experimental observations fell naturally into three groups:

1. Copper-cobalt alloys containing no visible zones or quite small coherent zones differed little in radiation response from elemental copper. Initially faulted loops were observed, followed by coalescence into a dislocation network and the nucleation and growth of voids. Loop and dislocation mobility was high during irradiation.

2. Copper-cobalt alloys containing initially incoherent precipitate particles did not exhibit faulted loop formation during the first part of the irradiation. Dislocation mobility was low during the irradiation, a result of pinning at the precipitate-matrix interfaces. Void nucleation and growth did ultimately occur, but at an appreciably higher dose than in the alloys noted in (1) above. Clear examples of void nucleation and growth at precipitate interfaces were observed.

3. Copper-titanium alloys were transformed to a modulated structure by aging at 683 K before 1-MeV electron irradiation at 573 K. The modulation wave length was about 55 Å along  $\langle 100 \rangle$ . These alloys did not nucleate voids up to about 40 dpa. Higher exposures have not yet been investigated.

The structural changes that accompany precipitation in these alloys are the formation of a high density of coherent zones, followed by coarsening and loss of coherency. In the case of aluminum-copper and copper-titanium alloys the coherency strains have tetragonal symmetry; the strains are spherically symmetric in copper-cobalt alloys. The results indicate that in these systems a high concentration of coherent strain centers is necessary but not sufficient for suppression of void nucleation. The observations of void nucleation in the copper-cobalt alloys indicates that the strain centers cannot be spherically symmetrical to suppress void nucleation; they must be at least tetragonal. This research is continuing.

#### 4.1.6 Effect of Structural Inhomogeneity on the Swelling of Nickel Binary Alloys — E. A. Kenik

The investigation was designed to increase the understanding of the interrelation of short-range and long-range order, second-phase precipitates and morphologies, and alloy thermal stability with the swelling behavior of four nickel-base alloys systems — Ni-Mo, Ni-Al, Ni-V, and Ni-Ti. These alloy systems are the primary subsystems of most nickel-base precipitation-hardening alloys being considered for advanced fuel cladding systems. In addition, the effects of various

irradiating species, and of the type, morphology, and kinetics of the different ordering, precipitation, and resolution reactions may be studied in these four systems.

Heavy-ion (Ni) irradiations of nickel single-crystal specimens were performed to supply a data base for comparison with the binary alloy data. Both step-height measurements of swelling and transmission electron microscopic (TEM) examination of the damage microstructures of these specimens have been completed. A peak swelling temperature of about 950 K was determined with a step-height of about 180 nm (~30% swelling) at 100 dpa. Possible reasons for this unusually high peak temperature are being investigated.

On the basis of step-height measurements the dilute Ni-V and Ni-Ti alloys exhibit similar temperature regimes for swelling to those of the single-crystal nickel. However, the degree of swelling is reduced by a factor of 2 to 3 for the alloys. In the two-phase Ni-V and Ni-Ti alloys, the limited step-height data indicate that the swelling decreases in the Ni-V system but increases in the Ni-Ti system.

From both preliminary TEM investigations of the damage structures in the Ni-V and Ni-Ti alloys and recent information in the literature, it appears that step-height measurements may not be ideally suited for measurement of swelling in systems capable of precipitation or ordering during irradiation. Changes due to irradiation in the dynamic state of the microstructures may appear as step heights or mask step heights associated with swelling. The possibility of such behavior requires TEM examination of the damage structures and comparison with observed step-height measurements in these binary nickel alloys. This is in progress.

#### 4.1.7 Tracing the Evolution of Bubbles in Helium-Injected Aluminum by Means of Positron Annihilation<sup>5</sup> — C. L. Snead, Jr.,<sup>6</sup> A. N. Goland,<sup>6</sup> and F. W. Wiffen

Pure aluminum was injected with 0.6 at. ppm He. Positron lifetime measurements were performed following isochronal annealing between 300 and 873 K. Transmission electron micrographs were taken after several of these anneals. The results are consistent with a model in which the injected helium quickly becomes substitutional. This substitutional helium is a trapping site for positrons. Monitoring the concentration and size of this trapping site through the measurement of the positron lifetimes shows that migration of the helium begins at about 375 K and that helium continually agglomerates up to about 525 K. Above this temperature the increasing size of the trapping site indicates bubble growth. Bubble growth proceeds up to 875 K, but whether by continued arrival of helium at nucleation sites, bubble migration and coalescence, or both is indeterminable. The major stage of bubble growth is between 575 and 875 K. The electron microscopy verified the presence of bubbles

---

<sup>5</sup>Summary of a paper submitted to *Journal of Nuclear Materials*.

<sup>6</sup>Brookhaven National Laboratory.

in both grain boundaries and matrix after annealing to 900 K, but cavities were observed only in grain boundaries on annealing to 575 K. Positron-lifetime measurements are a useful complement to electron microscopy in the study of bubbles in metals, especially in the early stages of the nucleation and growth of small cavities.

#### 4.1.8 Low-Activation Materials for Fusion Reactors: Radiation Damage Considerations in Aluminum Alloys<sup>7</sup> - K. Farrell

Many aluminum alloys have low residual radioactivity after neutron irradiation. They are also compatible with solid lithium and lithium oxide for some conceptual fusion reactor designs using the D-T reaction. But can they withstand neutron damage in a first-wall environment in a fusion reactor? This question may be answered by considering the nature of radiation damage in aluminum. This damage stems from two sources, the first of which is displacement of atoms from their lattice sites by fast neutrons and the aggregation of the resulting point defects (vacancies and interstitial atoms) into larger structural flaws such as dislocations and voids. This displacement damage results in significant hardening of the host material (and consequent loss in ductility) and gross swelling from void formation. Such damage is very sensitive to temperature and can not survive when the irradiation temperature is greater than about  $0.5T_m$  [ $\sim 200^\circ\text{C}$  (473 K) for aluminum]. The second source of damage is transmutation products, principally hydrogen and helium from  $(n,p)$  and  $(n,\alpha)$  reactions with fast neutrons and silicon from an  $(n,\gamma)$  reaction with thermal neutrons. These foreign elements are essentially insoluble in aluminum and are produced at all irradiation temperatures. The rates of production of transmutation products are functions of the neutron energies; in current fission reactors the hydrogen and helium production rates do not exceed about 120 and 20 at. ppm per year, respectively, but the silicon production rate can be as high as 1.5 at. % per year. In a fusion reactor first wall, where a much greater fraction of the neutrons have energies greater than the threshold values for  $(n,p)$  and  $(n,\alpha)$  reactions, the corresponding annual production rates are estimated to be about 1000 at. ppm H and 450 at. ppm He; production of silicon will be low compared with existing fission reactors in which aluminum alloys are now serving. Hydrogen can diffuse and escape from aluminum, but helium is relatively immobile and becomes trapped, often in gas bubbles on grain boundaries where it causes gas bubble swelling and premature intergranular failure. Experiments on irradiated aluminum-lithium alloys in which the lithium is transmuted to tritium and helium have established that gas levels of 1000 at. ppm or more can cause extensive swelling and intergranular fissuring at temperatures above 373 K ( $100^\circ\text{C}$ ), even in the absence of applied stress, the effects becoming more pronounced with increasing temperature. Since a fusion reactor first wall is not likely to operate

---

<sup>7</sup>Summary of a contribution to an EPRI conference on Low-Activation Materials for Fusion Reactors, San Francisco, Feb. 19-20, 1976. To be published in Conference proceedings.

below about 473 K (200°C) we conclude that swelling and very low ductility associated with high helium levels will preclude the use of aluminum and its alloys. Also, at such temperatures aluminum alloys have low flow stresses compared with stainless steels and refractory metals, and attempts to purify aluminum alloys to reduce highly radioactive elements may further weaken the alloys, since some residual elements are needed to stabilize precipitates and prevent grain growth. Aluminum alloys may find application in fusion reactors in positions where the neutron spectrum is more thermalized and where the operating temperatures are below about 370 K (100°C). For such purposes the radiation-induced changes in microstructures and mechanical properties of commercial aluminum alloys are reviewed.

#### 4.1.9 Simulation of Helium Effects: Introduction of Helium from Charged Particle Accelerators and Alpha Particle Sources<sup>8</sup> — K. Farrell

The question of simulating the effects of helium on elevated-temperature ductility of metals, otherwise known as helium embrittlement, is addressed in terms of introducing helium from charged particle accelerators and isotopic alpha particle sources. These two implantation techniques are currently used as pretreatments for studies of displacement damage structures, and to a small extent for mechanical property changes. Helium embrittlement is associated with grain boundaries, and simulation requires that specimens be thick enough to exhibit bulk, polycrystalline mechanical behavior. The depth of penetration of the alpha particles is a function of the energy of the incident particle and in the case of isotopic alpha particles, where the initial energy is usually only 5 or 6 MeV, the penetration is quite shallow, of the order of a few tens of micrometers, making this technique suitable only for studies of "skin" effects. With accelerated charged particles, whose initial energies may exceed 50 MeV, the depths of penetration may approach 1 mm, and this technique is thus more suitable for studies of bulk embrittlement. However, neither technique on its own is considered wholly satisfactory, the major objections being (1) failure to achieve a suitable distribution of helium, (2) poor control of implantation temperature, (3) inadequate balance of displacement damage structure and helium level, and (4) curtailment of diffusion processes that may be important to development of helium embrittlement. Nevertheless it is felt that the techniques offer potential for isolating and identifying mechanistic aspects of embrittlement.

The advantages and disadvantages of implanting helium from accelerators are discussed with particular emphasis on means of attaining temperature control and uniform helium distribution. The ORNL technique with the Oak Ridge Isochronous Cyclotron using 50-MeV alpha particles is described and the pros and cons are listed. Similar considerations are given to

---

<sup>8</sup>Summary of a contribution to Task Group D of ASTM Subcommittee E10.08 "Procedures for Simulating Damage Produced in Fission and Fusion Reactors." Presented at ASTM Committee Meetings, St. Louis, Mo., May 3-6, 1976.

implantation from isotopic alpha particle sources, where the prime limitation is the shallow depth of penetration of the helium. ORNL experience with  $^{244}\text{Cm}$  sources is discussed.

## 4.2 THEORETICAL STUDIES

### 4.2.1 Effect of a Surface Layer on Void Nucleation — W. G. Wolfer<sup>9</sup> and L. K. Mansur

Solute segregation and gas adsorption at free surfaces change the chemical composition of the topmost layers relative to the bulk composition. This fact is well known and originates from thermodynamic requirements that the surface and the layers beneath it will be enriched by constituents so as to minimize the surface free energy. Under irradiation, further segregation of solutes may take place by a dragging mechanism involving self-interstitials and/or vacancies. In any event, it is unlikely that the bulk composition and bulk properties will be homogeneous up to the surface for any solid material containing even small quantities of impurities and solutes.

Apart from lowering the surface free energy, surface segregation also changes the elastic properties of the surface region. This change alters radically the image interaction of self-interstitials with voids. This is demonstrated by the results shown in Fig. 4.2 for a void with a surface layer whose thickness is one-tenth the void radius. The shear modulus of the bulk matrix,  $\mu_m$ , is assumed to change abruptly at the interface to a value,  $\mu_s$ . If  $\mu_m = \mu_s$ , the image interaction is attractive and rapidly increasing as the void is approached. This case corresponds to voids without a surface layer. If  $\mu_s$  differs from  $\mu_m$ , the image interaction becomes repulsive before or behind the interface, depending on whether  $\mu_m < \mu_s$  or  $\mu_m > \mu_s$ . Thus, if  $\mu_s \neq \mu_m$ , the image interaction introduces an activation barrier, which is of the order of 0.1 eV for the self-interstitials.

In the absence of this surface barrier, the attractive image interaction causes small voids to have such a large preference for self-interstitials that void nucleation (but not bubble nucleation) becomes impossible. In Fig. 4.3, the free energy to form a cluster with  $N$  vacancies at  $T = 500^\circ\text{C}$  is shown as computed by the nucleation theory of Katz, Wiedersich, and Russell. The nucleation rates, critical cluster size, and maximum nucleation barrier are given in Table 4.2 together with other pertinent parameters. Curve A in Fig. 4.3 is obtained for voids with no surface barrier. As seen in Table 4.2 the corresponding nucleation rate is vanishingly small. However, voids with a modest surface barrier of only 0.01 eV are nucleating at a rate of  $7.9 \times 10^{13}$  voids  $\text{m}^{-3} \text{sec}^{-1}$ . Thus, the inevitable conclusion is that surface layers must form for void

---

<sup>9</sup>Present address Department of Nuclear Engineering, University of Wisconsin, Madison.

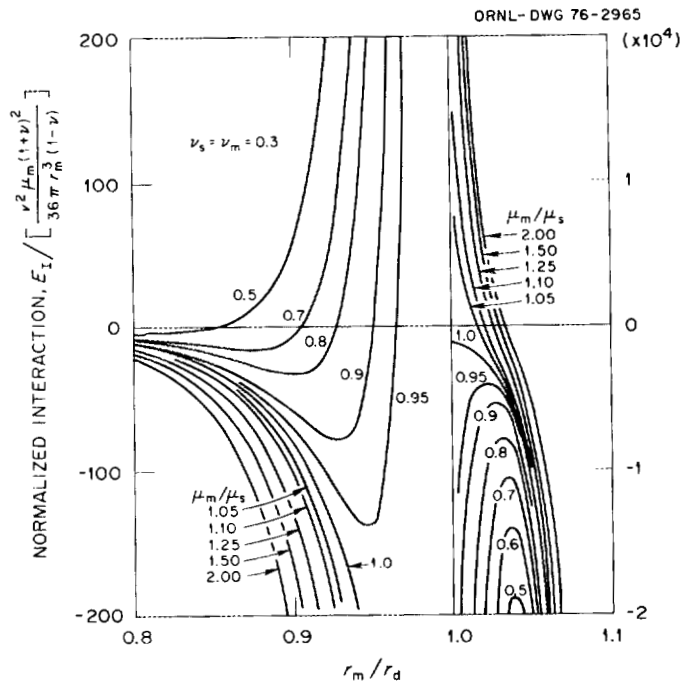


Fig. 4.2. Interaction Energy of a Center of Dilatation with a Coated Void, Showing Defect within as Well as Outside the Coating.

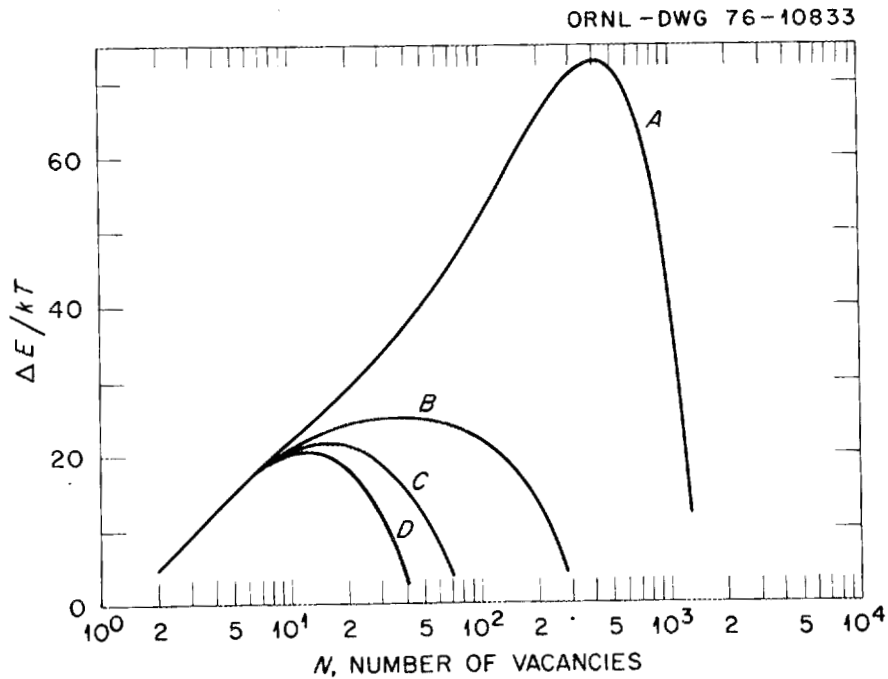


Fig. 4.3. Activation Energy for Void Nucleation with a Range of Elastic Energy Barriers.

Table 4.2. Parameters for Nucleation Calculations

Parameters Related to Specific Curves in Fig. 4.3:			
Curve	Surface Barrier (eV)	Critical Size (Number of Vacancies)	Nucleation Rate (Voids $m^{-3} sec^{-1}$ )
A	none	900	$1.49 \times 10^{-8}$
B	0.01	40	$7.88 \times 10^{13}$
C	0.05	20	$1.24 \times 10^{16}$
D	0.10	20	$1.42 \times 10^{16}$

General Parameters:	
Surface energy, $J/m^2$	0.8
Dislocation Bias Factor	1.5
Flux at $>0.1$ MeV, $n m^{-2} sec^{-1}$	$1 \times 10^{19}$
Irradiation temperature, K	873
Vacancy formation energy, eV	1.6
Vacancy migration energy, eV	1.4
Dislocation density, $m^{-2}$	$1 \times 10^{14}$

nucleation to be feasible. Impurity segregation can be markedly affected by alloy composition and minor additions of alloying elements. At present, it is not clear which impurity elements segregate at surfaces and which alloying elements inhibit segregation.

#### 4.2.2 The Effect of Stress-Induced Diffusion on Void Nucleation<sup>10</sup> -- W. G. Wolfer<sup>9</sup> and M. H. Yoo

Interstitials and vacancies interact with voids through the image force as well as forces induced by the surface stress and gas pressure in the void. These forces cause a drift of the point defects to the void and thereby give rise to a bias. The bias of voids increases with decreasing void radius. Thus, it mainly influences the nucleation of voids rather than their growth. We have incorporated this bias of voids into the nucleation theory developed by Katz, Wiedersich, and Russell, and studied the effect of surface energy, surface stress, temperature, dislocation bias, and gas pressure on the void nucleation. We find

<sup>10</sup> Abstract of pp. 458-73 in *Radiation Effects and Tritium Technology for Fusion Reactors* (Proc. Int. Conf., Gatlinburg, Tenn., Oct. 1-3, 1975) Vol. II, CONF-750989. Also ORNL/TM-5398 (May 1976).

that the critical void size is to a large extent determined by the condition that the interstitial bias of voids is equal to the bias of dislocations. Although the height of the activation barrier for nucleation depends on the bias factors also, it is affected more by surface energy, temperature, and, above all, gas content. Since the bias of dislocations is largest when produced by small dislocation loops, void nucleation depends critically on the evolution of the dislocation structure. To obtain nucleation rates as observed experimentally one of or preferably all the following conditions must be met: large dislocation bias, a reduction of the surface energy through contamination of the void surface, and a reduction of the void bias through impurity segregation.

#### 4.2.3 Some Aspects of Void and Loop Nucleation and Growth in the Vicinity of a Finite Dislocation Loop — W. A. Coghlan

The existence of a preferential attraction for interstitials by dislocations is the basis for all the existing models for void swelling in irradiated materials. This preferential attraction results from the strong interaction between the elastic stress field of the dislocation and the interstitial. The diffusion solution for these defects has a very nonhomogeneous distribution of point defects in the vicinity of the loop, reflecting the complicated nature of the stress field near the loop. In particular, vacancies are attracted into the region inside an interstitial loop, while interstitials are attracted to the outside regions. If a small vacancy cluster is formed in the region outside the loop, the increased concentration of interstitials will lead to annihilation of the cluster. Alternatively if a small vacancy cluster is formed above or below the center of the loop, the absence of interstitials and the surplus of vacancies in this region will encourage growth of the cluster.

This tendency for a neutral vacancy cluster to grow or an interstitial cluster to shrink can be described quantitatively by use of a parameter we call the growth function,  $D_V C_V - D_I C_I$ . In it,  $D_V$  and  $D_I$  are the diffusivities of the vacancy and interstitial, respectively, and  $C_V$  and  $C_I$  are their concentrations. Figure 4.4 is a number of contour plots of this growth function in the vicinity of faulted loops in aluminum. The top row of plots represents a loop placed in a region in a crystal where  $D_V C_V = D_I C_I$  far from the loop. This condition results in very rapid loop growth because of the preferential attraction for interstitials. The lower row of plots describes a loop in a region where the outer concentration of interstitials is such that the fluxes of vacancies and interstitials are the same and the loop will not grow. This condition will always result in the absence of other defect sinks.

In all the cases calculated, above the plane of an interstitial loop a region exists where void nucleation is much more likely because of the enhanced growth function. Also, the most likely region for interstitial clusters to form is outside the loop in the loop plane. Work is continuing to explore the consequence of these ideas in the overall description of defect nucleation and growth leading to void swelling.

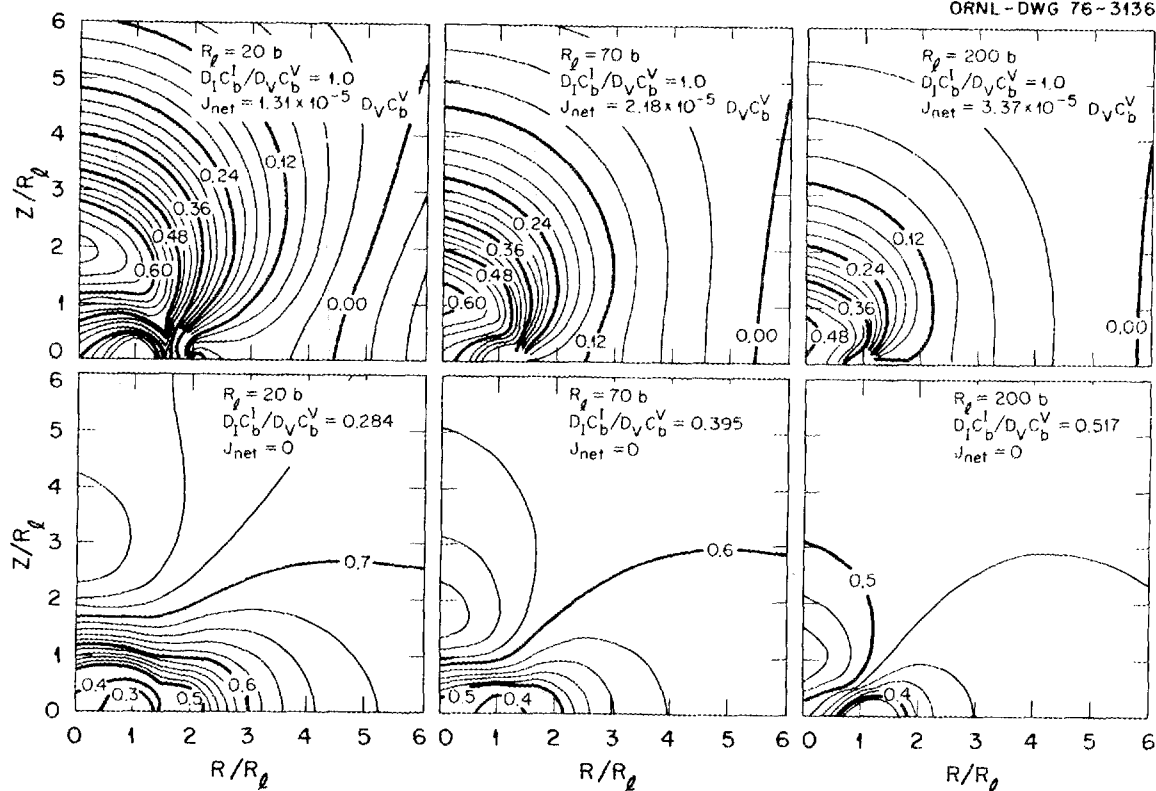


Fig. 4.4. Contours of the Growth Function for Interstitial Loops in Aluminum, Including Both the Size and Modulus Interaction. Each  $J_{net}$  value shown is the flux of interstitials minus the flux of vacancies.

#### 4.2.4 Evolution of Dislocation Density and Dose Exponents of Void Growth — L. K. Mansur

The question of the expected dose dependence of radiation-induced swelling is currently the object of renewed interest. By use of a continuum reaction rate theory to evolve the microstructure, predictions for dose dependences can be obtained.<sup>11,12</sup> In general this is done numerically. However, analytic predictions can be made for certain

<sup>11</sup>L. K. Mansur et al., "Void Coalescence and Growth in Metals under Irradiation," *International Conference on Defects and Defect Clusters in BCC Metals and Their Alloys* (held at National Bureau of Standards, Aug. 14-16, 1973), *Nuclear Metallurgy* Vol. 18, ed. by R. J. Arsenault, National Bureau of Standards, Gaithersburg, MD., 1973.

<sup>12</sup>L. K. Mansur et al., "Surface Reaction Limited Void Growth," pp. 272-89 in *Properties of Reactor Structural Alloys after Neutron or Particle Irradiation*, ASTM STP 570, American Society for Testing and Materials, Philadelphia, 1975.

limiting cases. The conditions for which limiting cases can be derived are often observed experimentally. These limiting equations also provide a means to explore the influence of important variables.

We have developed a table of dose dependences under a wide range of limiting conditions. For simplicity, voids, dislocations, and mutual annihilation are considered the only modes of point defect loss. As shown previously,<sup>13</sup> the dose dependence of the relative strength of these modes and the mechanism of point defect absorption at voids determine the dose dependence of swelling. Thus, several mechanisms of void growth, dose dependences of dislocation density, and relative strengths of sinks versus recombination are considered. Specifically the absorption at voids may be surface-reaction limited or diffusion limited for both vacancies and interstitials or surface-reaction limited for interstitials while diffusion limited for vacancies. The converse of course results in no void growth. For the dislocations several types of analytic behavior, each of which is an approximation to a large class of experimental observations, are allowed:

1. Dislocation loops growing with loop nucleation ceased -- often observed at low doses:

$$L = 4\pi\alpha(N_v N_l / 3\Omega)^{1/2} r_v^{3/2}$$

where

- $\alpha$  = lattice parameter,
- $\Omega$  = atomic volume,
- $N_v$  = number density of voids,
- $N_l$  = number density of loops,
- $r_v$  = average void radius,
- $L$  = dislocation density;

2.  $L$  is constant -- often observed at moderate to high doses;

3.  $L = 1/At$ ,

where  $A$  is a constant. Dislocations annihilate at a rate proportional to the square of their instantaneous density. This is observed in soft materials at higher doses.

Finally, either sinks or mutual recombination may be the dominant mode of point defect loss, and for either of these situations either sink may be the dominant absorber. The predicted dose dependences are given in Table 4.3.

---

<sup>13</sup>L. K. Mansur, K. Farrell, and J. O. Stiegler, "Comparison of Void Growth Kinetics in Irradiated Stainless Steels and Pure Metals," *Trans. Am. Nucl. Soc.* 21: 163-64 (1975).

Table 4.3. Dose Exponents of Void Growth for Limiting Cases and Different Mechanisms of Point Defect Absorption at Void

Dominant Sink	Recombination Importance	Value of $n$ in $\Delta V/V \propto (\text{dose})^n$ for Each Model		
		Dislocation Loop Growth	Constant Dislocation Density	Dislocation Mutual Annihilation
<u>Both Defects Diffusion Controlled</u>				
Dislocation	Minor	$6/7^{a,b}$	$3/2^c$	3
Dislocation	Dominant	$3/2^b$	$3/2^b$	$3/2$
Void	Minor	$6/5^b$	$3/4^c$	0
Void	Dominant	$2^{b,d}$	$1^{b,d}$	$\Delta V/V \propto \ln(\text{dose})^d$
<u>Both Defects Surface Controlled</u>				
Dislocation	Minor	$6/5^a$	$3^e$	6
Dislocation	Dominant	3	3	3
Void	Minor	$6/7$	$3/5^e$	0
Void	Dominant	2	1	$\Delta V/V \propto \ln(\text{dose})$
<u>Interstitial Surface Controlled, Vacancy Diffusion Controlled</u>				
Dislocation	Minor	$6/7$	$3/2$	3
Dislocation	Dominant	$3/2$	$3/2$	$3/2$
Void	Minor	$6/7$	$3/5$	0
Void	Dominant	2	1	$\Delta V/V \propto \ln(\text{dose})$

<sup>a</sup>Worked out previously by A. D. Brailsford, *Metall. Trans. A* 7A: 333 (1976).

<sup>b</sup>Worked out previously by A.J.E. Foreman, pp. 121-32 in *Proceedings of the British Nuclear Energy Society Conference on Voids Formed by Irradiation of Reactor Materials, held at Reading University, March 24 and 25, 1971*, ed. by S. F. Pugh, N. H. Loretto, and D.I.R. Norris, British Nuclear Energy Society.

<sup>c</sup>Standard result.

<sup>d</sup>Worked out previously by S. B. Fisher and K. R. Williams, *Radiat. Eff.* 14: 165 (1972).

<sup>e</sup>Worked out previously by L. K. Mansur, K. Farrell, and J. O. Stiegler, *Trans. Am. Nucl. Soc.* 21: 169 (1975).

Several observations can be based on this table:

1. This table provides the answer to the question "What is the expected dose dependence of swelling?" A wide range of dose dependences is possible. The regime, which can be determined from measured dislocation and void parameters, determines the precise value.

2. If experimental measurements of dislocation density with dose as well as void size distributions are available, the mechanisms of void growth can be established. Thus, surface-reaction-limited kinetics has been deduced for voids in stainless steels.<sup>11,12</sup>

3. During a single irradiation of long enough duration, several regimes will be traversed. The usual sequence expected in an annealed material is recombination dominant to recombination minor, dislocations dominant to voids dominant, and dislocation loop growth to dislocation density constant.

#### 4.2.5 Growth Kinetics of Frank Loops in Nickel during Electron Irradiation — M. H. Yoo and J. O. Stiegler

Nickel foil specimens of thickness 0.44  $\mu\text{m}$  prepared from zone-refined high purity grade were irradiated at temperature 725 K with 650-keV electrons in a Hitachi high-voltage electron microscope. The formation of defect clusters was observed during irradiation, and they were identified to be interstitial-type Frank loops. Their number density was essentially constant at  $5 \times 10^{20}/\text{m}^3$  during irradiation, and the average growth rate of the loops was proportional to a smaller power of the irradiation time than unity ( $n = 0.78$ ) under a constant irradiation, which gives the defect generation rate of  $6.4 \times 10^{-5}$  dpa/sec.

Based on earlier works<sup>14,15</sup> (see also Sect. 4.2.2), a model is developed for the growth kinetics of dislocation loops during irradiation. A method of determining the "sink strength parameter,"  $\beta$ , from a given micrograph is introduced. We find that for the present model to predict the observed average loop growth rate, the sink strength ratio,  $\beta_i/\beta_v$  (i.e., the ratio of the sink strength for interstitials to that for vacancies), must be an increasing function of the average sink size. This is contrary to an expectation based on the calculated results of so-called "bias factors" of dislocation loops.<sup>15-17</sup> Since the previous calculations were made for the case of one sink in an infinite medium, effects of sink size, geometry, and number density on the effective capture radius will be investigated.

---

<sup>14</sup>M. H. Yoo, W. H. Butler, and L. K. Mansur, "Defect Annealing and Clustering in the Elastic Interaction Force Field," pp. 804-11 in *Fundamental Aspects of Radiation Damage in Metals* (Proc. Int. Conf. Gatlinburg, Tenn., Oct. 6-10, 1975) Vol. 2, CCNF-751006P2.

<sup>15</sup>M. H. Yoo and W. H. Butler, "Steady State Diffusion of Point Defects in the Interaction Force Field," to be published in *Physica Status Solidi (b)*.

<sup>16</sup>W. G. Wolfer and M. Ashkin, "Stress Induced Diffusion of Point Defects to Spherical Sinks," *J. Appl. Phys.* 46: 547-57 (1975).

<sup>17</sup>W. A. Coghlan and M. H. Yoo, "The Diffusion of Point Defects to Finite Dislocation Loops," (to be published).

When only interstitial loops are present, more vacancies than interstitials must be lost to the foil surfaces for the loops to grow. The model predicts that the loop growth rate increases from zero at the foil surface to a maximum value near the surface and diminishes to a small value at the midthickness. To test the model the depth-dependent loop sizes at increasing electron fluences will be determined stereoscopically.

#### 4.2.6 Transient and Steady-State Diffusion Solution for Point Defects in a Stress Field<sup>18</sup> — W. A. Coghlan

The exact solution of the three-dimensional diffusion of point defects in a stress field is important in many areas of materials science, including phase transformations, radiation damage, deformation, and fracture. Analytical transient and steady-state solutions are intractable except for some very simple cases. Computer simulation offers a method to solve this problem for a large variety of initial and boundary conditions. A straightforward numerical method using a difference equation to replace the governing differential equation has been developed to simulate the transient behavior of the point defect concentration field. The method allows easy display of the results and simple modification to time- and position-dependent boundary and initial conditions. It was applied to find the time dependence of the vacancy concentration profile and defect current to a  $5b$ -radius dislocation loop in quenched aluminum. The calculation of the interaction between the defects and the internal stress gradient includes both the size and modulus effects of elastic interaction.

#### 4.2.7 Diffusion of Point Defects to a Toroidal Sink in a Finite Medium — W. A. Coghlan

Diffusion of defects to a toroidal or disk-shaped sink is important for many metallurgical problems, including dislocation loop growth in radiation damage, disk-shaped precipitate growth, and annealing of faulted and unfaulted vacancy loops. An analytical solution available<sup>19</sup> for some time describes the defect flux to such a sink in an infinite medium. This solution is inadequate for many applications because in many physical problems the sinks are much too dense and the diffusion fields overlap. We have extended the analytical solution to include an outer spherical surface at a constant concentration at a fixed radius

---

<sup>18</sup>Abstract of pp. 166-76 in *Proceedings of Conference on Computer Simulation for Materials Application* (Held April 19-21, 1976, Gaithersburg, Maryland) National Bureau of Standards, Gaithersburg, Md., 1976.

<sup>19</sup>D. N. Seidman and R. W. Balluffi, "On the Annealing of Dislocation Loops by Climb," *Phil. Mag.* 13: 649-54 (1966).

from the sink and also have found a simple empirical expression that extends the usefulness of a simplified expression for the solution over a wider range of geometric parameters.

#### 4.2.8 Morphologies of Precipitates on Voids and Loops Resulting From Irradiation-Induced Segregation — W. A. Coghlan

Segregation of solute atoms to voids and dislocation loops in materials undergoing irradiation appears to be a very general phenomenon and is thought to play a major role in controlling the swelling behavior of the low-swelling stainless steels. When this segregation reaches a high enough level near these voids and loops, precipitate particles are often found on the surface of the voids and along the dislocations. Sometimes the precipitate is found as continuous sheets on the voids and sometimes as discrete particles near the voids. Similarly the precipitate along dislocations sometimes breaks up into a string of separate particles.

We have begun an investigation into the stable morphologies for these precipitates based on surface energy considerations and have found that a toroidal precipitate particle will decompose into a string of spheres if the loop diameter is about 20 times the minor diameter of the toroid. Work is continuing to consider the stable morphology of precipitates on or near void surfaces and also the role that kinetic phenomena play in developing these morphologies in both voids and loops.

#### 4.2.9 Distributions of Point Defects in Bounded Media Under Irradiation<sup>20</sup> — M. H. Yoo and L. K. Mansur

The steady-state diffusion profiles of vacancies and interstitials in a semi-infinite medium and in a foil under irradiation at elevated temperatures are calculated by solving the general rate equations. The calculations include spatial variation of defect production and of size and number distributions of internal sinks, preferential absorption of point defects at internal sinks, thermal equilibrium vacancies, and the image interaction of point defects with free surfaces.

Numerical calculations are made for nickel in the temperature range  $0.3T_m$  to  $0.5T_m$  ( $T_m$  is the absolute melting temperature) during irradiation by heavy ions in an accelerator and by electrons in a high-voltage electron microscope. Conclusions of the present calculations are as follows: (1) the effect of the image elastic interaction of point defects with a free surface is relatively unimportant at  $T \geq 0.3T_m$ , (2) the peaks of free defect concentration profiles do not coincide with that of the ion energy deposition in a semi-infinite medium bombarded by self-ions, (3) pronounced spatial fluctuations of the defect diffusion

<sup>20</sup> Summary of a talk presented at 105th AIME Annual Meeting, Las Vegas, Nev., Feb. 22-26, 1976. Abstract published in *J. Met.* 27: A60 (1975), also accepted for publication in *Journal of Nuclear Materials*.

profiles may result directly from the nonuniform sink size and number distributions, (4) the additional effect of thermal equilibrium vacancies on the defect diffusion profiles is relatively important at  $T \geq 0.5T_m$  but not at  $T = 0.42T_m$ , and (5) the effect of biased internal sinks on defect diffusion profiles is the most pronounced and important one, especially when defects are predominantly annealed by loss to the internal sinks.

4.2.10. The Use of Pressurized Eccentric Tubes to Study the Effect of Hydrostatic Stress on Swelling — W. G. Wolfer<sup>21</sup> and T. C. Reiley

It has recently been postulated<sup>22</sup> that the rate of swelling under neutron irradiation is given by  $(\Delta\dot{V}/V) = (\Delta\dot{V}/V)_0 (1 + P\sigma_H)$ , where  $(\Delta\dot{V}/V)_0$  is the stress-free swelling rate,  $P$  is a constant and  $\sigma_H$  is the hydrostatic pressure. This stress dependence is also reflected in the associated expression for the radiation-induced deformation rate:

$$\dot{\epsilon}_{ij} = \delta_{ij}(\Delta\dot{V}/V)/3 + 3S_{ij}[C + D(\Delta\dot{V}/V)]/2 ,$$

where  $\delta_{ij}$  is the Kronecker delta,  $C$  and  $D$  are constants, and  $S_{ij}$  is the deviatoric stress tensor. The value of  $P$ , the coefficient of the stress effect on swelling, has been difficult to measure experimentally, even though it may be of fundamental significance in the description of reactor materials.

A technique outlined here allows the measurement of  $P$ , using a pressurized eccentric tube; that is, a tube with inner and outer surfaces having different centers of revolution. As the tube is pressurized it deforms elastically with the thin-walled side convex. During the irradiation of this pressurized tube in a fast-neutron flux, stress-enhanced swelling leads to a further increase of the curvature. The curvature  $\kappa_0$  due to the elastic loading is given by<sup>23,24</sup>

$$\kappa_0 = (1 - 2\nu)p_0K(\rho, \epsilon)/Er_1 , \quad (1)$$

<sup>21</sup>Present address Department of Nuclear Engineering, University of Wisconsin, Madison.

<sup>22</sup>W. G. Wolfer, M. Ashkin, and A. Boltax, "Creep and Swelling Deformation During Fast-Neutron Irradiation," pp. 233-58 in *Properties of Reactor Structural Alloys After Neutron or Particle Irradiation*, ASTM STP 570, American Society for Testing and Materials, Philadelphia, 1975.

<sup>23</sup>E. Weinel, "Über einige ebene Randwertprobleme der Elastizitätstheorie," *Z. Angew. Math. Mech.* 17: 276-87 (1937).

<sup>24</sup>W. Wuest, "Theorie des Hochdruckmessrohres mit Ausmittiger Bohrung," *Ingenieur Archiv.* 19: 12-21 (1951).

where  $p_0$  is the gas pressure,  $E$  the Young's modulus,  $\nu$  the Poisson's ratio,  $r_1$  the outer radius of the tube, and  $K$  is a function of the ratio  $\rho = r_0/r_1$  (where  $r_0$  is the inner radius of the tube) and the eccentricity parameter  $\epsilon = e/(r_1 - r_0)$  (where  $e$  is the distance between the centers of the two cylindrical surfaces). The function  $K(\rho, \epsilon)$  is shown in Fig. 4.5. After irradiation and depressurization, the residual curvature is given<sup>25</sup> by

$$\kappa_p = \rho_0 P (\Delta V/V)_0 K(\rho, \epsilon) / r_1 \quad . \quad (2)$$

It appears that the residual curvature could be increased by increasing the pressure  $p_0$ . However, a practical limit is dictated by the yield stress of the material used. Plastic deformation during pressurization would not directly produce a curvature (if volume is conserved during plastic deformation), but it would introduce nonuniform cold-working and lead subsequently to a nonuniform stress-free swelling. It should be noted that under these conditions cold-working would be largest in the thinnest portion of the tube, resulting in a curvature opposite that produced by stress-enhanced swelling.

<sup>25</sup>W. G. Wolfer and T. C. Reiley, paper in preparation.

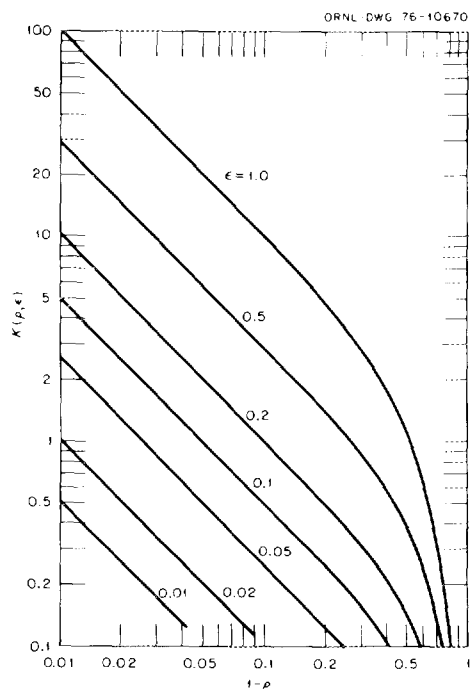


Fig. 4.5. The Factor  $K(\rho, \epsilon)$  Versus  $1 - \rho$ , where  $\rho = r_0/r_1$ , for Different Values of  $\epsilon = e/(r_1 - r_0)$ .

The maximum hoop stress occurs on the inside at the thinnest position of the tube. Assuming that yielding is governed by the Tresca condition, and that the stresses everywhere are below the yield point, then

$$\sigma_{\max} \leq \sigma_{\text{yield}}(T), \quad (3)$$

where

$$\sigma_{\max} = p_0 F(\rho, \epsilon), \quad (4)$$

and  $F$  is a function of the geometrical parameters  $\rho$  and  $\epsilon$  only. Hence, in terms of the maximum stress, the residual curvature is

$$\kappa_r = \sigma_{\max} P(\Delta V/V)_0 M(\rho, \epsilon)/r_1, \quad (5)$$

where  $M = K/F$  is shown in Fig. 4.6. It is seen that  $M$  is maximized for  $\epsilon \cong 0.5$  and  $(r_1 - r_0) \lesssim 0.4 r_1$ .

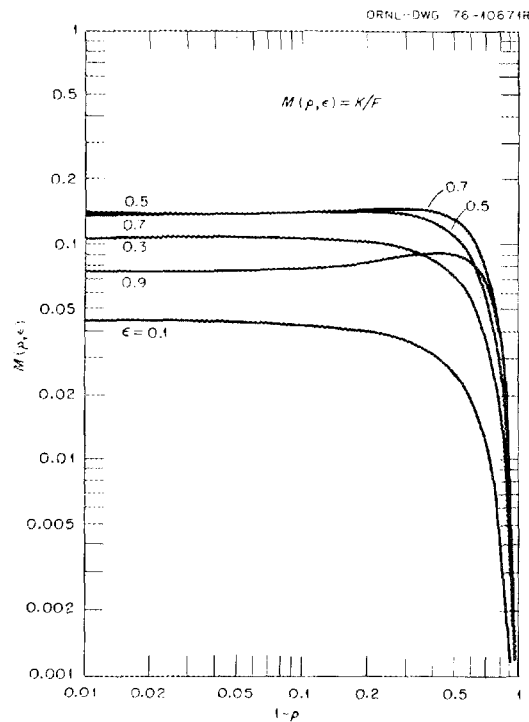


Fig. 4.6. The Factor  $M(\rho, \epsilon) = K(\rho, \epsilon)/F(\rho, \epsilon)$  Versus  $1 - \rho$  where  $\rho = r_0/r_1$ , for Different Values of  $\epsilon = e/(r_1 - r_0)$ .

It is convenient to measure the lateral deflection of the tube from the straight axis rather than measure the curvature. If  $\delta$  denotes the deflection and  $L$  the length of the tube, then

$$\delta/L = \kappa_r L/2 = LM(\rho, \epsilon) \sigma_{\max} P(\Delta V/V)_0 / 2r_1 . \quad (6)$$

For given values of  $\rho$  and  $\epsilon$ , the deflection per unit length increases with the ratio of length to diameter of the tube.

Tubes have been prepared from a high-swelling, high-purity heat of type 316 stainless steel, for which stress-free swelling data are available. These tubes have a length of 47 mm, a diameter of 5.8 mm, and geometric parameters  $1 - \rho = 0.24$  and  $\epsilon = 0.5$ . They will be placed in EBR-II in the coming year. (See Sect. 4.3.4).

### 4.3 FACILITY, EQUIPMENT, AND EXPERIMENT DEVELOPMENT

#### 4.3.1 The Simulation of Radiation-Enhanced Creep - T. C. Reiley, R. L. Auble,<sup>26</sup> and M. G. Duncan<sup>27</sup>

At present, our understanding of the enhancement of creep during neutron irradiation is limited. Some of these limitations stem directly from the difficulty and expense in performing instrumented, in-reactor creep experiments. The Oak Ridge Irradiation Creep Facility is being built for the simulation of neutron-irradiation creep through the use of light ion beams (e.g., 60-MeV alpha particles). Previous experiments by Harkness et al.<sup>28</sup> and Hendrick et al.<sup>29</sup> have demonstrated the feasibility of this simulation technique. This approach allows the relatively convenient study of relationships between structure and strain rate and transient behavior necessary to corroborate current theoretical treatments. Also, the Oak Ridge facility is to be used for testing pure materials and developmental alloys, in addition to reactor candidate alloys.

Experimental techniques for the optimization of beam extraction, the use of specimen thermocouples (0.02 mm diam), the improvement of the temperature control system, the operation of strain measuring devices, and the monitoring of beam current with a Langmuir probe device were studied in three cyclotron runs during this period. All these experimental features showed acceptable behavior under test conditions and

---

<sup>26</sup>Physics Division.

<sup>27</sup>Consultant, University of Tennessee.

<sup>28</sup>S. D. Harkness, F. L. Yaggee, and F. V. Wolfi, *Simulation of In-Reactor Creep of Type 304 Stainless Steel*, ANL-7883 (March 1972).

<sup>29</sup>P. L. Hendrick et al., "Simulation of Irradiation-Induced Creep in Nickel," *J. Nucl. Mater.* 59: 229 (1976).

are being incorporated into the apparatus. The fabrication of the apparatus is nearly finished, with the first irradiation creep experiment planned toward the end of calendar year 1976. The data handling system has been designed and is compatible with the CAMAC system being implemented at ORIC. Specimens have been prepared for testing (and for preirradiation in EBR-II) from the following 12 materials: Ni, Nb, Nb-1% Zr; 20%-cold-worked type 316 stainless steel; a "high-purity" high-swelling type 316 stainless steel; two developmental low-swelling alloys, D9 and D11; Nimonic PE16; Inconel 706; a nickel-base alloy M813; Zircaloy-2; Zircaloy-4.

4.3.2 The Oak Ridge CN Van de Graaff Facility for Heavy Ion Radiation Damage Studies<sup>30</sup> — M. B. Lewis, F. K. McGowan,<sup>26</sup> C. H. Johnson,<sup>26</sup> and M. J. Saltmarsh<sup>26</sup>

The ORNL CN Van de Graaff has been fitted with a model 910 Danfysik heavy-ion source for production of 4-MeV nickel ions. The source produces NiCl<sub>2</sub> gas by reacting CCl<sub>4</sub> with powdered nickel. The dissociation into Ni<sup>+</sup> ions occurs by an electron current contained in a magnetic field. The ions are extracted from a 1 mm<sup>2</sup> aperture, and the Ni<sup>+</sup> ions are then separated from other ions by a Wien velocity filter. After acceleration, the charge state of the Ni<sup>+</sup> ions is increased by passage through low-pressure argon gas. These ions are then energy and charge state analyzed by a 90° bending magnet. By different adjustments of the velocity filter and bending magnet, we learned that other useful ion species such as Cl<sup>+</sup>, O<sup>+</sup>, and C<sup>+</sup> could be extracted without further modifications of the ion source.

The beam is then focused uniquely by an especially designed electrostatic lens.<sup>31</sup> This lens radially deflects the Gaussian tail region of the beam into its more central portion, which is unchanged by the lens' field-free center. The cross-sectional diameter of the beam is reduced to about 15 mm, while the cross-sectional area is made uniform in intensity.

The beam is then collimated by a square aperture of 100 mm<sup>2</sup> just upstream from the target. The profile of the beam is monitored both before and after the special lens with Physicon model MS-10 vane profilometers. During a run the profile data are recorded and averaged by a Northern MS-570 signal averager. Using these methods, 1- and 2-μA beams of <sup>58</sup>Ni ions uniformly spread over a square centimeter area have been measured at the target site.

---

<sup>30</sup>Summary of pp. 15-40 in *Proc. Symp. Experimental Methods for Charged-Particle Irradiations* (Gatlinburg, Tenn., Sept. 30, 1975), CONF-750947.

<sup>31</sup>C. H. Johnson, "A Ring Lens for Focusing Ion Beams to Uniform Densities," *Nucl. Instrum. Methods* 127: 163-71 (1975).

#### 4.3.3 Experiments with the ORNL Heavy-Ion Bombardment Facility -- N. H. Packan, M. B. Lewis, F. V. McGowan,<sup>26</sup> and G. F. Wells<sup>26</sup>

During calendar year 1975, the 5-MV Ion Bombardment Facility functioned efficiently, yielding in 136 separate bombardment runs a total of 10,367 dpa in 359 hr of beam on target -- an average damage production rate of 29 dpa/hr. All experiments were conducted with a beam of 4.0-MeV  $^{58}\text{Ni}^{2+}$  ions, directed upon either an array of four disk specimens destined for transmission electron microscopy or else a stacked series of up to 15 specimens whose relative swelling behavior was to be assessed by step-height measurements. Doses per run ranged from the very low 0.2 to 1 dpa range up to 350 dpa; a bombardment to 600 dpa was carried out in early 1976. Bombardment temperatures ranged from room temperature to 700°C. Experiments supported by the Division of Physical Research used 60% of the total beam time, while alloy development work (Division of Reactor Development and Demonstration) accounted for 27% and outside users, 13%. The last category, in calendar year 1975, comprised five 250-dpa bombardments for a group from the Westinghouse Advanced Reactors Division and five room-temperature irradiations for J. Narayan of the ORNL Solid State Division.

One of the materials science experiments was a series of 1-dpa bombardments on pure nickel, performed to establish a correlation with neutron irradiation; the results are discussed in Sect. 4.1.3. Another experiment recently undertaken is an investigation of the effects, if any, of oxygen on void formation in one high-swelling and one swelling-resistant stainless steel. The method to produce oxygen (or carbon) beams employs an argon gas stripper already used to extract nickel ions. Carbon dioxide is fed directly into the arc chamber of the Van de Graaff ion source. The most plentiful  $\text{CO}^+$  ions are accelerated to  $\sim 1-4$  MeV. These ions are then dissociated by the stripper into  $\text{C}^+$ ,  $\text{C}^{2+}$ ,  $\text{O}^+$ ,  $\text{O}^{2+}$ , ... and energy-analyzed with the 90° bending magnet. The energy of the dissociated ions is  $MV/28$  where  $M$  is the C or O mass and  $V$  is the Van de Graaff potential. The range of these ions overlaps the range of 4 MeV Ni, so that O and C can be implanted before a nickel irradiation.

The 5-MV Ion Bombardment Facility is scheduled to undergo a number of significant modifications in the coming months. A new, multiple-furnace specimen chamber has been fabricated and tested; it will be installed as soon as the current series of bombardments is concluded. Besides permitting up to six runs to be made before we have to break vacuum, the new chamber will provide much improved knowledge of the temperature of every specimen, using both thermocouples and an infrared pyrometer. Most of the beam line will be replaced by larger diameter stainless steel piping having only ultrahigh-vacuum joints. Existing diffusion pumps on the beam line as well as the ion pump on the damage chamber are to be replaced by cryopumps, so that better vacuum throughout the system may be maintained.

Finally, before the end of calendar year 1976 the capability for performing simultaneous injection of helium together with heavy-ion bombardment should be realized. A 0.4-MV Van de Graaff has been acquired and installed. In the next few months, an ion optics system will be constructed. It will maintain a uniform helium beam over the array of

specimens while at the same time cyclically varying the voltage by about a factor of 2 to distribute the helium throughout the damage volume of a specimen. The helium injection rate during a typical several-hour ion bombardment should be adjustable over a range of perhaps 3 to 10,000 ppm, to allow the simulation of high-helium-generation conditions such as the fusion reactor environment as well as the slower generation appropriate for LMFB simulation.

#### 4.3.4 EBR-II Row 7 Irradiation Experiment -- M. L. Grossbeck

This experiment is a joint effort between programs at ONRL, HEDL, Battelle Pacific Northwest Laboratories, the University of Cincinnati, LASL, and Cornell University. The work is sponsored by ERDA Divisions of Reactor Development and Demonstration, Magnetic Fusion Energy, and Physical Research. The DPR-sponsored study consists of a series of experiments designed to provide information on the mechanisms of irradiation creep, irradiation-induced precipitation, segregation of solute elements, fracture mechanisms in irradiated materials, and the effect of stress on swelling.

Nine capsules will be placed within a standard hexagonal EBR-II subassembly. Three capsules will be filled with sodium and sealed but will be in thermal contact with the reactor coolant and will, therefore, operate at temperatures between 650 and 675 K. Three capsules will be heat-pipe temperature controlled and will be placed directly above and welded to three gas-gap-controlled capsules. The heat pipes have been designed by LASL personnel and are presently used by several EBR-II experimenters (LASL, NRL, and HEDL); thus feasibility of their use has been demonstrated. The temperature control capability of a heat pipe is shown in Fig. 4.7. The heat pipe capsules will operate at 850, 900, and 975 K. The gas-gap capsules have a specimen chamber surrounded by a gap containing low-pressure inert gas to conduct heat to the reactor coolant. The feasibility of the gas-gap concept has been demonstrated in several EBR-II experiments (e.g., X-034, X-035, X-100, and X-100A). Two of the capsules are designed to operate at 800 K, the remaining one at 850 K.

Specimens will be positioned in racks with provision for irradiation-induced swelling. Since refractory metals will be included, each of the six capsules operating above reactor coolant temperature will contain high-purity zirconium foil as a getter for oxygen.

Plans are for inclusion of the capsules in a modified M-1A subassembly for irradiation in the 7N4 position of EBR-II. Irradiation of approximately 18 months is planned to give a neutron fluence on the reactor midplane of about  $4 \times 10^{26}$  n/m<sup>2</sup> (>0.1 MeV). Adequate neutron fluence dosimeters and temperature monitors have been included in the experiment.

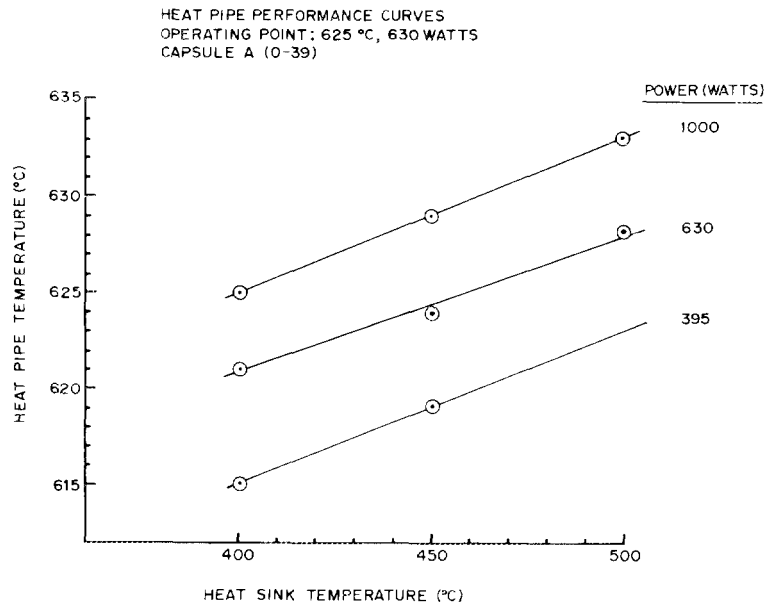


Fig. 4.7. Performance Curves for Heat Pipes.

#### 4.3.4.1 Precipitation of Solute Elements During Irradiation —

J. M. Leitnaker and D. N. Braski

Swelling resistance of many solid-solution (and possibly precipitation hardened) alloys is imparted by solute elements. Many of the elements known to be important are very reactive (e.g., Ti, C, Si), and the distribution of these elements between the matrix and second phases will change with time and may depend on fluence. Partitioning of elements between the matrix and second-phase precipitates will be examined by irradiating small slugs of the alloys of interest. Following irradiation, precipitates will be extracted, and the amount and composition of second phases and the composition of the matrix will be determined. Results will be compared with thermal control samples. The experiments will give quantitative information on precipitation kinetics and precipitate composition. This information will be of significant value in understanding swelling behavior during neutron irradiation. Alloys to be considered are variations of type 316 stainless steel with additions of titanium and silicon. Specimens will be irradiated at all five temperatures in both high- and low-flux positions.

#### 4.3.4.2 Irradiation Creep Simulation — T. C. Reiley

An apparatus has been designed and is being constructed to investigate irradiation creep phenomena by irradiating samples with high-energy alpha particles (60 MeV) produced by Oak Ridge Isochronous

Cyclotron (ORIC). To examine the effect of accumulated fluence on creep behavior, samples of developmental stainless steel alloys, nickel, niobium, Zircaloy-2, Zircaloy-4, and nickel-base alloys will be neutron irradiated before testing in the simulation experiments.

Preirradiation is necessary to avoid the microstructural transients that would occur upon testing unirradiated material. Eight specimens will be irradiated in a swelling-driven holder using a high-swelling type 316 stainless steel. This will remove structural transients associated with stress.

#### 4.3.4.3 Segregation of Solute Elements to Grain Boundaries — R. E. Clausing and C. L. White

Irradiation-induced segregation of solute elements is now an experimentally and theoretically established phenomenon. Segregation to grain boundaries could be playing an important role in the observed grain-boundary embrittlement of austenitic stainless steels. This phenomenon could also be important in other alloy systems that might be used in advanced LMFBR fuel systems and fusion reactor first walls. Irradiation-induced segregation can be effectively studied by Auger spectroscopy. Samples are fractured *in situ* in a modified Auger spectrometer, and the fracture surface is analyzed to detect segregation.

#### 4.3.4.4 Correlation of Neutron Damage with Ion Damage — N. H. Packan

Previous experiments have studied the effects of ion bombardment as well as low-fluence neutron irradiation. The purpose of this irradiation is to extend the existing correlation data to a higher damage level.

Eight specimen disks are to be irradiated at each of six temperatures. Sets of specimens will be placed at the top and at the bottom of the capsules in thermal contact with reactor coolant in order to achieve an additional irradiation temperature. Five disks of each set are to be zone-refined nickel; the remaining will be P7 (high-purity type 316 stainless steel). All specimens will be fully annealed.

Upon completion of irradiation, the specimens will be thinned for transmission electron microscopy.

#### 4.3.4.5 Swelling in Neutron Irradiated Pure Binary and Ternary Alloys — L. K. Mansur

The variation in radiation-induced microstructural response with changes in composition will be investigated in the Fe-Ni-Cr ternary system. Recent experiments at high dose under ion bombardment have produced extreme variations in swelling with changes in composition. The present experiments will determine the possible correlation of these

results with those obtained under neutron irradiation. In addition, parametric values of quantities to be used in theoretical predictions of high-dose neutron irradiation behavior will be determined.

#### 4.3.4.6 Effect of Stress on Swelling — W. G. Wolfer<sup>32</sup> and T. C. Reiley

The objective of this test is to detect a possible effect of stress on swelling or whether volume is not conserved in irradiation creep. Pressurized eccentric tubes made of type 316 stainless steel will be irradiated at 800 and 850 K. If either effect exists, the pressurized eccentric tubes will become bent during the irradiation. The accuracy with which a small curvature of the bent tube can be measured allows a detection of the possible effect even if it contributes only about 10% to the total stress-induced deformation (i.e., deformation excluding stress-free swelling). In the absence of any stress effect, the tube will remain straight after depressurization.

#### 4.3.4.7 Neutron-Induced Defect Characterization of Several BCC Metals and Alloys — J. Moteff,<sup>33</sup>

This experiment has the following objectives: (1) comparison of irradiation-induced defects in molybdenum with three different levels of interstitial impurities and (2) correlation of defect characteristics formed at high fluence ( $4 \times 10^{26}$  n/m<sup>2</sup>) with those of samples previously irradiated at low fluence ( $1 \times 10^{26}$  n/m<sup>2</sup> in EBR-II Row 7) as well as with ion-bombardment specimens. Characterization will be made with TEM observations.

Niobium and Nb-1% Zr with various oxygen contents irradiated by ion bombardment by B. A. Loomis (ANL) and neutron-irradiated material will also be studied with transmission microscopy.

#### 4.3.4.8 Atom-Probe, Field-Ion Microscope Investigation of Radiation Damage in Refractory Metal Alloys — D. N. Seidman,<sup>34</sup>

The atom-probe can examine the microstructural features and determine the chemical composition of a specimen on an atomic scale and will be used to study the general area of the interaction of point defects with impurities.

---

<sup>32</sup>Present address Department of Nuclear Engineering, University of Wisconsin, Madison.

<sup>33</sup>University of Cincinnati.

<sup>34</sup>Cornell University.

The goals of the experiments involving materials scheduled for irradiation are:

1. To elucidate the effect of titanium, zirconium, and rhenium on void formation in molybdenum-base alloys. In particular it is planned to determine if radiation induces segregation of any of these elements to voids.
2. To investigate the formation of radiation-induced phase changes. Specifically it is planned to determine the density, particle size, morphology, and chemical composition of the radiation-induced precipitates in a series of tungsten-rhenium alloys.
3. To determine the mechanism responsible for the suppression of swelling in iron-based alloys due to the addition of silicon. Among the numerous possible effects involving the silicon, changes in the spatial distribution of the silicon and trapping of gaseous impurities at the silicon will be studied.
4. To determine how well electron and ion irradiations simulate fast neutron damage by comparing the results obtained on the specimens irradiated in EBR-II with electron and ion-irradiated specimens.

#### 4.3.4.9 Status of Experiment

The design of the experiment has been completed. All capsule parts and specimen racks have been fabricated except an outer housing tube, which is now being machined. The hazards analysis is now completed. The experiment is expected to be shipped to EBR-II in September.

#### 4.3.5 Analytical Electron Microscopy -- R. W. Carpenter

The application of analytical electron microscopy to phase transformations and radiation damage in solids is presently being investigated with a JEOL-100 C transmission electron microscope equipped to operate in the following modes:

1. Scanning transmission electron imaging (STEM), for examination of the internal defect structure in electron transparent specimens;
2. scanning electron microscopy using secondary electron images (SEM), for examination of the surface topography of various specimens;
3. transmission electron microscopy (TEM), the imaging mode familiar to all electron microscopists;
4. the following diffraction modes:
  - a. convergent beam diffraction (static or dynamic),
  - b. micro-micro-diffraction,
  - c. Grigson diffraction,<sup>35</sup>
  - d. selected area diffraction,
  - e. small angle diffraction;

---

<sup>35</sup>C.W.B. Grigson and P. I. Tillet, "On Scanning Electron Diffraction, II," *Int. J. Electron.* 24: 101-38 (1968).

5. energy-dispersive x-ray chemical analysis for elements heavier than sodium.

Other imaging modes are also possible. Some very interesting results have been obtained so far. The STEM imaging mode can be used to measure the relative intensity distribution across features in the image directly from the photomultiplier tube output. This will be useful for comparing calculated contrast profiles with actual images; an example is stacking fault fringes, or fringes associated with precipitate particles. The Grigson coils, located slightly below the projector lens, have enabled the electronic measurement of intensity distribution in diffraction patterns. The output from these measurements is similar to that from an x-ray diffractometer, obviously much more convenient for measurement of intensity than the usual photographic recording method. Preliminary results indicate that the Grigson technique can also be used to measure the intensity distribution in TEM images electronically rather than relying on densitometer traces from photographic plates.

The small-angle scattering capability is very large. Fourteen orders of Bragg diffraction have been recorded from a simple magnification calibration grid having an effective lattice constant of 4630 Å using nominal camera lengths of 50 and 70 m at 120 keV. In principle the Grigson coils can be used to increase this camera length by a factor of up to  $3 \times 10^5$ ; the system limit then becomes the signal-to-noise ratio in the photomultiplier-amplifier detector system. This capability will be applied to the study of diffraction effects from ordered loop cluster arrays and void arrays in irradiated metals.

The energy dispersive x-ray chemical analysis system has been successfully applied to qualitative analysis of radiation-induced solute segregation. It has been established that transmutation-produced silicon migrates to  $\theta'$  precipitate particle interfaces in the aluminum-copper alloys (Sect. 4.1.5). Other results pertaining to steels are described elsewhere in this report. During the next year methods for adapting this system to quantitative analysis will be investigated.

#### 4.3.6 High-Voltage Electron Microscopy — R. W. Carpenter

During FY 1976 the feasibility of converting the HVEM to side-entry configuration, so that gas-solid reaction cells and *in situ* deformation stages can be used in the microscope, was investigated. The conversion is feasible, and the necessary components have been ordered.

## APPENDIX

### 1. STAFF ASSIGNMENTS

G. S. Painter, Institut für Festkörperforschung, Kernforschungsanlage, Jülich, FRG; H. H. Wills Physics Laboratory, University of Bristol, England; June 1974--September 1975.

D. L. McElroy, AERE, Harwell, England; September 1974--September 1975.

D. M. Kroeger, Institut für Festkörperforschung, Kernforschungsanlage, Jülich, FRG; September 1974--September 1975.

T. S. Lundy, ORNL, Planning and Analysis Group and Central Management Offices; October 1974--July 1976.

R. L. Beatty, Swiss Federal Institute for Reactor Research (EIR), Wurenlingen, Switzerland; June 1976--June 1977.

J. Brynestad, Norwegian Institute of Technology, Trondheim, Norway; October 1975--December 1975.

J. B. Hastings, Stanford Synchrotron Radiation Project, Stanford, California; January 1976--January 1977.

### 2. GUEST ASSIGNMENTS

H. P. Krautwasser, Institut für Reaktorwerkstoffe, Kernforschungsanlage, Jülich, FRG; May 1975--September 1976.

G. Bauer, Institut für Festkörperforschung, Kernforschungsanlage, Jülich, FRG; March 1975--May 1976.

P. Jung, Institut für Festkörperforschung, Kernforschungsanlage, Jülich, FRG; June 1976--July 1977.

D. J. Griffiths, Oregon State University; September 1974--September 1975.

D. G. Hall, ORAU Doctoral Student from University of Tennessee; September 1975--August 1976.

T. K. Holder, ORAU Graduate Student from Tennessee Technological University; January 1976--June 1976.

J. W. Masey, ORAU Graduate Student from Tennessee Technological University; June 1975--October 1975.

O. C. Sartain, Indiana State University; Summer 1975.

P. L. Leath, Rutgers University; Summer 1975.

H. Eaton, Vanderbilt University; Summer 1975.

R. W. Gould, University of Florida; Summer 1975.

W. Oliver, University of Tennessee; Summer 1975.

D. G. Dunmire, Thiel (Pennsylvania) College; Summer 1975.

R. Bayuzick, Vanderbilt University; Summer 1975; Summer 1976.

B. Gyorffy, H. H. Wills Physics Laboratory, University of Bristol, England; Summer 1975; Summer 1976.

R. A. Hartsell, Carnegie-Mellon University; Summer 1976.

### 3. STAFF CHANGES

R. O. Williams to Materials Compatibility, Metals and Ceramics Division.

H. F. Holmes to Chemistry Division (on loan from that Division).

G. J. Yurek to Department of Metallurgy, Mass. Inst. of Technology.

W. G. Wolfer to Department of Nuclear Engineering, University of Wisconsin.

J. J. Olson to Department of Physics, University of California-San Diego.

R. A. McKee from National Bureau of Standards to ORNL.

Amit Das Gupta from Nuclear Research Center, Karlsruhe, FRG, to ORNL.

J. S. Lin from Department of Physics, University of Missouri-Columbia, to ORNL.

### 4. ORNL-UT JOINT APPOINTMENTS FOR ACADEMIC YEAR 1975-1976

B. S. Borie, Professor, Metallurgical Engineering.

C. J. McHargue, Professor, Metallurgical Engineering.

R. A. Vandermeer, Professor, Metallurgical Engineering.

W. A. Coghlan, Assistant Professor, Metallurgical Engineering.

## 5. PRESENTATIONS AT TECHNICAL MEETINGS

Compiled by Stephanie B. Davison

International Conference on Radiation Test Facilities for the CTR Surface and Materials Program, Argonne National Laboratory, Argonne, Illinois, July 15-18, 1975

M. J. Saltmarsh\* and J. A. Horak, "A Large-Volume Intense Neutron Source for CTR Materials Studies"

Crystal Growth Conference, Stanford University, Stanford, California, July 16, 1975

G. W. Clark, C. B. Finch, J. D. Holder,\* and H. L. Yakel, "Unidirectional Solidification of MnO-Mn<sub>2</sub>SiO<sub>4</sub> Eutectic by the Edge-Defined, Film-Fed Method"

G. W. Clark,\* "Eutectic Solidification" (invited paper)

30th Annual Calorimetry Conference, Seattle, Washington, July 16-19, 1975

J. M. Leitnaker\* and D. N. Braski, "Activity Coefficients of Ti in a Nickel- and Iron-Base Alloy"

1975 International Cryogenic Materials Conference, Queens University, Kingston, Ontario, Canada, July 22-25, 1975

D. S. Easton\* and C. C. Koch, "Mechanical Properties of Superconducting Nb-Ti Composites"

Twelfth Biennial Conference on Carbon, Pittsburgh, Pennsylvania, July 28-August 1, 1975

P. Krautwasser,\* C. S. Yust, H. Lühleisch, H. Nickel, and E. Pollmann, "Identification of Three Components in Pyrocarbon Coatings by TEM and Measurements of Microporosity, Inner Surface, Degree of Order, and Crystallite Size"

P. Krautwasser,\* "Influence of Low-Order Material on the Irradiation Behavior of Pyrocarbon Coatings"

C. S. Yust,\* E. Pollmann, and H. Nickel, "The Evaluation of Pyrocarbon Fuel Sphere Coatings by Transmission Electron Microscopy"

24th Annual Denver X-Ray Conference, Denver, Colorado, August 6-8, 1975

C. J. Sparks, Jr.,\* "Quantitative X-Ray Fluorescence Analysis Using Fundamental Parameters" (invited paper)

Annual Meeting of the Electron Microscopy Society of America, Las Vegas, Nevada, August 11-15, 1975

D. N. Braski\* and G. A. Potter, "Jet-Polishing Iridium for TEM"

---

\*Speaker.

IV HVEM Conference, Toulouse, France, September 1-4, 1975

R. W. Carpenter,\* "Effects of Precipitation on Electron Displacement in FCC Alloys: Copper Alloys with Random and Modulated Microstructures"

Conference on *In Situ* Composites-II. Lakeville, Connecticut, September 2-5, 1975

J. D. Holder\* and G. W. Clark, "Directional Solidification by Internal Zone Melting of Cr<sub>2</sub>O<sub>3</sub>-Mo Composites"

EMAG 75: Development in Electron Microscopy and Analysis, University of Bristol, Bristol, UK, September 8-11, 1975

R. W. Carpenter,\* "Observations of Huang Scattering in BCC Alloys"

United States-Japan Seminar on Radiation-Produced Defects and Defect Clusters and their Effects on Metals, Ames, Iowa, September 28-30, 1975

K. Farrell,\* "Some Effects of Gases in Neutron Irradiated Metals"

International Conference on Radiation Effects and Tritium Technology for Fusion Reactors, Gatlinburg, Tennessee, October 1-3, 1975

W. G. Wolfer\* and M. H. Yoo, "Stress-Assisted Void and Bubble Growth in CTR First Wall Materials"

K. Farrell\* and J. T. Houston, "Combined Effects of Displacement Damage and High Gas Content in Aluminum"

International Conference on Fundamental Aspects of Radiation Damage in Metals, Gatlinburg, Tennessee, October 5-12, 1975

R. W. Carpenter\* and J. C. Ogle, "The Effect of Solute Content and Precipitate Distribution on Fast Neutron Damage in Aluminum-Copper Alloys"

J. O. Stiegler,\* "Elevated Temperature Fracture of Neutron Irradiated Metals"

W. G. Wolfer,\* "Segregation of Vacancies and Interstitials by Internal Stress Fields"

M. H. Yoo,\* W. H. Butler, and L. K. Mansur, "Defect Annealing and Clustering in the Elastic Interaction Force Field"

1975 SSRP Users Group Meeting, Stanford, California, October 22-24, 1975

C. J. Sparks, Jr. and J. B. Hastings,\* "X-Ray Monochromator Design for Synchrotron Radiation"

Seminar at Naval Research Laboratory, Washington, D. C., October 29, 1975

C. C. Koch,\* "Research on Superconducting Materials in the Metals and Ceramics Division, Oak Ridge National Laboratory"

ASM Chapter, Louisville, Kentucky, November 7, 1975

John D. Holder,\* "Eutectic Solidification"

ASM Materials Science Seminar, Cincinnati, Ohio, November 9-10, 1975

E. E. Bloom,\* "Irradiation Strengthening and Embrittlement"

ASM Educators Session on Materials Sciences, Cincinnati, Ohio, November 10-12, 1975

C. J. McHargue,\* "The New Graduate at a National Laboratory"

TMS-AIME Fall Meeting, Cincinnati, Ohio, November 10-13, 1975

R. W. Carpenter\* and J. C. Ogle, "The Effect of Precipitate Distribution on Fast Neutron Displacement Damage in Al-3.8% Cu Alloys"

W. A. Coghlan,\* N. H. Packan, and M. J. Saltmarsh, "A Method for Doping Irradiation Samples with He Using  $Cm^{244}$ "

C. C. Koch\* and J. O. Scarbrough, "The Influence of Yttrium on the Superconducting Properties of Nb-Ti Alloys"

C. L. White,\* L. Heatherly, and R. E. Clausing, "Solute Segregation to Grain Boundaries in Ir-0.3% W"

1975 Southeastern Regional Meeting of the American Physical Society, Auburn, Alabama, November 13-15, 1975

W. H. Butler,\* J. S. Faulkner, and J. J. Olson, "Calculation of the Superconducting Transition Temperature of the BCC Transition Metals"

Sixth Symposium on Engineering Problems of Fusion Research, San Diego, California, November 18-21, 1975

D. S. Easton,\* R. E. Schwall, and W. A. Fietz, "Degradation of Multifilament Nb<sub>3</sub>Sn Superconductor by Tensile Strain"

US-UK Fast Reactor Exchange Meeting, Oak Ridge National Laboratory, November 1975

L. K. Mansur,\* "Void Growth and Coalescence in Irradiated Metals"

Seminar, Vanderbilt University, Department of Materials Science and Metallurgical Engineering, Nashville, Tennessee, December 2, 1975

R. W. Carpenter,\* "Oxygen Absorption in a Typical V-IV BCC Solid Solution Alloy: Ta-8W-2Hf, Kinetics, Morphology, and Mechanical Properties"

Midwinter Solid State Research Conference, Laguna Beach, California, January 12-16, 1976

C. J. Sparks, Jr.,\* "Inelastic (Raman) Resonances Scattering of X Rays"

International Symposium on Atomic, Molecular, and Solid State Theory,  
Sanibel Island, Florida, January 18-24, 1976

J. S. Faulkner,\* "The Theory of Excitations in Disordered Solids"  
(invited paper)

American Crystallography Association Winter Meeting, Clemson, South  
Carolina, January 19-23, 1976

R. W. Hendricks,\* "A 10-Meter Small-Angle X-Ray Scattering  
Spectrometer Utilizing a Two-Dimensional Position-Sensitive  
Proportional Counter"

R. W. Hendricks,\* "Crystallographic Applications of One- and Two-  
Dimensional Position-Sensitive Proportional Counters"

Conference on Low Activation Materials in Controlled Thermonuclear  
Reactors, San Francisco, California, February 19-20, 1976

K. Farrell,\* "Bulk Radiation Damage in Aluminum Alloys" (invited  
paper)

AIIME Annual Meeting, Las Vegas, Nevada, February 22-26, 1976

R. E. Clausing, C. L. White,\* L. Heatherly, and D. N. Braski,  
"Intergranular Embrittlement of Hastelloy N by Tellurium"

W. A. Coghlan,\* "Some Aspects of Void and Loop Nucleation and  
Growth in the Vicinity of a Finite Dislocation Loop"

D. S. Easton,\* "The Effect on Critical Current of Tensile Stress  
in Nb<sub>3</sub>Sn and Nb-Ti Superconducting Composites"

A. Das Gupta,\* W. Gey, J. Halbritter, H. K pfer, and J. A. Yasaitis,  
"Inhomogeneities in Superconducting Niobium Surfaces"

C. C. Koch,\* A. Das Gupta, and D. M. Kroeger, "The Peak Effect in  
Superconducting Nb-Hf Alloys"

L. K. Mansur\* and W. G. Wolfer, "The Interaction of Point Defects  
with Coated Spherical Surfaces"

Roy A. Vandermeer,\* "The Phase Transformation Characteristics of a  
Uranium + 14 at. % Niobium Alloy"

C. L. White\* and D. F. Stein, "A Parallel Tangent Construction for  
Solute Segregation to Grain Boundaries"

M. H. Yoo\* and L. K. Mansur, "Distribution of Point Defects in  
Bounded Media Under Irradiation"

Seminar at Argonne National Laboratory, Argonne, Illinois, March 3, 1976

W. G. Wolfer,\* "Effect of Surface Composition on Void Nucleation  
and Growth"

1976 March Meeting of the American Physical Society, Atlanta, Georgia,  
March 29-April 1, 1976

W. H. Butler,\* "Superconductivity in the Transition Metals"

J. S. Faulkner,\* "A Band Theory Calculation of the Fermi Surface of Technetium"

D. G. Hall\* and J. S. Faulkner, "Exact Spectral Density Function for a One-Dimensional Model of an Amorphous Solid"

D. M. Kroeger,\* "Magnetic History Effects and Waveform Asymmetry in ac Magnetization Measurements on Type-II Superconductors"

G. S. Painter\* and J. Harris, "A Surface Molecule Study of O Chemisorption on Al"

Seminar, Department of Metallurgical Engineering, Ohio State University, Columbus, Ohio, April 2, 1976

R. A. Vandermeer,\* "Shape Memory Effects in Uranium Alloys"

Third NBS-ARPA Workshop, Vail, Colorado, April 5-7, 1976

D. S. Easton,\* "Stress Effects on Mechanical and Superconducting Properties of Commercial Conductors at 4.2K"

University of Virginia, Charlottesville, Virginia, April 9, 1976

W. G. Wolfer,\* "Mechanisms of Radiation-Induced Creep"

Department of Physics, Ohio State University, Columbus, Ohio, April 15, 1976

G. S. Painter,\* "Multiple-Scattering Calculations of the Electronic Structure and Bonding Properties of Transition Metal Surfaces"

Conference on Computer Simulation for Materials Application, Gaithersburg, Maryland, April 19-21, 1976

W. A. Coghlan,\* "Transient and Steady State Diffusion Solution for Point Defects in a Stress Field"

Joint Meeting, Tampa Chapters of American Society for Metals and American Society for Mechanical Engineers, Tampa, Florida, April 22, 1976

C. J. McHargue,\* "Engineering Requirements for Fusion Reactors"

American Physical Society Meeting, Washington, D. C., April 26-29, 1976

V. W. Lindberg,\* J. D. McGervey, and R. W. Hendricks, "Positron Lifetimes in Annealed, Neutron-Irradiated Aluminum"

Second Rochester Conference on d- and f-Band Superconductors, Rochester, New York, April 30-May 1, 1976

W. H. Butler\* and P. B. Allen, "Gap Anisotropy and  $T_c$  Enhancement: General Theory, and Calculations for Nb, Using Fermi Surface Harmonics"

78th Annual Meeting and Exposition of the Nuclear Division of the American Ceramic Society, Cincinnati, Ohio, May 1-6, 1976

C. S. Yust, V. J. Tennery,\* H. P. Krautwasser, and R. L. Beatty, "Structural Characterization of HTGR Pyrocarbon Fuel Particle Coatings"

C. S. Yust\* and V. J. Tennery, "Optical and Electron Microscopy of Vapor Deposited Silicon Carbide"

ASTM National Meeting, St. Louis, Missouri, May 2, 1976

E. A. Kenik\* and L. K. Mansur, "Variation in Microstructure of Iron-Nickel-Chromium Alloys Under Irradiation"

Preliminary Draft for Discussion by ASTM Subcommittee E10.08 (Procedures for Simulating Damage Produced in Fission and Fusion Reactors) St. Louis, Missouri, May 4-6, 1976

K. Farrell,\* "Task Group D, 'Procedures for the Simulation of Helium Effects,' Section 4 - "Introduction of Helium from Charged Particle Accelerators and Alpha Sources"

Workshop on Correlation of Neutron and Charged Particle Damage, Oak Ridge National Laboratory, May 8, 1976

L. K. Mansur,\* "Void Growth Kinetics"

Conference on Neutron Scattering, Gatlinburg, Tennessee, June 6-10, 1976

D. G. Hall\* and J. S. Faulkner, "Spectral Density Functions for Amorphous Solids"

J. Schelten\* and D. M. Kroeger, "Distribution of Transport Currents in Type II Superconductors Investigated by Neutron Small Angle Scattering"

1976 Annual Meeting of the American Nuclear Society, Toronto, Ontario, Canada, June 13-18, 1976

A. A. Solomon,\* C. S. Yust, and N. H. Packan, "Transient Deformation of Oxide Fuels"

"Carbon 76" International Carbon Conference, Baden-Baden, West Germany, June 28-July 2, 1976

P. Krautwasser, H. Nickel,\* and C. S. Yust, "Influence of Heat Treatments on the Microstructure of Pyrocarbon Coatings"

P. Krautwasser, H. Nickel,\* and C. S. Yust, "Influence of Annealing on the Microstructure of Pyrocarbon Coatings"

Invited Lecture at National Academy of Sciences - Solid State Sciences Committee Forum on Major Facilities and Equipment for Materials Research, Argonne National Laboratory, June 30-July 1, 1976

R. W. Carpenter,\* "High Voltage Electron Microscopy: Current State of Research and Future Prospects"

## 6. PUBLICATIONS -- Compiled by Judy Young

E. E. Bloom, J. O. Stiegler, A. F. Rowcliff, and J. M. Leitnaker, "Austenitic Stainless Steels with Improved Resistance to Radiation-Induced Swelling," *Ser. Metall.* 10(4): 303-08 (April 1976).

E. E. Bloom, K. Farrell, J. O. Stiegler, and M. H. Yoo, "Void Nucleation as Inferred from Neutron Irradiations," pp. 330-50 in *Consultant Symposium on the Physics of Irradiation Produced Voids, Harwell, 1974*, ed. by R. S. Nelson, H. M. Stationary Office, London, 1975.

C. R. Brinkman, R. K. Williams, R. L. Klueh, and T. L. Hebble, "Mechanical and Physical Properties of 2 1/4 Cr-1 Mo Steel in Support of CRBRP Steam Generator Design," *Nucl. Technol.* 28(3): 490-505 (March 1976).

P. T. Carlson, "Interdiffusion and Intrinsic Diffusion in Binary Vanadium-Titanium Solid Solutions at 1350°C," *Metall. Trans.* 7A(2): 199-208 (February 1976).

R. W. Carpenter, "Effects of Precipitation on Electron Displacement Damage in fcc Alloys: Copper Alloys with Random and Modulated Microstructures," pp. 221-24 in *Microscopie électronique à haute tension 1975* (Proc. 4th Int. Congress, Toulouse) ed. by B. Jouffrey and P. Favord, Société Française de Microscopie Electronique, Paris, 1976.

R. W. Carpenter and C. T. Liu, "Surface Reaction Controlled Oxygen Absorption in a Ta-8 W-2 Hf Alloy: Kinetics and Concentration Gradients," *Metall. Trans.* 6A(12): 2235-41 (December 1975).

J. V. Cathcart, "Gaseous Oxidation of Uranium Alloys," pp. 775-813 in *Physical Metallurgy of Uranium Alloys* (Proc. 3rd Army Materials Technol. Conf.) ed. by J. J. Burke, D. A. Colling, A. E. Gorum, and J. Greenspan, Brook Hill Publishing Company, Chestnut Hill, Massachusetts, 1976.

J. V. Cathcart, "Mechanisms of Stress Generation and Relaxation During the Oxidation of U Alloys," pp. 114-32 in *Stress Effects and the Oxidation of Metals*, ed. by J. V. Cathcart, The Metallurgical Society of AIME, New York, 1975.

Ji Young Chang, *Hot Pressing Study on Mixed Uranium-Plutonium Nitride for Advanced Reactor Fuel*, ORNL-5051 (November 1975).

R. E. Clausing and E. E. Bloom, "Auger Electron Spectroscopy of Fracture Surfaces in Irradiated Type 304 Stainless Steel," pp. 491-505 in *Grain Boundaries in Engineering Materials*, ed. by J. L. Walter, J. H. Westbrook, and D. A. Woodford, Claitor's Publishing Division, Baton Rouge, 1975.

W. A. Coghlan, "Transient and Steady State Diffusion Solution for Point Defects in a Stress Field," pp. 166-76 in *Proc. Conf. Computer Simulation for Materials Application*, ed. by R. J. Arsenault, J. I. Beeler, Jr., and J. A. Simmons, Gaithersburg, Maryland, 1976.

J. G. Cook, J. P. Moore, T. Matsumura, and M. P. Van der Meer, *The Thermal and Electrical Conductivity of Aluminum*, ORNL-5079 (September 1975).

A. E. Curzon and C. C. Koch, "Direct Observation of the Flux Distribution in the Mixed State of V-Ga Alloys Using a Scanning Electron Microscope," *J. Phys. D.: Appl. Phys.* 9(4): 611-13 (March 1976).

R. G. Donnelly, V. J. Tennery, D. L. McElroy, T. G. Godfrey, and J. O. Kolb, *Industrial Thermal Insulation - An Assessment*, ORNL/TM-5283 (March 1976).

D. S. Easton and C. C. Koch, "Tensile Properties of Super-conducting Composite Conductors and Nb-Ti Alloys at 4.2 K," pp. 431-44 in *Shape Memory Effects in Alloys*, ed. by J. Perkins, Plenum, New York, 1976.

K. Farrell and J. T. Houston, *Combined Effects of Displacement Damage and High Gas Content in Aluminum*, ORNL/TM-5395 (May 1976).

K. Farrell and A. E. Richt, "Postirradiation Properties of the 6061-T6 Aluminum High Flux Isotope Reactor Hydraulic Tube," pp. 311-25 in *Properties of Reactor Structural Alloys After Neutron or Particle Irradiation*, Am. Soc. Test. Mater. Spec. Tech. Publ. 570, American Society for Testing and Materials, Philadelphia, 1976.

J. S. Faulkner, "Electronic States of Sub-Stoichiometric Compounds and Application to Palladium Hydride," *Phys. Rev. B* 13(6): 2391-97 (March 1976).

C. B. Finch and J. P. Young, "Effect of Temperature on the Self-Luminescence of SrCl<sub>2</sub> Doped with <sup>244</sup>Cm or <sup>253</sup>Es: Observation of Host Defect Emissions," *J. Inorg. Nucl. Chem.* 38(1): 45-48 (January 1976).

C. B. Finch, G. W. Clark, and O. C. Kopp, "Growth of Single-Crystal Mn<sub>2</sub>SiO<sub>4</sub> (Tephroite) by Czochralski and Edge-Defined Film-Fed (EFG) Techniques," *J. Cryst. Growth* 29(3): 269-72 (July 1975).

D. J. Griffiths, C. C. Koch, and J. P. Charlesworth, "The Frequency Dependence of AC Losses in Type II Superconductors," *Phil. Mag.* 33(3): 505-28 (March 1976).

A. Das Gupta, W. Gey, J. Halbritter, H. Kupfer, and J. A. Yasaitis, "Inhomogeneities in Superconducting Niobium Surfaces," *J. Appl. Phys.* 47(5): 2146 (May 1976).

R.O.A. Hall, M. J. Mortimer, D. L. McElroy, W. Müller, and J. C. Spirlet, "The Specific Heat of Americium-241 Metal from 15 to 300 K," pp. 139-46 in *Transplutonium 1975* (4th International Symposium, Baden-Baden, Spet. 13-17, 1975), ed. by W. Müller and R. Lindmer, North-Holland, Amsterdam and Oxford, 1976.

J. Harris and G. S. Painter, "Oxygen Chemisorption on a Small Aluminum Cluster," *Phys. Rev. Lett.* 36(3): 151-54 (January 1976).

J. A. Horak and T. H. Blewitt, "Fast- and Thermal-Neutron Irradiation and Annealing of Cu, Ni, Fe, Ti, and Pd," *Nucl. Technol.* 27(3): 416-38 (November 1975).

J. A. Horak, "Fuels for Pulsed Reactors — Preface," *Nucl. Technol.* 38(1): 7–8 (January 1976).

J. A. Horak, C. J. McHargue, and M. J. Saltmarsh, "The Need for a Neutron Irradiation Facility," Chap. 2 in *INGRID, A Proposal for an Intense Neutron Generator for Radiation-Induced Damage Studies in the CTR Materials Program*, ORNL/TM-5233 (January 1976).

J. A. Horak, "Nuclear Materials Education — A Viewpoint from the National Laboratories," (Summary) *Trans. Am. Nucl. Soc.* 23(TANSAO 23): 181 (June 1976).

J. A. Horak, "Summary of Unpublished Presentations for Fuels for Pulsed Reactors," *Nucl. Technol.* 28(1): 87–91 (January 1976).

R. O. Jones, P. J. Jennings, and G. S. Painter, "Cluster Calculations of the Electronic Structure of Transition Metal Surfaces," *Surf. Sci.* 53(1): 409–28 (December 1975).

D. H. Klein et al. including J. C. Ogle, "Pathways of Thirty-Eight Trace Elements Through a Coal-Fired Power Plant," *Environ. Sci. Technol.* 9: 973–78 (October 1975).

C. C. Koch and D. M. Kroeger, "Fluxoid-Pinning in Niobium Containing Small Amounts of Yttrium or Gadolinium," pp. 164–67 in *International Discussion Meeting on Flux Pinning in Superconductors*, ed. by Peter Haaren and H. C. Freyhardt, Akademie der Wissenschaften in Göttingen, Germany, 1975.

C. C. Koch, "Superconductivity in the Technetium-Titanium Alloy System," *J. Less-Common Met.* 44: 177–81 (January 1976).

P. Krautwasser, C. S. Yust, H. Lühleich, H. Nickel, and E. Pollmann, "Identification of Three Components in Pyrocarbon Coatings by Transmission Electron Microscopy (TEM) and Measurements of Microporosity, Inner Surface, Degree of Order, and Crystallite Size," pp. 157–58 in *12th Bienn. Conf. Carbon Extended Abstracts and Program* (July 28–August 1, 1975, Pittsburgh, Pennsylvania) Co-sponsored by the American Carbon Society and the School of Engineering, University of Pittsburgh.

P. Krautwasser and C. S. Yust, "Influence of Low-Order Material on the Irradiation Behavior of Pyrocarbon Coatings," pp. 159–60 in *12th Bienn. Conf. Carbon Extended Abstracts and Program* (July 28–August 1, 1975, Pittsburgh, Pennsylvania) Co-sponsored by the American Carbon Society and the School of Engineering, University of Pittsburgh.

L. K. Mansur, P. R. Okamoto, A. Taylor, and Che-Yu Li, "Surface Reaction Limited Void Growth," pp. 272–89 in *Properties of Reactor Structural Alloys After Neutron or Particle Irradiation*, *Am. Soc. Test. Mater. STP 570*, American Society for Testing and Materials, 1975.

D. L. McElroy, H. R. Haines, R.O.A. Hall, and J. A. Lee, "The Specific Heat of  $\text{PuC}_{1-x}$  and  $\text{Pu}_2\text{C}_3$  from 10 to 300 K," pp. 267–76 in *Plutonium and Other Actinides* (5th International Conference, Proc. Baden-Baden, September 10–13, 1975), ed. by H. Blank and R. Lindmer, North-Holland, Amsterdam and Oxford, 1976.

J. P. Moore and T. G. Godfrey, "Comment on 'Thermal Conductivity of KCl Alloys,'" *J. Am. Ceram. Soc.* 58(7): 344 (August 1975).

J. P. Moore, R. S. Graves, M. B. Herskovitz, K. R. Carr, and R. A. Vandermeer, *Nicrosil II and Nisil Thermocouple Alloys: Physical Properties and Behavior During Thermal Cycling to 1200 K*, ORNL-TM-4954 (August 1975).

J. J. Olson, "Anderson-McMillan Prescription for the Density of States of Liquid Iron," *Phys. Rev. B* 12(8): 2908-16 (October 1975).

R. E. Pawel and J. J. Campbell, "Some Oxidation Characteristics of Ta-10W and Ta-10W-2.5 Hf Alloys," pp. 330-39 in *Stress Effects and the Oxidation of Metals*, ed. by J. V. Cathcart, The Metallurgical Society of AIME, New York, 1975.

R. A. Perkins, *Oxygen Diffusion in  $\beta$ -Zircaloy*, ORNL/NUREG/TM-19 (July 1976).

T. C. Reiley, *Deposition Profiles from Electron Beam-Heated Evaporation Sources*, ORNL-TM-5194 (January 1976).

Edwin Roedder and Otto C. Kopp, "Check on the Validity of the Pressure Correction in Inclusion Geothermometry, Using Hydrothermally Grown Quartz," pp. 431-46 in *IMA - Papers 9th Meeting, Berlin - Regensburg 1974*, December 1975.

J. Schelten and R. W. Hendricks, "A New Small-Angle X-Ray Scattering Facility Utilizing a Rotating Anode, Pin-Hole Collimation and a Position-Sensitive Proportional Counter," *J. Appl. Cryst.* 8(4): 421-29 (August 1975).

R. N. Shelton, T. F. Smith, C. C. Koch, and W. E. Gardner, "T<sub>C</sub> and Its Pressure Dependence for Technetium-Based HCP Solid Solution Alloys," *J. Phys. F*: 5(10): 1916-30 (October 1975).

P. S. Sklad and T. E. Mitchell, "Effects of Electron Irradiation on Precipitation in Al-3.5% Cu," *Acta Metall.* 23(11): 1287-1302 (November 1975).

C. J. Sparks, Jr., "Excess Diffuse X-Ray Scattering and Anomalous Dispersion," pp. 175-92 in *Anomalous Scattering*, ed. by S. Ramaseshan and S. C. Abrahams, Munksgaard, Copenhagen, 1975.

A. A. Solomon, C. S. Yust, and N. H. Packan, "Transient Deformation of Oxide Fuels," (Summary) *Trans. Am. Nucl. Soc.* 23(TANSAO 23): 176 (June 1976).

D. F. Stein, W. C. Johnson, and C. L. White, "Study of Grain Boundary Segregation Using Auger Electron Spectroscopy," pp. 301-51 in *Grain Boundary Structure and Properties*, ed. by G. A. Chadwick and D. A. Smith, Academic Press, London, 1976.

H. D. Stidham, J. B. Bates, and C. B. Finch, "Vibrational Spectra of Synthetic Single Crystal Tephroite, Mn<sub>2</sub>SiO<sub>4</sub>," *J. Phys. Chem.* 80(11): 1226-34 (May 1976).

J. O. Stiegler, J. M. Leitnaker, and E. E. Bloom, "Effects of Solute Interstitial Elements on Swelling of Stainless Steel," pp. 136-41 in *Physical Metallurgy of Reactor Fuel Elements*, ed. by J. E. Harris and E. C. Sykes, The Metals Society, London, 1975.

R. A. Vandermeer, "Aging Induced Shape Instability in an Elastically Bent Uranium + 7.5 Wt % Niobium + 2.5 Wt % Zirconium Alloy," *Metall. Trans.* 7A(6): 871-78 (June 1976).

R. A. Vandermeer, "Recent Observations of Phase Transformations in U-Ti and U-Nb-Zr Alloys," pp. 219-57 in *Physical Metallurgy of Uranium Alloys* (Proc. 3rd Army Materials Technol. Conf.), ed. by J. J. Burke, D. A. Colling, A. E. Gorum, and J. Greenspan, Brook Hill Publishing Company, Chestnut Hill, Massachusetts, 1976.

R. O. Williams, *A Computer Program for the Simulation of Solid Solutions*, ORNL-5140 (May 1976).

R. O. Williams, "Concerning the Question of Recovery Before Recrystallization," *Scr. Metall.* 10(6): 661-62 (June 1976).

R. O. Williams, "Discussion of 'Mathematical Representation of Thermodynamic Properties of Binary Systems and Solution of Gibbs-Duhem Equation'," *Metall. Trans.* 6A(10): 1962-63 (October 1975).

R. O. Williams, "Flip-Flop Decomposition Within Miscibility Gaps," *J. Mater. Sci.* 10(7): 1228-30 (July 1975).

W. G. Wolfer, M. Ashkin, and A. Boltax, "Creep and Swelling Deformation in Structural Materials During Fast-Neutron Irradiation," pp. 233-58 in *Properties of Reactor Structural Alloys After Neutron or Particle Irradiation*, Am. Soc. Test. Mater. Spec. Tech. Publ. 570, American Society for Testing and Materials, Philadelphia, 1976.

W. G. Wolfer and M. H. Yoo, *The Effect of Stress-Induced Diffusion on Void Nucleation*, ORNL/TM-5398 (May 1976).

H. L. Yakel, "The Crystal Structure of a Boron-Rich Boron Carbide," *Acta Cryst. B* 31(Part 7): 1797-1806 (July 1975).

H. L. Yakel, "A Review of X-Ray Diffraction Studies in Uranium Alloys," pp. 259-308 in *Physical Metallurgy of Uranium Alloys* (Proc. 3rd Army Materials Technol. Conf.), ed. by J. J. Burke, D. A. Colling, A. E. Gorum, and J. Greenspan, Brook Hill Publishing Company, Chestnut Hill, Massachusetts, 1976.

H. L. Yakel, *Three Computer Codes of General Use in X-Ray Crystallography*, ORNL-TM-5177 (January 1976).

G. J. Yurek, *Interface Stability During Oxidation of Binary Alloys*, ORNL-5116 (April 1976).

C. S. Yust, E. Pollmann, and H. Nickel, "The Evaluation of Pyro-Carbon Fuel Sphere Coatings by Transmission Electron Microscopy," pp. 7-8 in *12th Bienn. Conf. Carbon Extended Abstracts and Program* (July 28- August 1, 1975, Pittsburgh, Pennsylvania) Co-sponsored by the American Carbon Society and the School of Engineering, University of Pittsburgh.

## Publications Pending

J. Bentley and E. A. Kenik, "Energy Dispersive X-Ray Measurements of Thin Metal Foils," paper presented at Electron Microscopy Society of America, Miami Beach, Florida, August 9-13, 1976. To be published in the proceedings.

D. S. Billington, "Radiation Damage (Radiation Effects) in Materials," to be published in *Encyclopedia Science and Technology*, ed. by Daniel N. Lapedes, McGraw-Hill, New York.

E. E. Bloom, "Irradiation Strengthening and Embrittlement," paper presented at American Society for Metals Materials Science Seminar, Cincinnati, Ohio, Nov. 9-10, 1975. To be published in the proceedings.

W. H. Butler, "A One-Dimensional Model for Transition Metals and Their Alloys," to be published in *Physical Review*.

W. H. Butler, J. J. Olson, J. S. Faulkner, and B. L. Gyorffy, "The Electron Phonon Interaction in Cubic Systems: Application to Niobium," to be published in *Physical Review*.

W. H. Butler and P. B. Allen, "Gap Anisotropy and  $T_c$  Enhancement: General Theory, and Calculations for Nb, Using Fermi Surface Harmonics," paper presented at Second Rochester Conference on d- and f-Band Superconductors, Rochester, New York, April 30-May 1, 1976. To be published in the proceedings.

W. A. Coghlan, "Transient and Steady State Diffusion Solution for Point Defects in a Stress Field," paper presented at Conference on Computer Simulation for Materials Applications, NBS, Gaithersburg, Maryland, April 19-21, 1976. To be published in the proceedings.

D. S. Easton and C. C. Koch, "Mechanical Properties of Superconducting Nb-Ti Composites," paper presented at 1975 International Cryogenic Materials Conference, Queens University, Kingston, Ontario, Canada, July 22-25, 1975. To be published in the proceedings.

D. S. Easton, D. M. Kroeger, and A. Moazed, "Thermomechanical Heat Generation in Copper and a Nb-Ti Superconducting Composite," to be published in *Applied Physics Letters*.

D. S. Easton and R. E. Schwall, "Performance of Multifilamentary Nb<sub>3</sub>Sn Under Mechanical Load," to be published in *Applied Physics Letters*.

K. Farrell, "Low Activation Materials for Fusion Reactors: Radiation Damage Considerations in Aluminum Alloys," paper presented at Workshop on Low Activation Materials for Fusion Reactors, San Francisco, California, February 19-20, 1976. To be published in the proceedings.

J. S. Faulkner, "Electronic States in Disordered Alloys II: Results for Real Solids," paper presented at International Symposium on Quantum Chemistry and Solid State Physics, Sanibel Island, Florida, January 18-24, 1976. To be published in *International Journal of Quantum Chemistry*.

D. G. Hall and J. S. Faulkner, "Spectral Density Functions for Amorphous Solids," paper presented at Conference on Neutron Scattering, Gatlinburg, Tennessee, June 6-10, 1976. To be published in the proceedings.

D. G. Hall, "The Quasicrystalline Approximation: Comparison of the Spectral Density with Exact Results," to be published in *Solid State Communications*.

L. A. Harris, T. Rose, L. DeRoos, and J. Greene, "Quantitative Analyses of Pyrite in Coal by Optical Image Techniques," to be published in *Journal of Economic Geology*.

J. D. Holder and G. W. Clark, "Directional Solidification by Internal Zone Melting of  $\text{Cr}_2\text{O}_3$ -Mo Composites," paper presented at Conference on *In Situ* Composites-II, Lakeville, Conn., September 2-5, 1975. To be published in the proceedings.

Edward A. Kenik, "Radiation-Induced Solute Segregation in a Low Swelling 316 Stainless Steel," to be published in *Scripta Metallurgica*.

C. C. Koch, "Technetium," to be published in *Metals Handbook*, Vol. 1.

D. M. Kroeger and J. Schelten, "Bending of Flux Lines by Transport Currents in Type-II Superconductors Measured by Neutron Diffraction," to be published in *Journal of Low Temperature Measurements*.

P. L. Leath, "Cluster Shape and Critical Exponents Near Percolation Threshold," to be published in *Physical Review Letters*.

P. L. Leath, "Cluster Size and Boundary Distribution Near Percolation Threshold," to be published in *Physical Review*.

R. A. McKee, "Solute and Solvent Diffraction for an Alloy in Dissociative Equilibrium," to be published in *Physical Review B*.

J. P. Moore, R. K. Williams, and R. S. Graves, "Thermal Conductivity, Electrical Resistivity and Seebeck Coefficient of High Purity Chromium from 280 to 1000 K," to be published in *Journal of Applied Physics*.

G. S. Painter, R. O. Jones, and P. J. Jennings, "Bonding Properties of Stepped Transition Metal Surfaces," paper presented at National Bureau of Standards, Gaithersburg, Maryland, Dec. 7-9, 1975. To be published in the proceedings.

R. A. Perkins and R. A. Padgett, Jr., "Sputter Sectioning of Diffusion Specimens," to be published in *Metallurgical Transactions*.

T. C. Reiley, "Deposition Profiles from Electron-Beam-Heated Evaporation Sources," to be published in *Journal of Vacuum Science and Technology*.

M. H. Yoo and W. H. Butler, "Steady State Diffusion of Point Defects in the Interaction Force Field," to be published in *Acta Metallurgica*.

G. J. Yurek, J. V. Cathcart, and R. E. Pawel, "Microstructures of the Scales Formed on Zircaloy-4 in Steam at Elevated Temperatures," to be published in *Oxidation of Metals*.

## Patent

C. J. Sparks and J. C. Ogle, *Window for Radiation Detectors and the Like* (to U.S. Energy Research and Development Administration). U.S. Patent 3,916,200.

## Theses

D. G. Hall, "Spectral Density Functions for Disordered Systems," Ph.D. Thesis, Physics Department, University of Tennessee, Knoxville, Tenn., 1976. To be published as ORNL-5184.

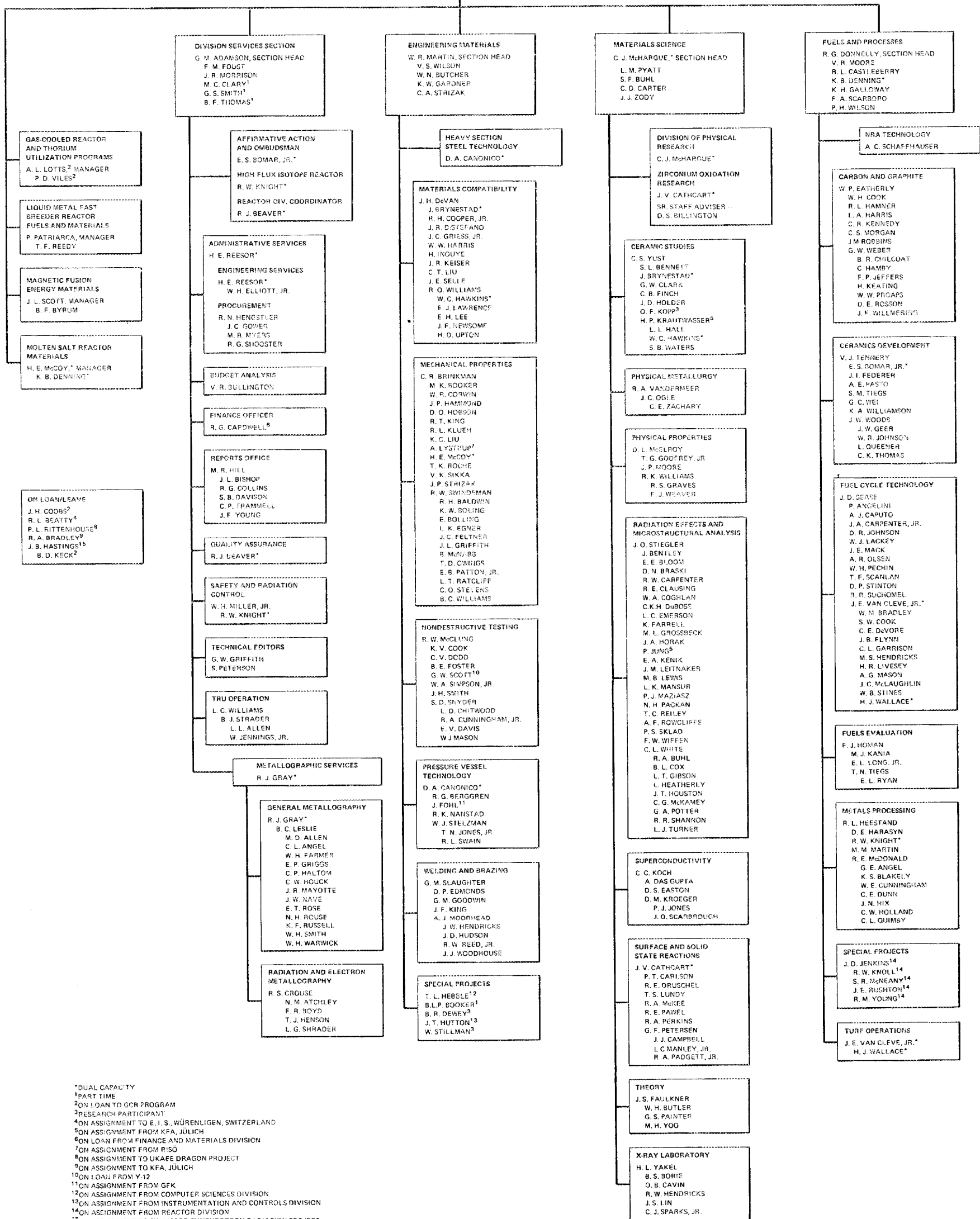
T. K. Holder, "Thermal Conductivity, Electrical Resistivity, and Absolute Seebeck Coefficient of High-Purity Iron and Selected Iron-Alloys from 90 to 400 K," M.S. Thesis, Department of Chemical Engineering, Tennessee Technological University, Cookeville, Tenn., 1976. To be published as ORNL/TM-5339.

J. Masey, "The Thermal Conductivity of Iron and Iron-Base Alloys," M.S. Thesis, Department of Chemical Engineering, Tennessee Technological University, Cookeville, Tenn., 1975.

# METALS AND CERAMICS DIVISION

JULY 1, 1976

DIRECTOR J. R. WEIR, JR.  
F. R. COX  
ASSOCIATE DIRECTOR J. E. CUNNINGHAM  
M. B. WHITE



<sup>1</sup>DUAL CAPACITY  
<sup>2</sup>PART TIME  
<sup>3</sup>ON LOAN TO GCR PROGRAM  
<sup>4</sup>RESEARCH PARTICIPANT  
<sup>5</sup>ON ASSIGNMENT TO E. H. S. WÜRENLIGEN, SWITZERLAND  
<sup>6</sup>ON ASSIGNMENT FROM KFA, JÜLICH  
<sup>7</sup>ON LOAN FROM FINANCE AND MATERIALS DIVISION  
<sup>8</sup>ON ASSIGNMENT FROM P-50  
<sup>9</sup>ON ASSIGNMENT TO UKAEA DRAGON PROJECT  
<sup>10</sup>ON ASSIGNMENT TO KFA, JÜLICH  
<sup>11</sup>ON LOAN FROM Y-12  
<sup>12</sup>ON ASSIGNMENT FROM GFK  
<sup>13</sup>ON ASSIGNMENT FROM COMPUTER SCIENCES DIVISION  
<sup>14</sup>ON ASSIGNMENT FROM INSTRUMENTATION AND CONTROLS DIVISION  
<sup>15</sup>ON ASSIGNMENT FROM REACTOR DIVISION  
<sup>16</sup>ON ASSIGNMENT TO STANFORD SYNCHROTRON RADIATION PROJECT



## INTERNAL DISTRIBUTION

1-2.	Central Research Library	65.	J. A. Horak
3.	Document Reference Section	66.	L. H. Jenkins
4-13.	Laboratory Records Department	67.	P. R. Kasten
14.	Laboratory Records, ORNL RC	68.	O. L. Keller
15.	ORNL Patent Office	69.	E. A. Kenik
16.	G. M. Adamson	70.	C. C. Koch
17.	S. E. Beall	71.	W. C. Koehler
18.	S. L. Bennett	72.	D. M. Kroeger
19.	J. Bentley	73.	J. M. Leitnaker
20.	D. S. Billington	74.	M. B. Lewis
21.	B. S. Borie	75.	R. S. Livingston
22.	C. R. Brinkman	76.	A. L. Lotts
23.	J. Brynestad	77.	T. S. Lundy
24.	W. H. Butler	78.	F. C. Maienschien
25.	D. A. Canonico	79.	L. K. Mansur
26.	P. T. Carlson	80.	W. R. Martin
27.	R. W. Carpenter	81.	R. W. McClung
28.	J. V. Cathcart	82.	H. E. McCoy
29.	G. W. Clark	83.	H. F. McDuffie
30.	J. F. Clarke	84.	D. L. McElroy
31.	R. E. Clausing	85.	F. K. McGowan
32.	J. W. Cleland	86-135.	C. J. McHargue
33.	W. A. Coghlan	136.	R. A. McKee
34.	R. R. Coltman	137.	R. Minturn
35.	J. H. Coobs	138.	J. P. Moore
36.	J. A. Cox	139.	J. C. Ogle
37.	F. L. Culler	140.	S. M. Ohr
38.	J. E. Cunningham	141.	N. H. Packan
39.	A. Das Gupta	142.	G. S. Painter
40.	J. H. DeVan	143.	P. Patriarca
41.	R. G. Donnelly	144.	R. E. Pawel
42.	D. S. Easton	145.	R. A. Perkins
43.	W. P. Eatherly	146.	S. Peterson
44.	K. Farrell	147.	H. Postma
45.	J. S. Faulkner	148.	C. R. Richmond
46.	C. B. Finch	149.	M. T. Robinson
47.	R. J. Gray	150.	M. W. Rosenthal
48.	M. L. Grossbeck	151.	M. J. Saltmarsh
49.	W. O. Harms	152.	A. C. Schaffhauser
50.	R. L. Heestand	153.	J. L. Scott
51.	R. W. Hendricks	154.	S. T. Sekula
52.	R. F. Hibbs	155.	G. M. Slaughter
53-62.	M. R. Hill	156.	H. G. Smith
63.	J. D. Holder	157.	C. J. Sparks
64.	F. J. Homan	158.	D. Steiner

- |                            |                                     |
|----------------------------|-------------------------------------|
| 159. P. H. Stelson         | 172. R. F. Wood                     |
| 160. J. O. Stiegler        | 173. R. G. Wymer                    |
| 161. V. J. Tennery         | 174. W. J. Yaggi (Y-12)             |
| 162. D. B. Trauger         | 175. H. L. Yakel, Jr.               |
| 163. R. A. Vandermeer      | 176. M. H. Yoc                      |
| 164. P. R. Vanstrum (Y-12) | 177. F. W. Young, Jr.               |
| 165. J. R. Weir, Jr.       | 178. A. Zucker                      |
| 166. C. L. White           | 179. J. H. Frye, Jr. (consultant)   |
| 167. F. W. Wiffen          | 180. P. M. Brister (consultant)     |
| 168. W. J. Wilcox, Jr.     | 181. John Moteff (consultant)       |
| 169. M. K. Wilkinson       | 182. Hayne Palmour III (consultant) |
| 170. R. K. Williams        | 183. J. W. Frados (consultant)      |
| 171. C. E. Winters         | 184. N. E. Promisel (consultant)    |
|                            | 185. D. F. Stein (consultant)       |

## EXTERNAL DISTRIBUTION

186. S. Amelinckx, SCK/CEN, B. 2400 Mol, Belgium
187. K.H.G. Ashbee, H. H. Wills Physics Laboratory, University of Bristol, Bristol, England
188. R. W. Balluffi, 210 Bard Hall, Cornell University, Ithaca, NY 14850
189. W. Bauer, Physical Research, Sandia Laboratories, Livermore, CA 44550
190. Leo Brewer, Inorganic Materials Division, Lawrence Berkeley Laboratory, Berkeley, CA 94720
191. J. P. Charlesworth, AERE, Harwell, Didcot, Oxon, OX11, ORB, England
192. J. H. Crawford, Jr., Dept. of Physics, University of North Carolina, Chapel Hill, NC 27514
193. J. Dienes, Dept. of Physics, Brookhaven National Laboratory, Upton, NY 11973
194. B. T. Frost, Director, Materials Science Division, Argonne National Laboratory, 9700 South Cass Avenue, Argonne, IL 60439
195. A. N. Goland, Dept. of Physics, Brookhaven National Laboratory, Upton, NY 11973
196. D. Gurinsky, Applied Science Division, Brookhaven National Laboratory, Upton, NY 11973
197. P. Haasen, Institut für Metallphysik, University of Göttingen, Göttingen, Germany
198. W. Johnston, General Electric Research and Development Center, Schenectady, NY 12301
199. Librarian, Building 465, Atomic Energy Research Establishment, Harwell, Didcot, Oxon, OX11, ORB, England
200. K. Lücke, Technische Hochschule Aachen, Aachen, Germany
201. W. D. Manly, Stellite Division, Cabot Corp., 1020 Park Avenue, Kokomo, IN 46901
202. R. J. Mauer, Materials Research Laboratory, University of Illinois, Urbana, IL 61801
203. D. J. Michel, Met. Div., Code 6397, Naval Research Laboratory, Washington, DC 20375

204. T. E. Mitchell, Dept. of Met. and Mat. Sci., Case-Western University, Cleveland, OH 44106
205. M. Nevitt, Deputy Director, Argonne National Laboratory, 9700 South Cass Avenue, Argonne, IL 60439
206. H. Nichols, Director, Institut für Reaktorwerkstoffe, Kernforschungsanlage, Jülich GmbH, 517 Jülich 1, Postfach 1913, Germany
207. B. F. Oliver, Dept. of Chem. and Met. Eng., University of Tennessee, Knoxville, TN 37919
208. N. Peterson, Materials Science Division, Argonne National Laboratory, 9700 South Cass Avenue, Argonne, IL 60439
209. D. L. Price, Solid State Physics Division, Argonne National Laboratory, 9700 South Cass Avenue, Argonne, IL 60439
210. L. W. Roberts, Chemistry and Materials Science, Lawrence Livermore Laboratory, P.O. Box 808, Livermore, CA 84550
211. W. Schilling, Institut für Festkörperforschung, der Kernforschungsanlage, Jülich, D-517 1, Postfach 365, Germany
212. W. Schmatz, Institut für Festkörperforschung, der Kernforschungsanlage, Jülich, D-517 1, Postfach 365, Germany
213. A. Seeger, Institut für Theoret und Angew, Physik der Universität Stuttgart, 7000 Stuttgart 80-Pfaffenwaldring 57/V1, Germany
214. D. Seidman, Dept. Mat. Sci. and Eng., Cornell University, Ithaca, NY 14850
215. D. Shirley, Director, Inorganic Materials Division, Lawrence Berkeley Laboratory, Berkeley, CA 94720
216. S. Spooner, Dept. of Chem. Eng., Georgia Institute of Technology, Atlanta, GA 30332
217. R. Smallman, Dept. of Metallurgy, University of Birmingham, Birmingham, England
218. J. T. Stanley, College of Eng. Sci., Arizona State University, Tempe, AZ 85281
219. E. E. Stansbury, Dept. of Chem. and Met. Eng., University of Tennessee, Knoxville, TN 37919
220. H. Ullmaier, Institut für Festkörperforschung, Kernforschungsanlage, Jülich, D517, Jülich 1, Postfach 365, Germany
221. F. L. Vook, Dept. 5110, Sandia Laboratories, Albuquerque, NM 87115
222. J. B. Wagner, Dept. of Mat. Sci., Northwestern University, Evanston, IL 60201
223. M. S. Wechsler, Dept. of Metallurgy, Iowa State University, Ames, IA 50010
224. A. M. Weinberg, Institute for Energy Analyses, ORAU, Oak Ridge, TN 37830
225. C. Wert, Dept. Met. and Mining Eng., University of Illinois, Urbana, IL 61801
226. USERDA, Division of Buildings and Industry, Conservation Administration, Washington, DC 20545

R. Anderson

227. USERDA, Division of Conservation Research and Technology,  
Washington, DC 20545  
J. Neal
- 228--229. USERDA, Division of Fossil Energy Research, Washington, DC 20545  
A. Mills  
H. Frankel
- 230--234. USERDA, Division of Magnetic Fusion Energy, Washington, DC 20545  
K. M. Zwilsky  
T. C. Reuther  
O. Manly  
C. D. Henning  
C. Finfgeld
- 235--240. USERDA, Division of Physical Research, Washington, DC 20545  
J. S. Kane  
L. C. Ianniello  
D. Readey  
D. K. Stevens  
M. C. Wittels  
S. Wolf
- 241--243. USERDA, Division of Solar Energy, Washington, DC 20545  
H. R. Blieden  
M. P. Prince  
G. M. Kaplan
- 244--245. USERDA, Oak Ridge Operations Office, P.O. Box E, Oak Ridge, TN 37830  
Director  
Research and Technical Support Division
- 246--442. USERDA, Technical Information Center, Office of Information  
Services, P.O. Box 62, Oak Ridge, TN 37830  
For distribution as shown in TID-4500 Distribution Category,  
UC-25 (Materials)